CHEMICAL REVIEWS

pubs.acs.org/CR

Review

Engineering Anisotropy into Organized Nanoscale Matter

Wenjie Zhou,[¶] Yuanwei Li,[¶] Benjamin E. Partridge, and Chad A. Mirkin*

Cite This: *Chem. Rev.* 2024, 124, 11063−11107

Read Online

ACCESS | Metrics & More | Article Recommendations

ABSTRACT: Programming the organization of discrete building blocks into periodic and quasi-periodic arrays is challenging. Methods for organizing materials are particularly important at the nanoscale, where the time required for organization processes is practically manageable in experiments, and the resulting structures are of interest for applications spanning catalysis, optics, and plasmonics. While the assembly of isotropic nanoscale objects has been extensively studied and described by empirical design rules, recent synthetic advances have allowed anisotropy to be programmed into macroscopic assemblies made from nanoscale building blocks, opening new opportunities to engineer periodic materials and even quasicrystals with unnatural properties. In this review, we define guidelines for leveraging anisotropy of individual building blocks to direct the organization of nanoscale matter. First, the nature and spatial distribution of local interactions are considered and three design rules that guide particle organization are derived. Subsequently, recent examples from the literature are examined in the context of these design rules. Within the discussion of each rule, we delineate the examples according to the dimensionality (0D−3D) of the building blocks. Finally, we use geometric considerations to propose a general inverse design-based construction strategy that will enable the engineering of colloidal crystals with unprecedented structural control.

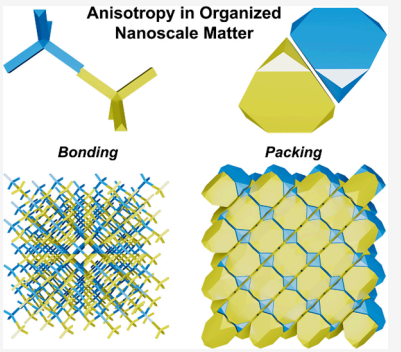

CONTENTS

Received: April 19, 2024
Revised: August 30, 2024
Accepted: September 6, 2024
Published: September 24, 2024

https://doi.org/10.1021/acs.chemrev.4c00299
Chem. Rev. 2024, 124, 11063−11107

1. INTRODUCTION

The organization of discrete building blocks into extended assemblies is a decentralized process, where order arises in an initially disordered system through a series of simple and well-defined local interactions.[1] This process is a hallmark of complex systems—the behavior of the entire system is intrinsically difficult to study, yet individual behaviors are narrowly defined and can be investigated.[2] The organization of complex systems is observed and appreciated across multiple length scales in many physical, chemical, biological, and cognitive settings, among which crystallization is arguably the most pertinent to the materials chemist.[3−6] In principle, crystallization, like all organization processes, is predictable, and an adequate understanding of how local interactions influence the overall generation of order should allow for the structures of those assemblies to be predicted. However, although crystallization is a ubiquitous process and can be predicted in certain cases, it is still not fully comprehended.

The outcomes of complex organization processes are dictated by the nature of local interactions, and the development of emergent order depends heavily on the number of encounters between individual objects—the more opportunities for interactions to occur, the more likely it is that a system will reach its final state, a local energy minimum. In the context of colloidal assembly, due to Brownian motion, nanoscale objects rapidly interact with each other and typically achieve their final state within experimentally feasible lengths of time.[7,8] These features make nanoscale assembly useful for investigating why and how order emerges as a result of complex organization processes. Using chemical principles, vast libraries of functional nanomaterials have been prepared that are often inaccessible through other means and that can be utilized to investigate assembly.[9−12]

The packing of isotropic nanoparticles—typically, uniformly functionalized nanoscale spheres or pseudospheres—has been extensively studied, and various packing modes have been empirically observed and theoretically explained.[13−17] However, the assembly of *anisotropic* nanoparticles—including asymmetrically functionalized spheres and pseudospheres or uniformly functionalized rods, plates, and polyhedral nanocrystals (i.e., the anisotropy is in the surface ligand placement or the core shape, respectively)—has not been as thoroughly explored in large part due to the synthetic challenges in realizing such types of nanoparticles.[18,19] Fortunately, advances in colloidal nanocrystal synthesis over the past decade have led to facile routes to a broad range of well-defined, anisotropic nanoscale building blocks with high purity and low dispersity.[20−22]

Though the assembly outcomes of some systems of anisotropic particles are expected (e.g., cubes assembling into simple cubic lattices, rods into hexagonal slabs, and plates into long extended pillars),[23] very few empirical rules have been articulated, and those that have are often challenged when unusual or unexpected outcomes are observed.[24,25] Moreover, the empirical rules do not accurately predict the behavior of increasingly complex nanoparticle systems, such as those involving hollow nanoframe particles, which have only recently become synthetically accessible.[26−28] Thus, there is a need to articulate general design principles that rationalize experimental observations with existing complex nanomaterials and also predict future avenues for the assembly of nanomaterials that have yet to be synthesized.

In this review, unified design principles that describe the role of anisotropic interactions in colloidal assemblies are presented. Rather than surveying the field through a lens of structural and functional diversity, as was superbly done by Deng et al.,[29] a geometric perspective is employed to understand how the relationship between individual nanoscale objects and emergent structural outcomes. First, the nature and spatial distribution of local interactions are considered, and three design rules that guide particle organization are summarized (Section 2). Then, examples from the literature are examined as case studies to assess how these design rules can be used to rationalize the assembly of complex systems (Section 3) involving constituent building blocks of increasing dimensions (from zero-dimensional (0D) to 3D). Though most case studies discussed herein focus on inorganic nanoparticles, proteins are a special class of anisotropic nanoscale building blocks and their assembly is of growing interest. Consequently, a brief survey of anisotropy in protein assembly is also included (Section 3.5). Finally, a vision of an inverse design-based geometric construction strategy that can be utilized to achieve sophisticated structural control is introduced (Section 4), and a brief outlook on the future of the field is offered (Section 5).

2. DESIGN PRINCIPLES FOR COLLOIDAL ORGANIZATION

As noted above, colloidal organization is a complex, fundamentally decentralized process. From a thermodynamic

https://doi.org/10.1021/acs.chemrev.4c00299
Chem. Rev. 2024, 124, 11063−11107

Table 1. Summary of Types of Ligands and Their Roles in Colloidal Crystallization

Type of Ligands	Chemical Characteristics	Roles in Colloidal Crystallization	Examples
Surfactant (Type I)	Amphiphilic small molecules	Act as a stabilizer by reducing surface tension, aiding in the dispersal and organization of nanoparticles.	51−53
Alkyl Chains (Type I)	Long carbon chains typically ending with a functional group	Provide steric stabilization by creating a physical barrier around nanoparticles, preventing aggregation.	18,54,55
Long-Chain Molecules (Type I)	Polymers or large organic molecules (e.g., PEG, polystyrene)	Provide steric stabilization and flexibility, impacting the viscosity and dynamics of particle movement in solution.	57,58
Supramolecular Ligands (Type II)	Molecules that form bonds based on molecular recognition	Facilitate selective and reversible interactions, allowing dynamic assembly processes and reconfiguration of structures.	40,56
Peptides and Proteins (Type II)	Amino acid sequences	Offer biospecificity, binding selectively to particle surfaces or specific crystal faces, guiding the assembly process.	59,60
Oligonucleotides (Type II)	Nucleic acid sequences (e.g., DNA, RNA)	Enables programmable assemblies due to specific base-pairing capabilities, supporting highly precise and complex structures.	23,27,61,62

perspective, the final assembly outcome is a product of the interplay between the entropy and enthalpy. Without a central organizing force, the assembly process is dictated by the nature of the local interactions between particles and the spatial organization of these interactions on individual particles. Therefore, the final organization of particles is heavily influenced by the local features of the individual particles, including their surface chemistry (local interactions), valency (tendencies to bind with other particles), and shape, all of which can be dictated by chemical design. In this section, these features are analyzed in turn, and their contributions to the three design principles that ultimately guide colloidal organization are delineated.

2.1. The Roles of Local Interactions

Colloidal assembly is intrinsically a hierarchical organization process, in which surface-bound ligands (Table 1) are collectively organized while an optimal packing of particle shapes is concomitantly achieved.[30,31] Therefore, assuming a sufficiently disordered initial state, the nature of the chemical interactions between building blocks is of utmost importance when trying to predict assembly outcomes.

Colloidal assembly approaches can be broadly categorized into two types: those in which nanoparticles assemble by reducing reaction volume or increasing internal pressure (concentration), often dominated by entropy (type I); and those in which nanoparticles assemble via induced accumulation, where reaction volume or internal pressure (concentration) is constant, often dominated by enthalpy (type II). In systems where organization is dominated by entropic factors (type I) (in general, where the particles have hard shapes and interactions are rigid), the total reaction volume tends to decrease. In this regime, to predict the assembly outcome, one essentially must compute the densest packing configuration of the initial particles. [Note that most real-world colloidal systems involve non-negligible enthalpic particle−particle interactions such that it is energetically favorable for there to be a closer distance or a larger contact area between certain regions of particular particles. In these systems, enthalpic and entropic contributions must be considered.]

In cases where enthalpic factors far exceed entropic ones (type II) (where the binding between particles is strong), one may ignore the volume and symmetry requirements. In this regime, the assembly outcome can be predicted by maximizing the contact area between specific regions on a nanoparticle surface. Geometrically, it is often easier to predict outcomes that maximize contact area rather than those that maximize packing density for certain shapes; brute-force computation is needed to make predictions about packing, and still there are grand challenges within this field.[30]

2.1.1. Entropy-Dominated (Type I) Colloidal Assembly. Type I, or entropy-driven, assembly can be achieved through multiple processes, including those that involve: 1) slow drying or solvent evaporation on 2D surfaces or in the 3D bulk;[15,32] 2) gravity or centrifugation;[33] and 3) applied fields.[34−36] The main consideration in these processes is the local volume exclusion of the surface-functionalized ligands. Given the ubiquity of ligands in colloidal systems, entropically driven type I assemblies have been investigated extensively, and empirical guidelines for their formation have been developed.[13,17] The ligand environment can be modified to tune the interparticle potential, which is mainly affected by van der Waals forces, steric stabilization interactions, and electrostatic interactions. However, these interactions are fundamentally isotropic in nature.

Anisotropic interactions in type I systems typically arise via shape-induced symmetry breaking, which will be discussed later (Section 2.3), or field-induced symmetry reduction. Magnetic field-assisted assembly—an important approach gaining an increasing amount of attention—relies heavily on magnetic anisotropy, which reduces the symmetries of the building blocks. However, the assembly outcomes often represent an optimal collective result of both field-alignment and shape packing.[34,36] In short, the local, entropically driven interactions of type I systems are more relevant to the organization of the isotropic building blocks. These systems have been discussed in multiple reviews,[13,37,38] including those covering sphere packing, and will not be discussed here.

2.1.2. Enthalpy-Dominated (Type II) Colloidal Assembly. In contrast to type I assembly processes, in which entropy is the primary determinant of the reaction product, type II assembly is dominated by enthalpic considerations, which stem from relatively strong chemical interactions such as hydrogen bonding. These interactions typically rely on the cooperative enthalpy-driven binding of multiple DNA strands, polymer chains, or supramolecular motifs.[39−42] Such short-range attractive interactions are characterized by their high directionality and programmable nature.[16,23,43] As a result, these systems often support facet registration between anisotropic particles, where maximizing facet−facet overlap enables the binding of a greater number of chemical moieties. Such assemblies are more thermodynamically stable than those where the individual components are poorly registered.[44]

Facet registration highlights a fundamental tension in preparing assemblies via type II processes: one must find a balance between: a) maximizing programmed contact area (maximizing local enthalpy) and b) maximizing final system

https://doi.org/10.1021/acs.chemrev.4c00299
Chem. Rev. 2024, 124, 11063−11107

entropy (reconciling internal repulsion). This tension leads to a more complex assembly behavior that may proceed via the distinct stepwise organization of local and long-range structures. Key kinetic insights can be drawn from the geometries of the building blocks; for example, large, flat facets bind preferably with other large, flat facets rather than with smaller ones. Moreover, type II assembly processes allow isotropic building blocks to be endowed with anisotropic assembly behavior through symmetry reduction processes (e.g., asymmetric ligand functionalization). In short, type II assembly processes are comparatively underexplored and not as well-understood, yet they offer the possibility of much finer thermodynamic and kinetic control over assembly outcomes. In addition, it is more feasible to deliberately design assembly outcomes based on geometric considerations in type II assemblies since such systems can be simplified to maximize preferred particle−particle contact. Consequently, the later discussion of specific design principles focuses mainly on type II assemblies.

2.1.3. Typical Types of Ligands and Local Interactions. Ligands play a crucial role in the assembly of colloidal nanoparticles by mediating interactions at the particle interface. The choice of ligands not only influences the stability and solubility of nanoparticles but also dictates the nature and strength of the interactions that drive the assembly processes. Here, we briefly discuss common types of ligands used in nanoparticle synthesis and their typical interactions:

2.1.3.1. Surfactants. Surfactants are amphiphilic molecules that adsorb to particle surfaces and stabilize nanoparticles by reducing the surface tension. In nanoparticle assembly, surfactants can act as steric stabilizers, preventing particles from approaching close enough to aggregate nonspecifically. The hydrophobic tails of these molecules interact with each other, while the hydrophilic heads remain exposed to the solvent, facilitating dispersion in various media.

2.1.3.2. Alkyl Chains. Alkyl chains are long carbon chains that may end with a functional group, enhancing the nanoparticle solubility in nonpolar solvents. Like surfactants, these ligands provide steric stabilization by creating a physical barrier around nanoparticles, which prevents agglomeration by maintaining a minimum distance between them.

2.1.3.3. Long-Chain Molecules. Polymeric ligands, such as poly(ethylene glycol) (PEG) and polystyrene, are high-molecular-weight molecules that attach to nanoparticle surfaces. These polymers enhance colloidal stability through steric hindrance and can be functionalized with various end groups to enable selective interactions. Their presence affects the viscosity of the nanoparticle dispersion and can modulate the dynamics of the particle movement and assembly in solution.

2.1.3.4. Peptides and Proteins. Peptides and proteins introduce biospecificity into nanoparticle interactions. Additionally, they may selectively bind to specific crystal faces of nanoparticles or to other molecular entities due to their complex tertiary structures.

2.1.3.5. Oligonucleotides. DNA and RNA strands form highly specific base-pair interactions, which can be harnessed to program the self-assembly of nanoparticles into predetermined structures. The specificity, reversibility, and stimuli-responsiveness of nucleic acid interactions allow for the creation of dynamic materials that can respond to changes in their environment such as temperature and pH shifts.

While specific interactions facilitated by ligands such as oligonucleotides allow for precise control over the assembly structures (Type II), hydrophobic interactions provide an alternative route for directing the anisotropic assembly of colloidal particles, capitalizing on the inherent nonpolarity of certain ligands. These interactions, predominantly entropic in nature (Type I), arise from the tendency of hydrophobic surfaces to minimize their exposure to polar solvents, thereby driving the assembly of colloidal particles in a manner that shields hydrophobic regions from the aqueous environment. Hydrophobic interactions are especially significant in the assembly of inorganic nanoparticles, where the surface ligands can be tailored to exhibit hydrophobic characteristics. This method has been effectively utilized in the formation of various nanostructures, as highlighted in several studies recently reviewed by Shao et al. and Zhang et al.[45,46]

Despite the broad array of ligands available to control and refine the anisotropic organization of nanoparticles at the nanoscale, accurately quantifying the local interactions between these nanoparticles poses significant challenges. Current methods for quantification include: (i) analysis of nanoparticle hybridization by monitoring surface plasmon resonance (SPR) as a function of temperature;[44] (ii) analysis of nanoparticle aggregation by *in situ* X-ray;[47] (iii) analysis of nanoparticle assemblies through *in situ* TEM;[48] (iv) analysis of assembly processes using isothermal titration calorimetry (ITC);[49] (v) computational modeling of interparticle potentials based on DLVO theory.[50] Despite these advances, the precise interactions among surface ligands and their complex interplay during the anisotropic organization of nanoscale building blocks remain open questions under active investigation.

2.2. Valency

The concept of valency is foundational to synthetic chemistry, providing chemists with a clear geometric framework to design and synthesize molecules based on the highly directional interactions between atoms. The most deeply rooted theory of valency is Valence Shell Electron Pair Repulsion (VSEPR) theory, which predicts over 15 geometric models based on the number and symmetry of bonding and nonbonding electron pairs around a central atom.[63] VSEPR theory is an extremely useful tool for understanding and designing chemical compounds composed of atoms, and it also provides a generalizable approach to rationalizing the interactions between any building blocks that interact based on their specific geometries. As a result, colloid chemists have seized upon VSEPR, leveraging these principles to explain colloidal assembly and, ultimately design, functional colloidal clusters and superlattices.[64,65] In short, colloid chemists use valency to categorize colloidal building blocks and geometrically bridge ligand-functionalized nanoparticles and assembled superlattices composed of them.

Before the salient similarities and differences between valency in atomic and colloidal systems are highlighted, two related concepts in colloidal organization must be delineated: *oligomerization* and *crystallization*. Colloidal building blocks may *oligomerize* into discrete "colloidal molecules." In other words, valency can lead to the formation of arbitrary chains or specific clusters in a manner conceptually akin to how atoms undergo chemical reactions to define molecular structures in synthetic chemistry.[66] In this regime, valency is employed to break symmetry and is therefore used to achieve structural

https://doi.org/10.1021/acs.chemrev.4c00299
Chem. Rev. 2024, 124, 11063−11107

control. However, a structure that is stable as a discrete oligomer may not propagate to fill 2- or 3D space; that is, crystallize. In *crystallization* processes, tessellation in 2- or 3D space is emphasized, and valency is used to understand and ultimately regulate crystallization by inducing well-controlled local environments. This type of chemistry is conceptually closer to that seen with metal- (MOFs), covalent- (COFs), and hydrogen-bonded-organic frameworks (HOFs).[67−69] In summary, valency plays a role in both *oligomerization* and *crystallization* of colloidal building blocks, albeit in different ways.

2.2.1. Number of Bonds. In order to understand the valency of specific building blocks, one must consider the number of bonds that can be formed. It is important to clarify that a single "bond" in a colloidal system may be composed of molecular interactions involving tens or even hundreds of individual ligand molecules. A discrete number of distinct colloidal bonds is typically defined from a collection of a much larger, unknown number of surface-bound ligands due to shape-induced symmetry breaking or the native geometry of a colloidal cluster. For example, a ligand-functionalized cube can participate in six octahedrally arranged bonding events, while a ligand-functionalized tetrameric colloidal cluster can be viewed as a building block with four tetrahedrally arranged preferred bonding elements, provided that the ligand shell is short and rigid enough to maintain and project the shape anisotropy of the underlying particle (Figure 1).[25] New synthetic strategies

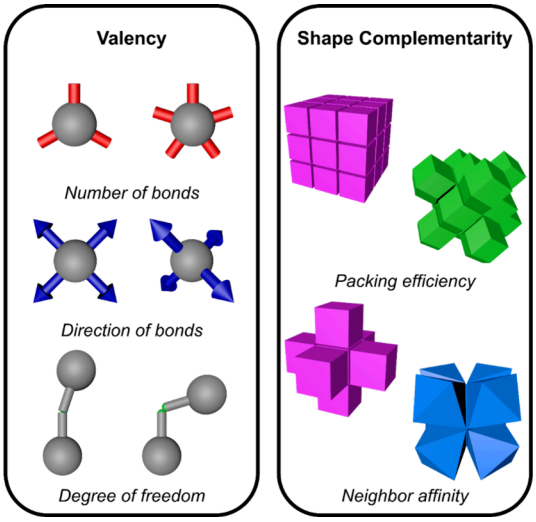

Figure 1. Schematics illustrating the main types of anisotropy in colloidal systems including valency and shape complementarity.

are already enabling systems with valency and coordination geometries not accessible with atoms and traditional VSEPR theory, including decavalent (and higher) colloidal clusters. Such valences are beyond the scope of traditional chemistry and are challenging to realize even in reticular systems, such as those involving MOFs and COFs.[67−69] Indeed, since examples of highly valent coordination environments in molecular coordination chemistry, such as dodecahedral or icosahedral arrangements, are lacking, it is important to explore colloidal systems with high valency particles if they can be prepared (e.g., dodecahedral nanoparticles or icosahedral colloidal clusters).

2.2.2. Directionality of Bonds. Bond directionality is another important component of valency in both atomic and colloidal systems. Tetrahedral and square-planar metal complexes are both four-coordinate, yet they each have distinct geometries; likewise, a cluster of six spherical particles can be positioned in an octahedral or tetrahedral arrangement (Figure 1). In fact, early studies have shown that the bonding angle of dimeric and trimeric colloidal clusters can be controlled in a relatively arbitrary fashion.[66] Different geometric arrangements of identical numbers of bonds are also manifested at the level of individual ligand-functionalized polyhedral nanocrystals. For example, rhombic dodecahedral (RD) and Platonic dodecahedral (PD) nanoparticles have distinct geometries, yet both of them have 12 preferred bonding directions: an RD nanoparticle creates a local face-centered cubic (*fcc*) coordination environment, whereas a PD nanoparticle creates a local *icosahedral* coordination environment.[70] The direction of the bonds accessible to colloidal building blocks, like the bond number, also surpasses what is offered by atomic examples: a Catalan trigonal bipyramidal nanocrystal, for example, has six highly symmetrical, defined bonding directions, yet this geometry is not found in traditional coordination chemistry.[70] The crystallization of particles with this unusual valency resulted in a series of complex clathrate-like structures.[71]

2.2.3. Degree of Conformational Freedom. The highly directional interactions of molecular coordination complexes are defined by molecular orbitals and their hybridization interactions, whereas the bonding interactions in colloidal assemblies enjoy additional degrees of conformational freedom (Figure 1). Illustrative of this example, a bivalent particle system, where spherical building blocks have two distinct collections of bonding entities positioned 180° apart, form Kagome lattices.[72] A rigid model of valency would predict that these particles should form extended 1D chains; however, they instead organize into an open 2D lattice when assembled on a surface (discussed in detail later; see Figure 5c). In the lattice, each bivalent building block connects with four other building blocks, two on each "patch." The Kagome lattice forms because: first, spherical patches tend to form triple clusters as their stable local packing; and second, the middle, nonbonding portion of the colloids has a repulsive force that prevents the collapse of the open lattice. Even when the number and directionality of the bonding interactions are both determined, the degree of conformational freedom can still affect the organizational outcome.[73] Therefore, the connections between colloidal building blocks with defined valencies should be considered flexible joints, which ultimately give colloids sufficient freedom to arrange into their most stable forms rather than rigid bonds. Although this additional freedom complicates efforts to program the assembly outcomes of nanoparticles, it provides another handle to use in the design of more sophisticated architectures.

2.3. Shape Complementarity

Analogies between bonding in atomic systems and the local ligand interactions of colloidal systems have permitted invaluable insights and furthered our understanding of complex colloidal systems.[42,74] Discussions of bonding and valency bridge synthetic chemistry and colloidal assembly, and continue to advance the pursuit of designer, programmable matter, a holy grail in materials science. However, in many ways, colloidal building blocks have additional design parameters that cannot be fully captured by using such analogies. For instance, polyhedral atoms do not exist, yet

https://doi.org/10.1021/acs.chemrev.4c00299
Chem. Rev. 2024, 124, 11063−11107

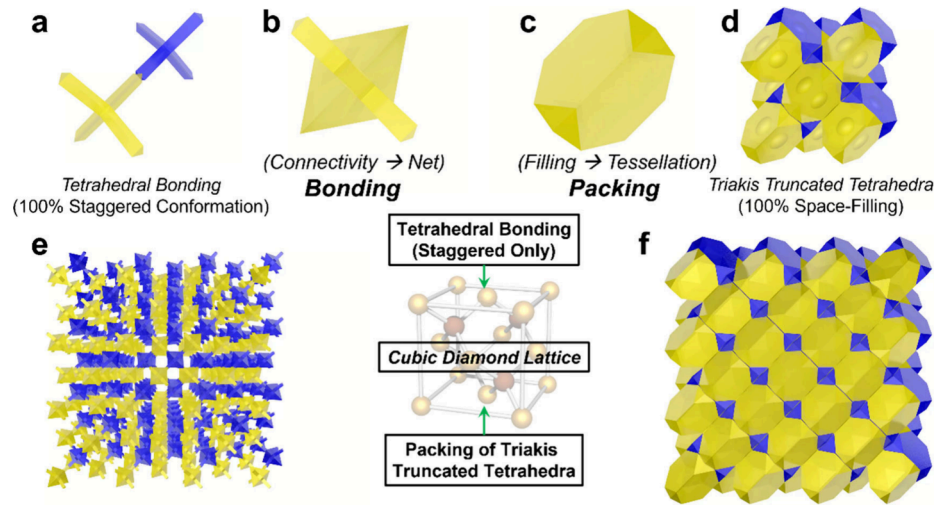

Figure 2. A construction of the cubic diamond crystal structure from the standpoints of valency and shape complementarity. Systems based on atoms and reticular chemistry are better viewed from a "directional linking" standpoint, while those based on colloids and their particle geometries are better viewed from a "bonding and packing" perspective.

polyhedral colloids of multiple shapes can be synthesized in high yield and low dispersity.[20] This example is a reminder that while analogies to traditional chemistry are conceptually useful, new mesoscale physical processes are occurring in colloidal systems that are very different from those seen in atomic systems (Figure 2). Topologies and networks seen in organic and inorganic crystals are sources of inspiration, but they cannot capture the full scope of possibilities available in the context of colloidal systems. With this in mind, shape complementarity is discussed from two viewpoints: space filling, which is more relevant in type I assemblies; and neighbor affinity, which is more relevant in type II assemblies. The discussion primarily focuses on the organization of polyhedral building blocks (Figure 1).

2.3.1. Space-Tiling of Complementary Shapes. From a space-filling point-of-view, shape complementarity drives a system to minimize the total volume of the final structures or optimize the packing of the building blocks at a high density. Many theoretical and computational works have offered valuable insights into the most stable structures into which hard polyhedral particles of various shapes can pack.[75−79] The simplest cases involve space-filling shapes, such as cubes, truncated octahedra, RD, and hexagonal prisms, which pack seamlessly into simple cubic (*sc*), body-centered cubic (*bcc*), *fcc*, and simple hexagonal (*sh*) symmetries, respectively. In general, cases that involve single-component, non-space-filling, hard polyhedra have mainly been studied through numerical approaches, providing experimentalists with a large library of promising building blocks to consider.[77,80]

It is not routine to experimentally realize sophisticated structures that have been identified by simulations, even if the nanoparticle building blocks can be synthesized with perfect monodispersities and ideal shapes. To date, most simulations consider only geometry-induced entropy, where particles generally experience strong repulsion upon contact and interact solely through excluded volumes, thereby maximizing space-filling (type I assembly; Section 2.1.1). Due to limitations in computational capabilities, it is currently impractical to account for all enthalpic and entropic contributions in a generic experimental system. As a result, the results of the simulations and the associated experiments typically deviate significantly when too many ligand interactions are computationally approximated. Furthermore, in practice, the surface-functionalized ligand shell is an important contributor to the overall particle shape and its interactions. Polyhedral nanoparticles functionalized with ligands that are long, relative to the nanoparticle dimensions, achieve assemblies different from those that would be predicted based on their geometric shape: nanocubes pack into rhombohedral, *bcc*, or even body-centered tetragonal (*bct*) lattices, when their surface ligands are sufficiently long and deformable.[24,25,81] In summary, although simulation can guide the determination of the optimal packing of particles of any arbitrary shape, experimental studies of shape-packing in complex systems provide important insights into the organization of building blocks with real, nuanced interactions for which a space-filling model may be overly simplistic.

2.3.2. Neighbor Affinity between Complementary Shapes. From a space-filling perspective, shape complementarity is a means to optimize packing density, while a neighbor affinity point-of-view considers shape complementarity as a route to maximize the contact area between two surfaces (Figure 1).[82] It is mainly valid to maximize the contact area in enthalpy-driven assemblies through the collective binding of multiple weak chemical bonds on particles with large facets (type II assembly; Section 2.1.2). Such interactions lead to facet registration and the formation of geometrically specific local clusters. These local clusters can act as predetermined nucleation sites for the growth of other particles. If, from a geometric perspective, these clusters are linked to others formed by local packing, the overall structure will propagate into an extended, ordered colloidal crystal or quasicrystal. Despite the relative infancy of neighbor affinity as a guiding principle for colloidal organization, several sophisticated crystalline and quasicrystalline structures have already been designed or rationalized using a neighbor affinity approach (Sections 3.4.4 and 4). Recent theoretical efforts have also suggested that this stepwise construction methodology can be used to generate novel structures using predefined local clusters as seeds.[76]

Despite the visual similarity between the dense packing of polyhedral nanocrystals and the representation of inorganic

https://doi.org/10.1021/acs.chemrev.4c00299
Chem. Rev. 2024, 124, 11063−11107

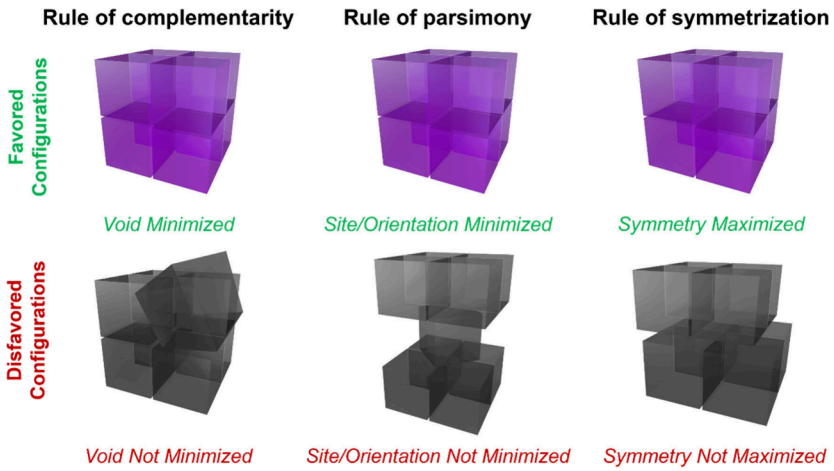

Figure 3. Tendencies in colloidal crystallization are summarized as three rules. In each case, the favored *sc* structure is shown in purple (top), while a less-favored structure disobeying each rule is shown in black (bottom). The rule of complementarity favors structures with high packing efficiencies. The rule of parsimony favors small repeating units (unit cells). The rule of symmetrization favors unit cells with a high rotational symmetry.

crystals as coordination polyhedra, the key concept—how the polyhedra pack—is very different in these two systems. Pauling's third rule for ionic crystals states that "the presence of shared edges and especially of shared faces [between anion polyhedra] in a coordinated structure *decreases* its stability."[83,84] Hence, neighboring anion polyhedra, such as tetrahedra and octahedra, tend to share only their corners and edges, not their faces. In stark contrast, the enthalpy-driven dense packing of polyhedral nanoparticles favors facet registration; that is, neighboring colloidal polyhedra interact via face-to-face contact, a packing motif that is rarely seen in inorganic crystals. This distinction has important consequences for designing new colloidal superlattices, whereby the *dual shapes* of anion polyhedra in an inorganic crystal must be considered to design new ones (Sections 4.1 and 4.2). In short, the ability to predict or explain complex structures formed by the enthalpy-driven crystallization of polyhedral nanocrystals offers the opportunity to construct a library of new structures from the bottom-up, a significant portion of which is likely not found in nature.

2.3.3. Packing of Multiple, Cooperatively Complementary Shapes. Although some shapes can pack alone into perfectly space-filling arrangements, as noted in Section 2.3.1, many more polyhedral shapes can fill space when packed with other polyhedra. Examples of such space-filling pairs include: tetrahedra and octahedra; octahedra and truncated cubes; and truncated tetrahedra and tetrahedra. Researchers have performed numerical simulations[66] to explore the concept of cooperative shape complementarity between multiple constituents, in large part due to the increased complexity inherent in systems with multiple different interaction geometries. One particularly interesting and fundamental question raised by these studies is: when do complementary shapes coassemble rather than phase-separate? Furthermore, do multicomponent systems assemble into different ordered lattices at different stoichiometries? Experimental efforts have yet to scratch the surface in exploring the massive number of potential experimental parameters related to these questions, but if answers to them were found, then the landscape of colloidal crystallization would be transformed.

2.4. A Colloidal Equivalent to Pauling's Rules

At the start of Section 2, it was noted that the outcome of colloidal organization can be programmed, in principle, by defining the local features of the individual particles. However, to control the organizational fate of any colloidal system, one must consider all these features—entropy, enthalpy, valency, and shape complementarity—a nontrivial pursuit for all but the simplest systems. Fortunately, by considering empirical observations,[13,41] guiding principles can be delineated that describe assembly in many colloidal systems, accounting for the specific local factors discussed earlier. Just as Pauling's rules provide a framework to rationalize and predict ionic crystal structure using atoms, guiding principles for colloidal crystallization can be formalized: 1) the rule of complementarity; 2) the rule of parsimony; and 3) the rule of symmetrization (Figure 3).[80,83] Like Pauling's rules, these principles may cooperate with or, at times, contradict each other, and therefore their contributions to an assembly outcome should always be discussed in a case-by-case manner.

2.4.1. Rule of Complementarity. *Colloidal arrangements where nanoparticles exhibit stronger local shape complementarity (minimum physical void space) and facet registration (maximum favorable chemical bonding) are favored. Such arrangements typically lead to smaller total volumes and greater number of interparticle facet contacts.*

This rule is based on creating favorable entropic (minimization of voids) and enthalpic (maximization of chemical bonds) situations. In space-filling configurations (constituents fill the space with 100% volume efficiency), these two factors are fulfilled simultaneously; in nonspace-filling configurations, these two factors often compete. The structures with the most favorable enthalpic arrangements, which maximize chemical bonding, are not also those with the most favorable entropic arrangement, which minimizes voids to create the highest degree of space-filling. This latter system allows one to deliberately engineer structures with large voids or open channels inside, which can then be used for the absorption of nanoscale guest species.[71]

2.4.2. Rule of Parsimony. *Colloidal arrangements are favored that minimize the number of distinct lattice sites and*

https://doi.org/10.1021/acs.chemrev.4c00299
Chem. Rev. 2024, 124, 11063−11107

nanoparticle orientations in a unit cell; thus, the smallest unit cell with the least number of distinct orientations is preferred.

This rule arises from entropic factors, where higher translational symmetry is preferred. Notably, systems with high translational symmetry also typically have a higher number of repeating units in a certain direction and therefore smaller unit cells. Alternatively, for a given lattice symmetry, as the number of distinct lattice sites increases, the size of the unit cell must increase. As a result, the system entropy will tend to be higher (preferred) if the constituent building blocks are in a configuration in which the translational symmetry is maximized.

In the context of the colloidal organization of anisotropic particles, the orientation of a particle is important in defining distinct lattice sites. [Plastic crystals, where the orientational order and therefore the anisotropy of the building blocks are lost, are a notable exception.] This unique structural feature is not relevant to atoms or isotropic particle building blocks. Many studies often consider the anisotropic building blocks in colloidal crystals simply as specially arranged points in space; however, such a simplification only frustrates efforts to understand structure formation. Indeed, particle orientation is just as important as particle position in the discussion of particle−particle interactions.

2.4.3. Rule of Symmetrization. *Colloidal arrangements that maximize the rotational symmetry of their unit cell are favored.*

This rule also arises from entropic factors, but the unit cell scale, rather than individual particle scale, is considered. It is entropically favorable for the system to maximize translational and rotational symmetry, as reflected by the number of rotational axes of a unit cell. For example, if one compares the symmetry of a cubic $(\frac{4}{m}\bar{3}\frac{2}{m})$ or hexagonal $(\frac{6}{m}\frac{2}{m}\frac{2}{m})$ cell to that of a monoclinic $(\frac{2}{m})$ or triclinic $(\bar{1})$ cell, one discovers that the former two have many more rotational axes and therefore will be preferred even if the latter two have an equal chance of forming. This tendency can be rationalized by considering the unit cell as an arbitrary parallelepiped: a more symmetrical parallelepiped can more easily pack into a periodic array and therefore is more likely to be the thermodynamically favored product. This rule explains the large portion of reported colloidal crystals that adopt cubic or hexagonal symmetries and emphasizes the overall challenge of reducing crystal symmetry (to obtain low-symmetry structures).

3. ORGANIZATION OF BUILDING BLOCKS OVER MULTIPLE DIMENSIONS

The nature of the particle−particle interactions that dictate colloidal organization differs across systems and length scales. However, shape factors generally play a role in assembly across the board (Figure 4). Therefore, to approach a universal understanding of the crystallization behaviors of anisotropic building blocks, representative examples of how anisotropy affects organization processes are surveyed and analyzed here. We organize the examples by the dimensionalities of their building blocks discussed within them, from 0D (patchy particles) through 1D (rod-like particles) and 2D (platelike particles) to 3D (polyhedral particles). Based on this analysis, geometric structure−unit relationships are developed, and each case is rationalized based on local particle−particle interactions, valencies, and shape complementarities.

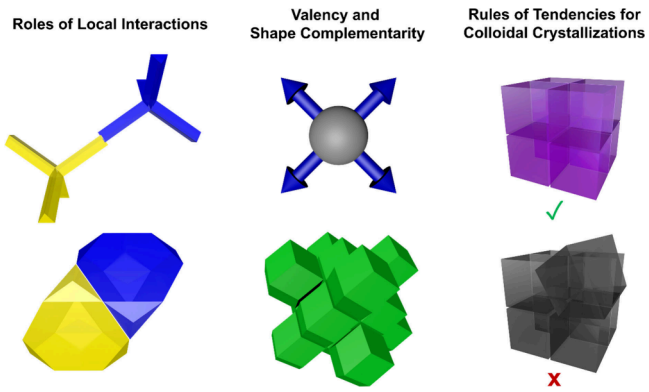

Figure 4. Graphical summary of design principles for colloidal organization.

3.1. Zero-Dimensional (0D) Building Blocks

Here, anisotropic 0D building blocks are defined as particles with an isotropic shape that engage in interactions that are anisotropic in nature. Such building blocks are usually based on spherical centers asymmetrically encoded with chemical functionalities that can afford attractive or repulsive interactions, that is, colloidal valency. The ability to design and assemble arbitrary, complex structures from 0D building blocks has been limited by the lack of specificity and directionality of their interactions, though recent progress in this area has been made.[85,86]

3.1.1. Organization of Spherical Particles with Interacting Patches. The symmetry of the isotropic particle surface must be broken to define valency with spherical 0D particles. One popular way to break symmetry is to synthesize "patchy" particles, complex colloidal spheres with anisotropically patterned surfaces. The patches on the surface of these particles may be based on surface chemistry (enthalpic patches), particle shape (entropic patches), or both.[87] By controlling the position, number, and physicochemical properties of the patches, particles can be assembled into ordered structures in ways that are reminiscent of how atomic bonding is leveraged to create molecules. Patchy particles can access a greatly enhanced range of assembled structures compared to isotropic 0D colloidal building blocks without patches.

The enthalpic interactions of patchy particles have been designed based on depletion forces, hydrophobic/solvophobic interactions, covalent or supramolecular coupling, DNA hybridization, and others modalities.[88] Hydrophobic patches can provide directionality to bond 0D building blocks but cannot be used to program interactions between specific patches on different spheres. DNA-coated patchy particles, however, provide a route to more chemically specific interactions between patches. Single-stranded "sticky" regions of DNA mediate interparticle binding through hybridization with complementary DNA strands attached to patches on other particles. The locations of the patches on the particles' surfaces provide directionality, whereas the sequence-dependent binding of DNA imparts specificity. Consequently, diverse artificial molecules can be synthesized by combining mixtures of particles that have matched valences and complementary DNA strands. In one example reported by Pine and coworkers, colloidal particles with chemically distinct surface patches were used to imitate hybrid atomic orbitals, including sp, sp^2, sp^3, sp^3d, sp^3d^2, and sp^3d^3 (Figure 5a).[89] Combining these particles yielded colloidal molecules (CMs) with AX to

https://doi.org/10.1021/acs.chemrev.4c00299
Chem. Rev. 2024, 124, 11063−11107

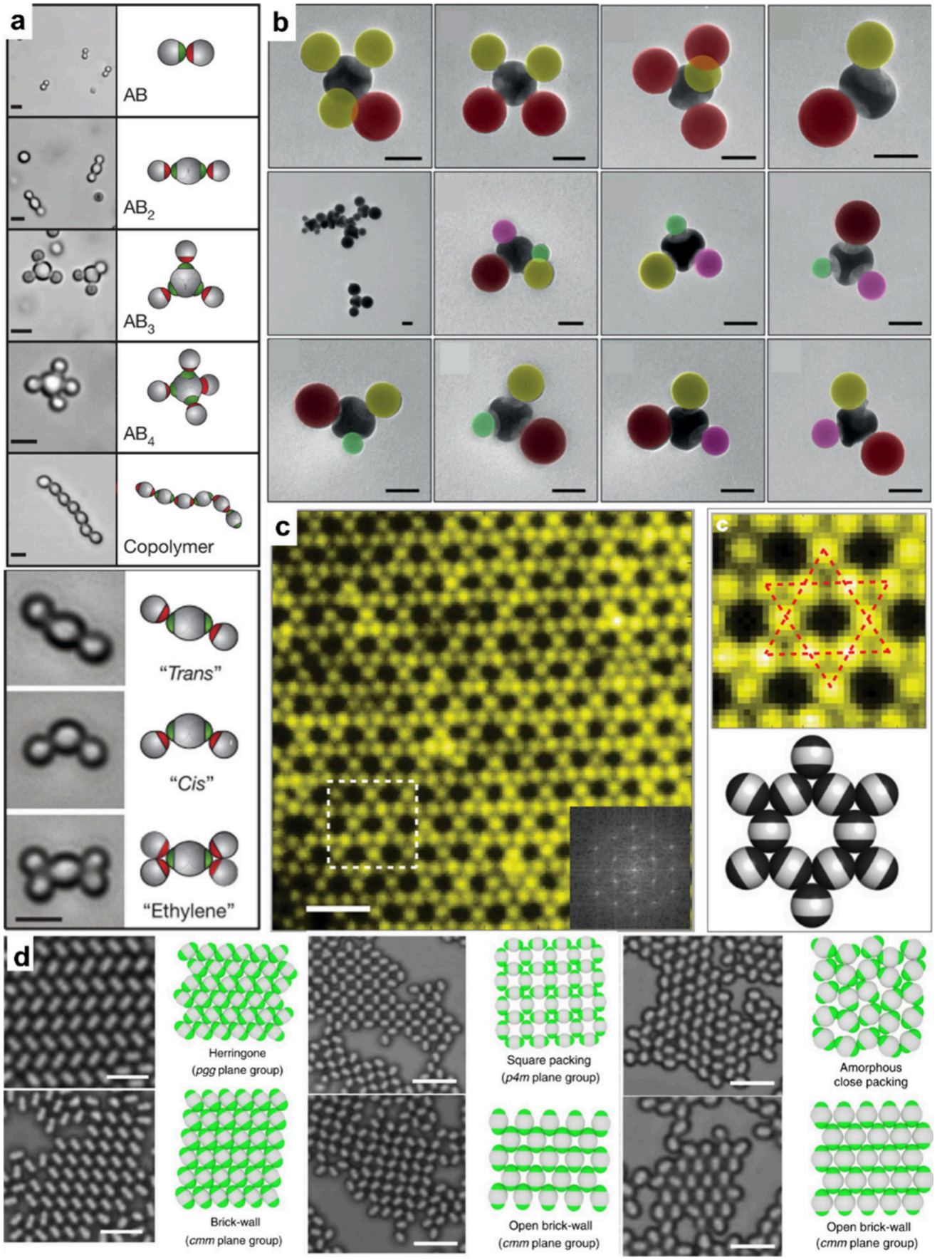

Figure 5. Organization of colloidal patchy particles into colloidal molecules (CMs) and extended lattices. (a) CMs from specific directional bonding between colloidal patchy particles observed with optical microscopes. Scale bars: 2 μm. Figures adapted with permission from ref 103.

https://doi.org/10.1021/acs.chemrev.4c00299
Chem. Rev. 2024, 124, 11063−11107

Figure 5. continued

Copyright 2012 Springer Nature. (b) False-colored TEM images of CMs obtained by mixing valence-endowed colloidal atoms with nanospheres. Scale bars: 100 nm. Figures adapted with permission from ref 94. Copyright 2018 Wiley-VCH. (c) Colloidal Kagome lattice from triblock Janus spheres with hydrophobic poles (black, with an opening angle of 65°) and charged regions at the equator (white). Scale bar: 4 μm. Figures adapted with permission from ref 72. Copyright 2011 Springer Nature. (d) Polymorphic 2D assemblies of triblock particles of polystyrene (PS), 3-(trimethoxysilyl)propyl methacrylate (TPM), and PS, induced by the surfactant and depletant, pluronic F127. Scale bars: 5 μm. Figures adapted with permission from ref 104. Copyright 2020 Springer Nature.

AX_4 stoichiometries, as well as copolymeric arrangements. By tuning of the patch-to-particle size ratio, more complex molecular motifs were observed, such as *cis* and *trans* configurations, which mimic the arrangements of atoms involved in a double bond. Stepwise assembly was demonstrated with particles bearing two types of DNA strands (i.e., one type on the patches and another type on the shell) by taking advantage of the 10 °C difference between the melting temperatures of patch and shell DNA duplexes.[90]

In the previous example, the particles are first synthesized and then site-specifically modified with DNA to prepare DNA-coated patchy particles. Methods, including this one, mostly result in particles with round patches, which bring about high degrees of conformational freedom (Section 2.2.3). To realize better structural control, Pine and co-workers recently reversed the conventional paradigm by introducing polymerizable liquid droplets with DNA coatings to form ordered superlattices.[91] Subsequent photopolymerization in the bulk superlattices converted the droplets into patchy particles with localized DNA facets. The facet size and DNA distribution were dictated by the balance between the elastic deformation energies of the droplets and the DNA binding energies. These faceted DNA-functionalized patchy particles were subsequently assembled into chain-like hybrid structures and CMs with AX_8 stoichiometry.

Shape complementarity has also been used as a recognition mechanism for directing the assembly of patchy particles. Pine and co-workers demonstrated that the assembly of patchy particles can be reduced to a simple geometrical problem based on a "lock-and-key" principle.[92] In this system, colloidal spheres were employed as "keys" and monodisperse colloidal particles with a spherical cavity acted as "locks," and these two particles bound spontaneously and reversibly via depletion interactions. Because irreversible chemical bonding was not involved, the formation of flexible dimeric, trimeric, and tetrameric CMs as well as more complex colloidal polymers was permitted. Similarly, Weck, Pine, and co-workers used dimpled silica microparticles with a well-defined number of cavities as locks and appropriately sized spheres as keys.[93] CMs with AX to AX_5 stoichiometries were prepared from dimpled particles with spherical, linear, triangular, tetrahedral, and pentagonal dipyramidal symmetries by changing the valency of the lock. More recently, Ravaine and co-workers demonstrated that different CMs could be obtained from di-, tri-, and tetravalent particles through the covalent coupling of aminated dimpled particles and complementary carboxylated silica nanospheres (Figure 5b).[94] Additional diversity was achieved when multiple types of silica particles were simultaneously employed as keys; in particular, chiral CMs were created by assembling a sp^3-like dimpled particle with four silica spheres of different sizes.

In addition to discrete CMs, extended colloidal superlattices have also been assembled by using patchy particles. In most cases, the formation of extended structures has relied on understanding and balancing the effects of multiple interactions. The Kagome structure reported by Granick and co-workers (introduced in Section 2.2.3) was obtained with triblock Janus particles (Figure 5c), micron-sized spheres that could engage in repulsive electrostatic interactions (in the middle) and attractive hydrophobic interactions (at their poles). To create these open Kagome structures, the interactions between the building blocks had to be sufficiently strong enough to overcome translational entropy while still allowing for a relatively high rotational and vibrational entropy.

Bharti and co-workers exploited magnetic field-induced interactions between metallodielectric patchy particles and isotropic, nonmagnetic "satellite" particles to assemble superparticles.[95] Specifically, they showed the assembly of 3D, multicomponent supraparticles that dynamically reconfigure in response to changes in the external field strength as a function of their connectivity, composition, and distribution. Elwenspoek and co-workers investigated the role of dipolar interactions in the assembly of millimeter-sized permanent magnets embedded in polymer shells of varying shapes.[96] They showed that 3D crystals could be assembled from objects in the micrometer range provided that the energies of the dipoles in the parallel and antiparallel states were equal (achieved by balancing dipolar and steric interactions). In a recent example, Weck and co-workers used regioselective depletion interactions to engineer the directional bonding and subsequent assembly of nonspherical colloidal hybrid microparticles into many different structures, including 1D cross-chains, ladder-like chains, tilted ladder-like chains, and 2D structures (Figure 5d).[97] Polymorphic 2D structures were observed, where particles of a specific aspect ratio simultaneously formed crystals with different symmetries.

The computational investigation of patchy particles has revealed complex assemblies that have not yet been realized experimentally. Glotzer and co-workers simulated a system of hard particles with attractive patches and showed that they could assemble into a diamond structure from an initially disordered state.[98] Subsequently, these researchers showed how specific crystalline assemblies, including *sc*, *bcc*, diamond, and dodecagonal quasicrystal, could be targeted by introducing geometric features to the entropically patchy particles via shape operations.[99] Moreover, Doye and co-workers developed a systematic approach to rationally design patchy particles to form desired crystal structures.[100] Their method ensures that a given target crystal structure represents the free-energy global minimum below some threshold temperature without nearby competing structures. Their most complex example was a clathrate with 46 particles in its primitive unit cell. More recently, Chakrabarti and co-workers simulated the hierarchical assembly of patchy particles into colloidal crystals via CMs by leveraging assembly pathways.[101] They also calculated the photonic band structures of the cubic and hexagonal polymorphs, which both support a complete photonic band gap.

https://doi.org/10.1021/acs.chemrev.4c00299
Chem. Rev. 2024, 124, 11063−11107

Together these experimental and computational examples highlight that patchy 0D particles can be used to define valency in periodic colloidal assemblies. An interesting next step would be to delineate design rules for how patchy particles can be utilized to form aperiodic target structures such as quasicrystals. Although patchy particles that can be used to form dodecagonal and metastable octagonal and decagonal quasicrystals in 2D have been identified, it is considerably more difficult to employ them to form 3D aperiodic structures, such as icosahedral quasicrystals.[102] Quasicrystal synthesis poses a particular challenge because elements of both order and disorder play a role, and quasicrystals are stabilized by the resulting entropy; consequently, a single global target structure does not exist. Researchers may need to modify existing simulations to permit some degree of promiscuity in the target structure.

3.1.2. Organization of Spherical Particles with DNA Origami. DNA origami has been used to introduce specific directional interactions into 0D building blocks to direct assembly. Indeed, the high degree of programmability and addressability of DNA origami has enabled the assembly of a wide variety of well-ordered colloidal architectures in 1-, 2-, and 3D. This is a field of intense research that was recently reviewed by Tian, Gang, and co-workers.[105] Consequently, only a few archetypal examples of the DNA origami-mediated organization of spherical colloidal particles in different dimensions are described briefly here.

Nanoparticles can be organized in 1- and 2D by DNA origami, where the nanoparticles are often functionalized onto the surface of the DNA structure. Yan, Chaput, and co-workers reported that Au nanoparticles could be synthesized *in situ* on DNA nanotubes using surface-immobilized peptides.[106] The arrangement of the peptides directed the *in situ* nucleation and growth of nanoparticles from soluble chemical precursors and templated their positions in a 1D array. Two-dimensional organizations of nanoparticles, including periodic arrays, simple shapes, and complex mesoarchitectures, were achieved by integrating nanoparticles with planar DNA origami structures. In one recent example, a high degree of order was achieved using tetravalent DNA-functionalized nanoparticles, which were bound by a highly ordered planar DNA origami structure with well-defined nanoparticle recognition sites.[107]

To gain directional control over spherical nanoparticle organization in 3D, Gang and co-workers designed different DNA origami polyhedral frames, including those with octahedron, cube, elongated square bipyramid, prism, and triangular bipyramid geometries, to encapsulate nanoparticle cargos and serve as programmable topological linkers between particles.[108] Varying the geometry of the DNA origami frame allowed a single type of spherical nanoparticle to assemble into a variety of lattice symmetries, including *fcc*, *bct*, *sc*, and hexagonal (Figure 6e–h). Importantly, Au particles could be encapsulated inside tetrahedral DNA frames to assemble superlattices from the cubic diamond family, the preparation of which had been a considerable challenge in the field of colloidal assembly (Figure 6a–d).[109] In addition, recent advances in DNA origami technology have allowed hybrid DNA origami–colloid structures in the micron-size regime to be prepared (Figure 6i).[110] Micron-sized chiral CMs were synthesized by mixing DNA-coated spheres with a central particle coated with an elastic DNA origami belt, which fixed the relative positions of the sticky patches on its surface and allowed control over the angles and positions of the constituent particles.

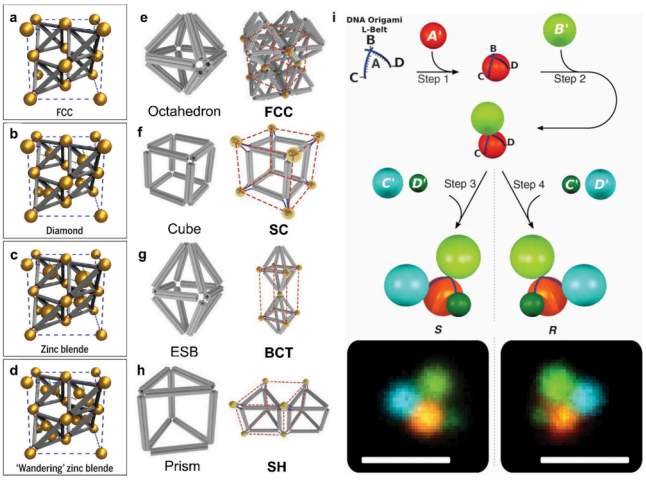

Figure 6. Organization of colloidal particles with DNA origami. (a–d) Diamond family of NP superlattices from tetrahedral DNA origami frameworks. Symmetries of Au NPs can be programmed into *fcc* (a), *diamond* (b), *zinc blende* (c), and *"wandering" zinc blende* (d). Figures adapted with permission from ref 111. Copyright 2016 American Association for the Advancement of Science. (e–h) Different shapes of DNA origami frames and the corresponding symmetries (with respect to the Au NPs) of the observed lattices when origami frames and Au NPs were cocrystallized. Octahedral frames arrange Au NPs into *fcc* symmetry (e), cubic frames arrange Au NPs into *sc* symmetry (f), elongated square bipyramidal (ESB) frames arrange Au NPs into *bct* symmetry (g), and triangular prism frames arrange Au NPs into *sh* symmetry (h). Figures adapted with permission from ref 112. Copyright 2016 Springer Nature. (i) Main steps in the synthesis of the DNA origami-functionalized colloidal clusters with controlled positions, dihedral angles, and chirality. Scale bars: 2 μm. Figures adapted with permission from ref 110. Copyright 2016 The American Association for the Advancement of Science.

3.2. One-Dimensional (1D) Building Blocks

The crystal engineering of 1D building blocks, like rod-shaped nanoparticles, is interesting due to the unique shapes of the building blocks and their associated near-IR absorbances and enhanced surface plasmon resonances (SPR).[113] These elongated shapes tend to pack on their sides, resulting in a series of planar structures. Because this tendency for planar organization is so strong, the assembly of 1D building blocks is synthetically robust and it is unlikely that more complex superstructures will emerge. Therefore, 1D building blocks are particularly attractive for generating 2D colloidal superstructures (that is, monolayers or few-layer structures), which is exciting because their 2D atomic counterparts (for example, graphene and boron nitride) are leading to the discovery of unprecedented chemical and physical phenomena.

3.2.1. Assembly via Side-to-Side Interactions. Rod-like 1D building blocks have a much larger surface area on their sides than their tips, so strong side-to-side interactions between particles are observed. This fact drives the vast majority of uniformly functionalized nanorods to assemble into simple hexagonal slabs regardless of whether their assembly is governed more by entropy (type I assembly) or enthalpy (type II). Side-to-side packing is the most volume-efficient particle arrangement and provides the largest interparticle contact area. For 1D building blocks assembled through type I and II processes, the number of hexagonal layers achieved

https://doi.org/10.1021/acs.chemrev.4c00299
Chem. Rev. 2024, 124, 11063–11107

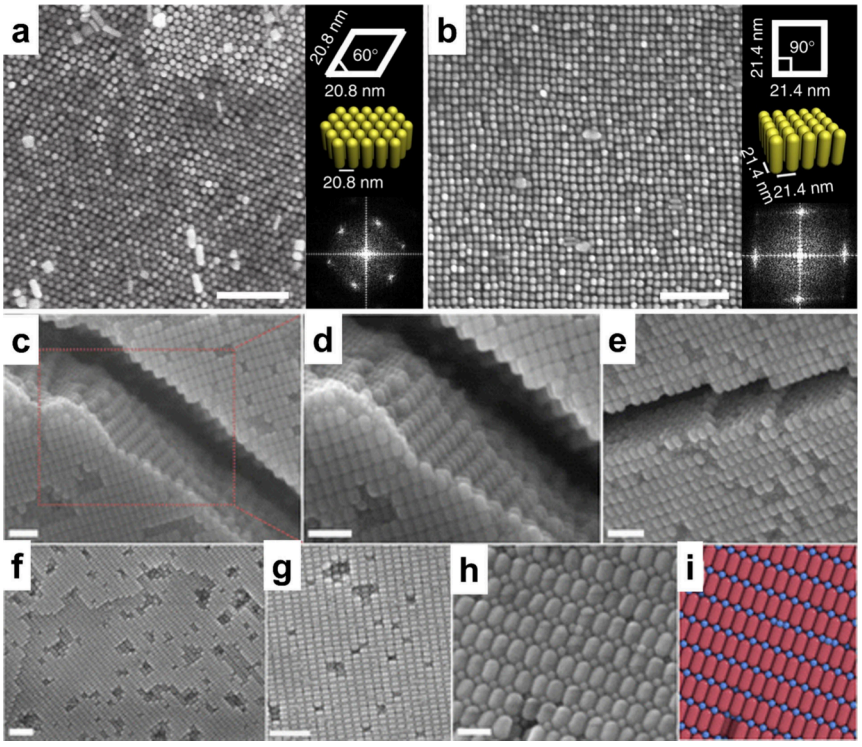

Figure 7. Side-to-side interactions in the organization of 1D building blocks. (a, b) Rhodamine 6G-mediated assembly of Au nanorods into hexagonal (a) and tetragonal (b) lattices. Scale bars: 200 nm. Figures adapted with permission from ref 115. Copyright 2017 Springer Nature. (c–h) SEM images of an AlB_2 binary superlattice assembled from $NaYF_4$ nanorods and Fe_3O_4 nanospheres close to a cracked region. Scale bars: (c–e) 100 nm, (f–g) 200 nm, (h) 50 nm. (i) Model of the binary superlattice. Figures adapted with permission from ref 118. Copyright 2013 American Chemical Society.

differs. Entropy-driven assembly favors volume exclusion over interparticle contact area, and therefore many layers are generated. These layers typically arrange in an ABCABC packing motif that resembles the *fcc* packing of spheres. In contrast, enthalpy-driven assembly maximizes interparticle contact area, and therefore, the number of layers is highly dependent on the aspect ratio (AR) of the rods. Longer rods have relatively less surface area on their tips, and interlayer interactions are not favored. Therefore, rods with higher ARs assemble into monolayers or multilayer structures with fewer layers than rods with lower ARs.

The hexagonal packing observed with many nanorod building blocks is dictated by the close packing of their essentially circular cross sections. However, as-synthesized nanorods are often not perfectly cylindrical. For example, the cross sections of noble metal nanorods generally exhibit four- or 5-fold symmetry, depending on whether they are single-crystalline or penta-twinned, respectively.[114] It is noteworthy that neither of these symmetries is hexagonal. Consequently, nonhexagonal packings can be realized by exploiting this inherent geometry. In one example, when Rhodamine 6G (R6G) molecules were introduced into a system containing gold nanorods partially covered with cetyl trimethylammonium bromide (CTAB), a more thermally stable tetragonal superstructure was the main product upon slow-drying (Figure 7a, b).[115] As a result of the single crystalline nature of these nanorods (they are, in fact, truncated squares in the cross section), a tetragonal arrangement was favored as the enthalpy-driven assembly outcome. R6G molecules are small enough that the shape anisotropy of the single crystalline nanorods was maintained, so with the introduction of R6G molecules, the system engages in type II, as opposed to type I, assembly. A more pronounced version of this effect was demonstrated when Au nanorods were overgrown into elongated, tetragonal-shaped Au@Ag nanorods.[116] These core–shell "nanobars" assembled into tetragonal superlattices, while the original core-only structures (Au nanorods) arranged into hexagonal superlattices. Although attempts have been made to explore these concepts using pentagonal nanorods with various ARs, structures with local 5-fold symmetry and ordered orientations have yet to be seen.[117] Instead, hexagonal superstructures are observed with random in-plane particle orientations.

The tips of nanorods are geometrically similar to spheres and can act like them during coassembly with spherical particles. When nanorods and small spheres were assembled, a lamellar phase and an AlB_2 coassembled superstructure were observed, with the exact structural outcome depending on the size ratio between the rod tips and spheres (Figure 7c–i).[118] The structural driving force for both ordered phases is still the hexagonal arrangement of the densely packed nanorods. When the spheres are comparatively small, they cannot occupy space as fixed lattice sites between the hexagonal rod layers and a lamellar phase is observed. However, when the spheres are large enough, they can occupy the boride lattice sites in the AlB_2 structure. This arrangement stabilizes the coassembled structures akin to the AlB_2 structure coassembled by spheres of two different sizes.[15] Notably, this approach is currently the only method of generating large-scale, vertically aligned hexagonal lattices of nanorods.

The structural sophistication of DNA origami templates has been utilized to realize helical arrangements of nanorods, in addition to those of spherical particles (Section 3.1.2). Using a

https://doi.org/10.1021/acs.chemrev.4c00299
Chem. Rev. 2024, 124, 11063–11107

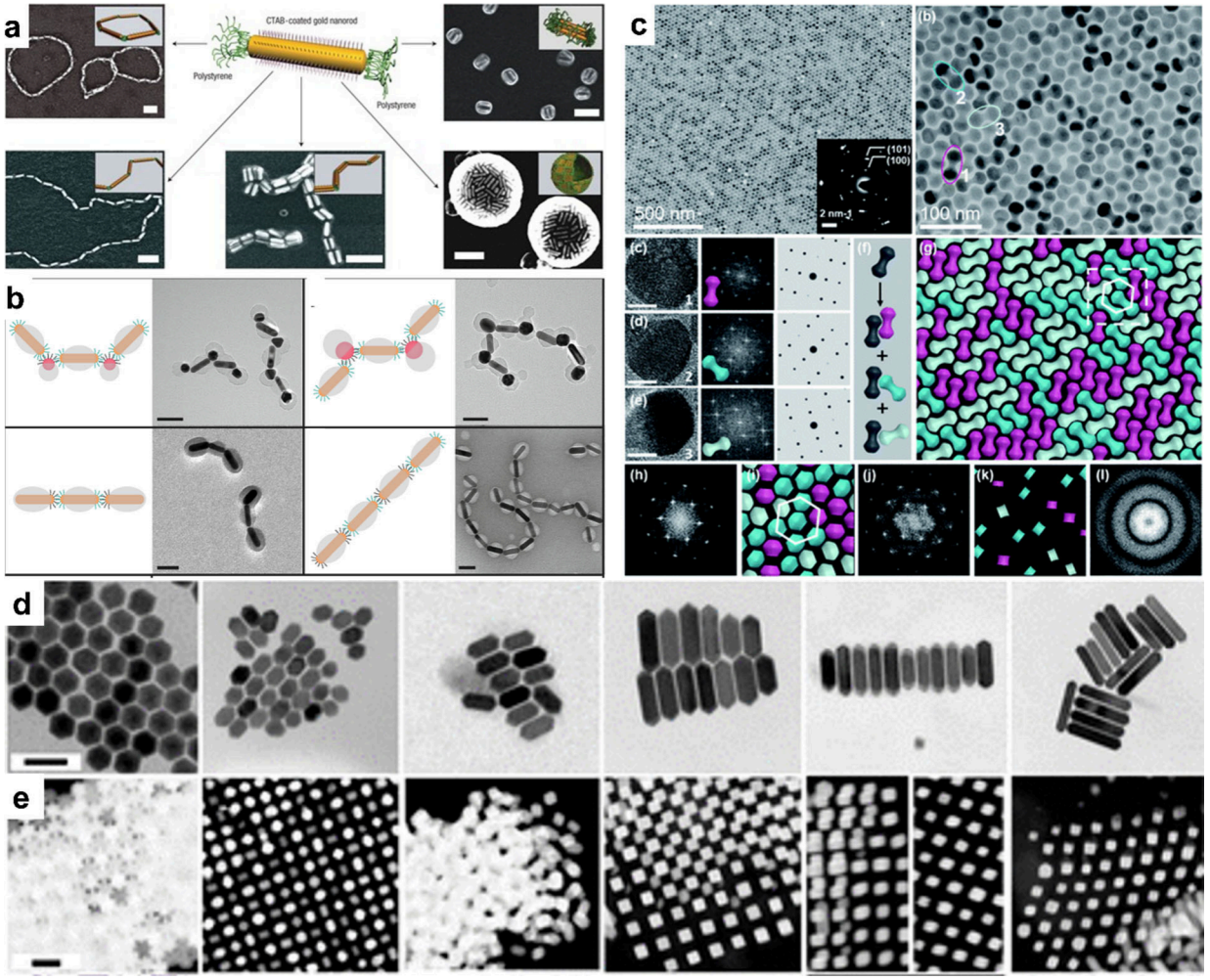

Figure 8. Tip-to-tip interactions in the organization of 1D building blocks. (a) Assembly of polymer-tethered Au nanorods in various solvents. An amphiphilic Au nanorod carrying a double layer of CTAB along the longitudinal side (the {100} facet) and polystyrene molecules were grafted to both tips. Scale bars: 100 nm. Figures adapted with permission from ref 120. Copyright 2007 Springer Nature. (b) Programmable assemblies built from regioselective surface-encoded nanoparticles. Scale bars: 50 nm. Figures adapted with permission from ref 121. Copyright 2018 Spinger Nature. (c) Monolayer membrane assembled from nanodumbbells on an ethylene glycol surface. Inset scale bars: 10 nm. Figures adapted from ref 122. Copyright 2020 Royal Society of Chemistry. (d, e) Elongated RD building blocks (d) crystallized into multiple lattice symmetries (e). From left to right, these particles have dimensions and ARs of 30.4 ± 2.4 and 1.1; 20.9 ± 1.4 and 1.6; 22.3 ± 1.2 and 2.8; 26.2 ± 1.9 and 4.3; 21.5 ± 2.4 and 5.0; 16.2 ± 2.4 and 9.0. Scale bars: 100 nm. Figures adapted with permission from ref 123. Copyright 2019 American Chemical Society.

hinged DNA "adapter," Lan and co-workers demonstrated that the conformation of the DNA component can be tuned to program the formation of various chiral supramolecular architectures, thereby regulating the chiral directional "bonding" of Au nanorods.[119]

3.2.2. Assembly via Tip-to-Tip Interactions. For decades, colloid chemists, to diversify the structures into which 1D building blocks can assemble, have primarily relied on the postsynthetic modification of nanorods. These approaches exploited the difference between the curvature of the sides of nanorods (low curvature) and those of their tips (high curvature). Importantly, this curvature difference leads to different ligand densities on the tips and sides of the nanorods, thereby allowing the tips and sides to be addressed selectively to permit asymmetric surface functionalization. Nie and co-workers functionalized the tips of nanorods with polystyrene (Figure 8a).[120] The assembly of these polymer-tipped nanorods led to a variety of assembly outcomes under different solvent conditions, including linear and staggered chains, loops, and clusters, all driven by tip-to-tip interactions. More broadly, researchers have developed a generalizable, regioselective surface-encoding platform for the site-specific modification of a variety of nanoparticles. By selectively blocking nanoparticle surfaces with a diblock copolymer (polystyrene-*b*-poly(acrylic acid)), Chen and co-workers functionalized nanorods with DNA on one tip, both tips, and both tips and one side (Figure 8b).[121] Dimers, trimers, and larger oligomers of nanorods were precisely generated on demand, significantly advancing possibilities for synthetic control over the colloidal organization.

One can also increase the role of tip-to-tip interactions by physically enlarging the nanorod tips. Liu and co-workers used a core−shell approach to synthesize nanodumbbells, essentially two spheres connected by a nanorod (Figure 8c).[122] During assembly, these dumbbell-shaped building blocks effectively act as dimers of spheres, generating a monolayer with a highly ordered hexagonal packing motif. Note that translational order was not observed in terms of dumbbell position, since the spherical tips are the structural motifs that organize, irrespective of the orientation of the dumbbells. Two, more

https://doi.org/10.1021/acs.chemrev.4c00299
Chem. Rev. 2024, 124, 11063−11107

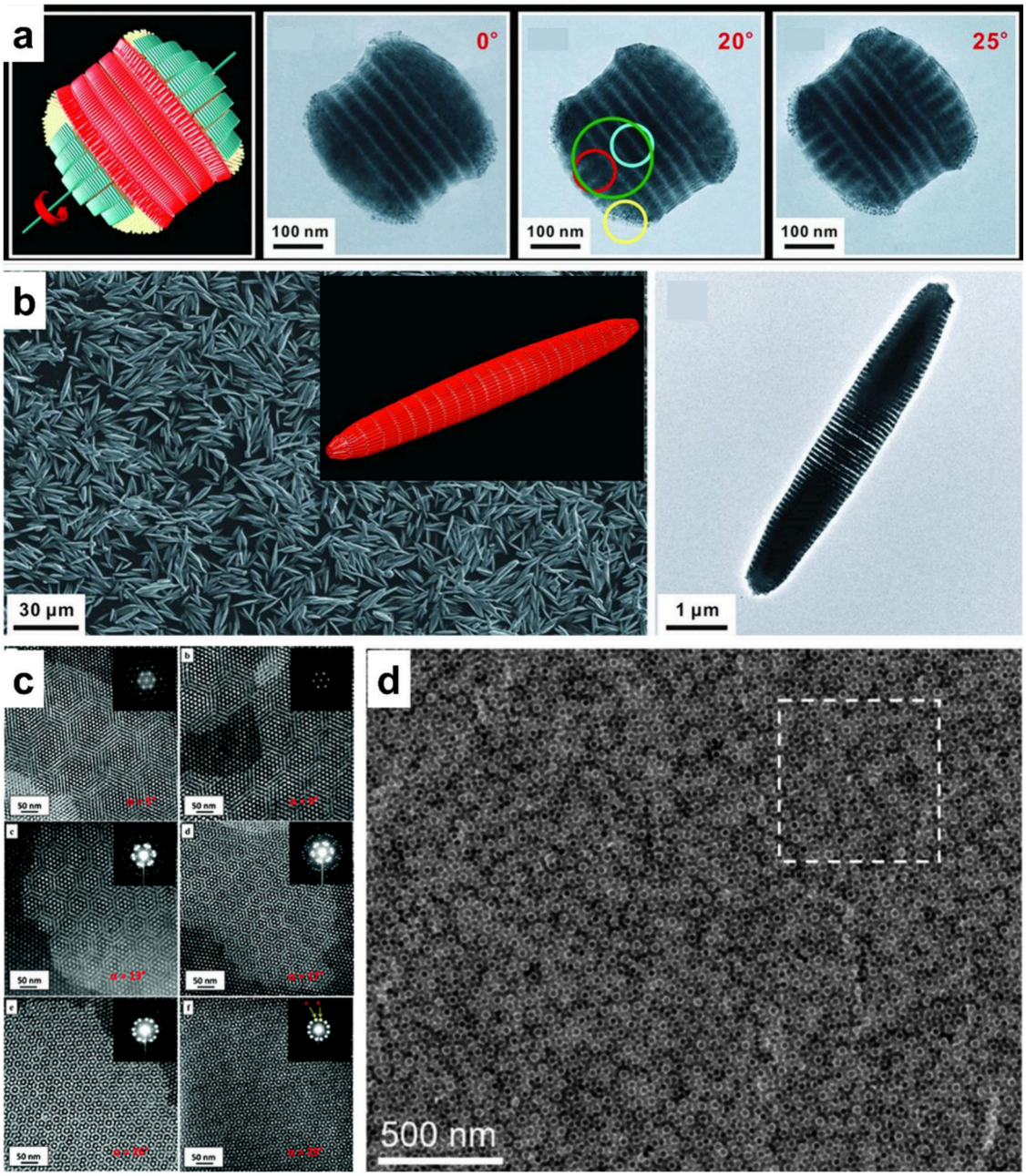

Figure 9. Superstructures in the organization of 1D building blocks. (a, b) Colloidal superparticles assembled from CdSe-CdS core−shell nanorods, including double-domed cylinder superparticles (a) and needle-like superparticles (b). Figures adapted with permission from ref 125. Copyright 2012 The American Association for the Advancement of Science. (c) Dark field (DF)-STEM images and the corresponding fast Fourier transform (FFT) and selected electron diffraction (SAED) patterns (inset) of Moiré patterns arising from the stacking of two sheets of vertically oriented CdS nanorod superlattice films. Misorientation angle: ∼5°, ∼9°, ∼13°, ∼17°, ∼26°, and ∼30°. When the misorientation angle between two CdS nanorod layers is close to 30°, the SAED pattern shows a 12-fold quasicrystalline-like pattern. Figures adapted with permission from ref 126. Copyright 2012 American Chemical Society. (d) Quasi-12-fold Moiré pattern generated from the bilayer stacking of nanodumbbells on the ethylene glycol subphase. Figure adapted from ref 122. Copyright 2020 Royal Society of Chemistry.

ordered, hexagonal phases with controllable interlayer packing, tilted or vertically aligned, were obtained when the ARs of the dumbbells was adjusted. These two arrangements are favored because they effectively represent two stable packings of spheres: an interlocked hexagonal lattice and a vertically aligned hexagonal lattice.

Both the tips and sides of the nanorods can have defined facets. Depending on the AR, these facets can induce very interesting intra- and interlayer packings. Laramy and co-workers synthesized elongated RD nanocrystals as "rod-like" building blocks.[123] When crystallized with self-complementary DNA, nanoparticles with an AR = 1.15, AR > 4, and AR > 5 exhibited *fcc* (the same as with RDs), *bct*, and hexagonal planar (*hp*) packing behavior, respectively (Figure 8d, e). This polymorphism arises from the enthalpy-driven (type II) nature of the DNA-mediated crystallization. At lower ARs, facet-to-facet interactions at the rod tips are significant in determining the overall packing, but at higher ARs, side-to-side interactions dominate, so the *hp* structure is favored.

https://doi.org/10.1021/acs.chemrev.4c00299
Chem. Rev. 2024, 124, 11063−11107

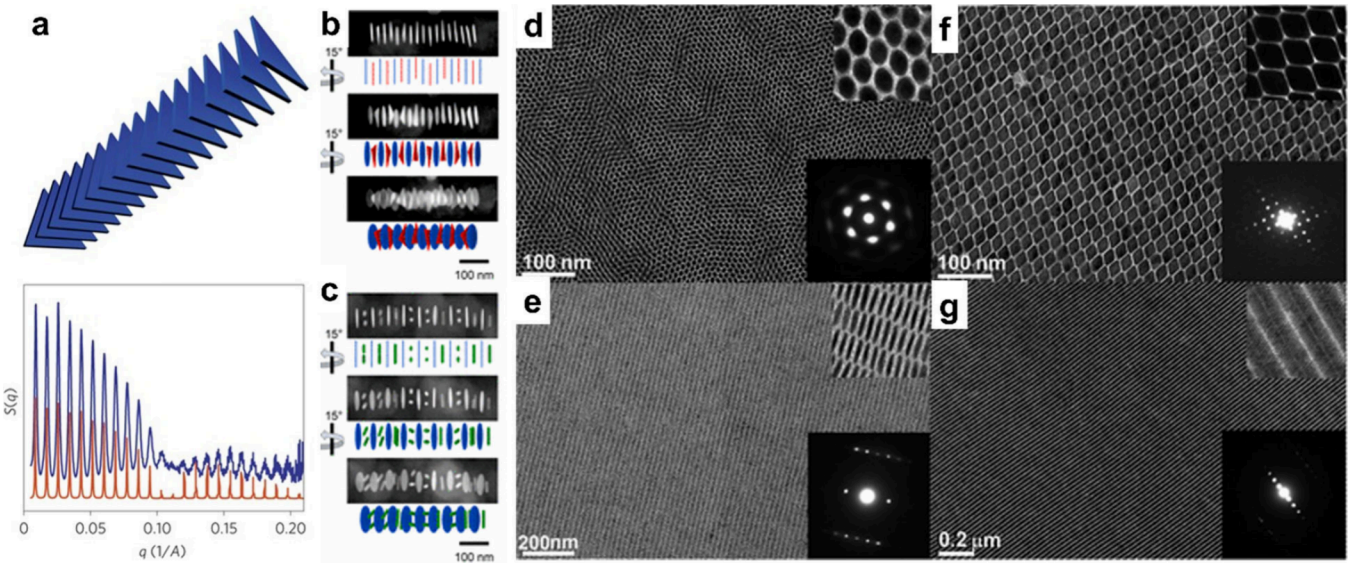

Figure 10. Face-to-face stacking in the organization of 2D building blocks. (a) SAXS characterization of primarily 1D lamellar assemblies of self-complementary DNA-functionalized Au triangular nanoprisms. Figures adapted from ref 23. (b, c) EM characterization of shape-biperiodic symmetry-broken nanoparticle superlattices. Arrays consist of alternating arrangements of circular disks and triangular prisms (b) or circular disks and rod dimers (c). Figures adapted with permission from ref 129. Copyright 2017 American Chemical Society. (d–g) TEM images of (d, f) columnar and (e, g) lamellar liquid crystalline superlattices through a liquid interfacial assembly technique. The top inset is a high-magnification TEM image, and the bottom inset is a small-angle electron diffraction pattern. Figures adapted with permission from ref 136. Copyright 2011 American Chemical Society.

3.2.3. Assembly into Superstructures. The ease of the synthesis of nanorods also has spurred investigations into more complex assemblies with multiple levels of structural control. Colloidal superparticles—discrete assemblies of multiple nanoparticles—and precise multilayer structures with offset rotation, which give rise to Moiré patterns, have been explored.

Unlike the superparticles generated from pseudospherical building blocks, which mostly have spherical morphisms with *fcc* or icosahedral particle arrangements, superparticles assembled from nanorods can present highly anisotropic structures.[124] Wang and co-workers reported the assembly of CdSe-CdS core–shell semiconductor nanorods, generating mesoscopic colloidal superparticles with multiple well-defined crystalline domains (Figure 9a, b).[125] By tuning the interplay of competing interactions during assembly, these nanorods generated double-domed cylinder-shaped superparticles with three distinct domains: a middle domain composed of multiple hexagonal layers of nanorods and two cap domains where multiple hexagonal layer domains were arranged perpendicular to the middle domain. To attain their pseudospherical shape, the caps also were composed of multiple domains, each perpendicular to the middle domain. Under conditions that do not favor the formation of the cap domains (with very high ARs), multilayer superparticles were observed, because these structures minimize the surface energy of the system. This work is the only report of highly anisotropic superparticles generated from nanoscale building blocks.

Given their strong tendency for side-to-side packing, nanorods are the ideal building block for generating stable and ordered monolayers, arguably even more so than spherical nanoparticles. Indeed, Singh and co-workers studied how hexagonal monolayers of vertically assembled nanorods generate Moiré patterns upon layering (Figure 9c).[126] Like with atomic Moiré patterns generated from twisted bilayer 2D materials,[127] small relative rotations (<20°) produced hexagonal patterns with increased unit cells, where the size of unit cell is determined by the rotation angle. Notably, when the rotation angle between two identical hexagonal patterns was close to 30°, a dodecagonal quasicrystal was generated, consistent with the behavior observed for graphene bilayers.[128] This structure has been observed for these nanorod bilayers as well as for bilayers of nanodumbbells (Figure 9d).[122]

3.3. Two-Dimensional (2D) Building Blocks

Whereas the structure of 1D nanorods is dominated by their shape along a single axis, 2D building blocks are characterized by their dominant shape lying along two axes, that is, planar structures with a comparatively small thickness. This geometry makes it favorable for 2D colloids to interact with each other via their planar faces to form face-to-face stacks. Like the assembly of monolayers from 1D nanoparticles, the formation of stacked columns from 2D colloids is both entropically and enthalpically favored: it is volume-efficient to stack 2D particles with facet registration (type I) and the largest possible contact area is also ensured (type II). There is, however, a nuance that distinguishes these two types of assembly: type I assembly processes favor the generation of hierarchical structures to ensure the densest packing, while type II assembly processes do not substantially favor such structures based on the comparatively weak side-to-side interactions. This weaker structural hierarchy in enthalpically driven systems tends to result in the formation of discrete columnar stacks first in a typical type II assembly process.

3.3.1. Assembly via Face-to-Face Stacking. As noted above, the pronounced anisotropy of 2D nanoparticles greatly favors face-to-face stacking rather than edge-to-edge tiling, since face-to-face assembly will always result in more excluded volume, more formed chemical bonds, and less exposed surface area. This effect is especially valid in type II assemblies; for example, when triangular Au nanoprisms are assembled using complementary DNA, 1D stacks of these prisms are the main

https://doi.org/10.1021/acs.chemrev.4c00299
Chem. Rev. 2024, 124, 11063–11107

product (Figure 10a).[23,129−134] Due to the strong cooperative effect of DNA binding between two flat nanoparticle facets, these columnar stacks typically exhibit a high degree of facet registration; there is little rotation of adjacent nanoprisms around the column axis. Their highly predictable stacking has also been used to engineer alternating structures consisting of two 2D nanoparticles with different shapes, such as triangular nanoprisms and circular nanodisks (Figure 10b).[129] Indeed, the anisotropy of these particles is so strong that even the coassembly of nanorods and nanodisks results in a similar alternating columnar structure, where a pair of nanorods resides between two neighboring nanodisks (Figure 10c).[129] Interestingly, it has been observed in enthalpy-driven systems that 2D particles with larger areas assemble into longer structures composed of more particles, compared to similar systems composed of smaller particles.

Since stacked structures are usually 1D ensembles covered with the same ligand as the constituent 2D particles, it is expected that 1D columns, if large enough, will further assemble into hierarchical structures. The outcome of this hierarchical assembly process can often be predicted by considering a simple 2D tessellation of the constituent facet shapes, that is, circular and hexagonal nanoplates assemble into *sh* columnar superlattices,[135] while triangular nanoplates assemble into *honeycomb* columnar superlattices.[52] However, complex assembly phenomena emerge when 2D nanoparticles cannot tessellate. For example, GdF_3 nanoplates with rhombic and ellipsoidal shapes have been assembled through the slow-drying of solvent to form two types of hierarchical liquid crystalline structures (Figure 10d−g).[136] As expected, the ability of rhombic shapes to tessellate generates long-range, positionally, and orientationally ordered columnar superlattices (*cmm* symmetry, Figure 10f) with a remarkably high degree of registration in the out-of-plane direction. In contrast, ellipsoidal plates lack a geometrically stable in-plane packing option. Instead, a columnar assembly with in-plane short-range positional order and liquid-crystal-like orientational order forms (Figure 10d). Moreover, the choice of substrate has a strong effect on the anchoring orientations of the resultant superlattices, indicating a complex kinetic difference between "columnar" and "lamellar" orientations.

3.3.2. Assembly via Edge-to-Edge Tiling. Although face-to-face interactions dominate the organization of 2D nanoparticles, the particle thickness cannot be neglected completely (Figure 11a). Indeed, leveraging the edges of nanoplates offers opportunities to fine-tune ligand distribution, and it has resulted in a series of intriguing 2D tilings through chemically engineered edge-to-edge interactions. Such a high level of control was elegantly demonstrated by Murray and co-workers in the context of the 2D assembly of rhombic and elongated rhombic (hexagonal) nanoplates through an interfacial approach.[137] Unlike rhombic plates, which assemble with *cmm* symmetry (as noted in the previous subsection),[136] elongated rhombic plates assemble into two types of highly ordered 2D tessellations, topologically noted as *cmm* and *pgg* (Figure 11b−d). The AR of these elongated rhombi can be synthetically tuned, while vertex angles and the symmetry of the shape are maintained. In this way, the phase diagram of *cmm* and *pgg* tessellations can be systematically explored. When only shape-induced entropic effects are considered, the *cmm* tiling is geometrically plausible for any AR; when the AR is tuned so that the elongated rhombus is a regular hexagon, the *pgg* tiling, where two orientations of hexagons tessellate in an alternating fashion, is also geometrically plausible (Figure 11c). In this situation, the two types of tessellations are entropically equal but enthalpically unequal. Interestingly, the *pgg* tiling is favored; the authors realized that the exposed facets of the A and B edges around the hexagonal plate differ and, as a result, ligand-induced reduction in the particle symmetry favors *pgg* over *cmm* tiling. This *interaction asymmetry* hypothesis was also confirmed by density functional theory (DFT) calculations and molecular dynamics (MD) simulations.[137]

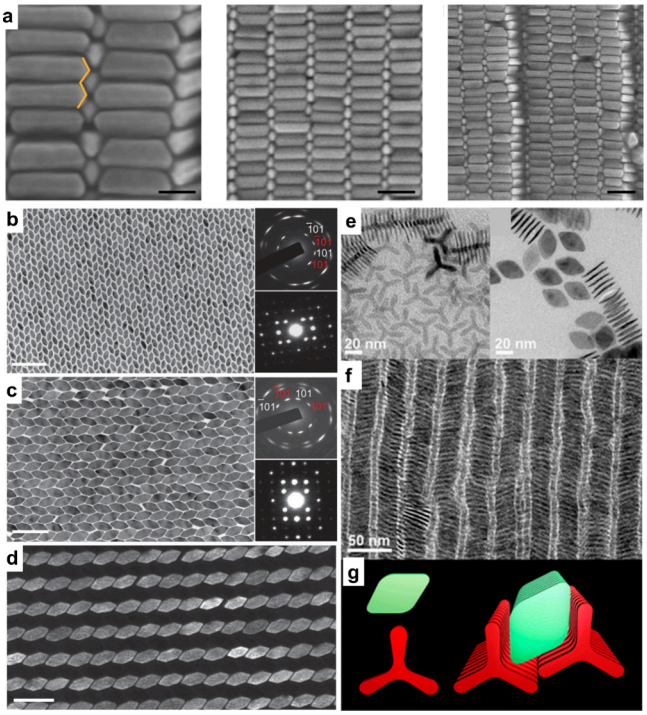

Figure 11. Edge-to-edge tiling in the organization of 2D building blocks. (a) Beveled gold triangular prism assembly via droplet evaporation. SEM images of the *ih* lattice (from left to right: high-magnification image, single layer, and multilayers). The orange lines highlight the beveled sides of the *ih* lattice. Scale bars: 40, 100, and 100 nm. Figures adapted with permission from ref 52. Copyright 2017 American Chemical Society. (b−d) 2D superlattices self-assembled from lanthanide fluoride nanoplates. (b, c) Alternating arrangements of hexagonal nanoplates with intermediate ARs, composed of DyF_3 (b) or TbF_3 (c). (d) Dark-field TEM image of the same area as shown in (c). Scale bars: 100 nm. Figures adapted with permission from ref 137. Copyright 2013 Springer Nature. (e−g) Shape-directed binary assembly of anisotropic nanoplates. (e, f) TEM images of (e, left) Gd_2O_3 tripodal nanoplates and (e, right) GdF_3 rhombic nanoplates and (f) a binary self-assembly of tripodal and rhombic nanoplates formed via a complementary-shape interaction. (g) Schematics of rhombic and tripodal nanoplates and their binary assembly. Figures adapted with permission from ref 55. Copyright 2013 American Chemical Society.

The unprecedented ability to tune enthalpy based on AR inspired a subsequent study of the dendrimer-directed assembly of rhombic plates. As noted, rhombic plates can only form one type of in-plane tessellation, *cmm*. Intriguingly, Murray and co-workers discovered that an ordered out-of-plane offset was observed when these nanoplates were functionalized with a series of dendrimers of different bulkiness.[31] Nanoplates modified with low-bulk ligands were assembled into the expected *cmm* columnar structures. However, medium-bulk ligands distorted the in-plane angle

https://doi.org/10.1021/acs.chemrev.4c00299
Chem. Rev. 2024, 124, 11063−11107

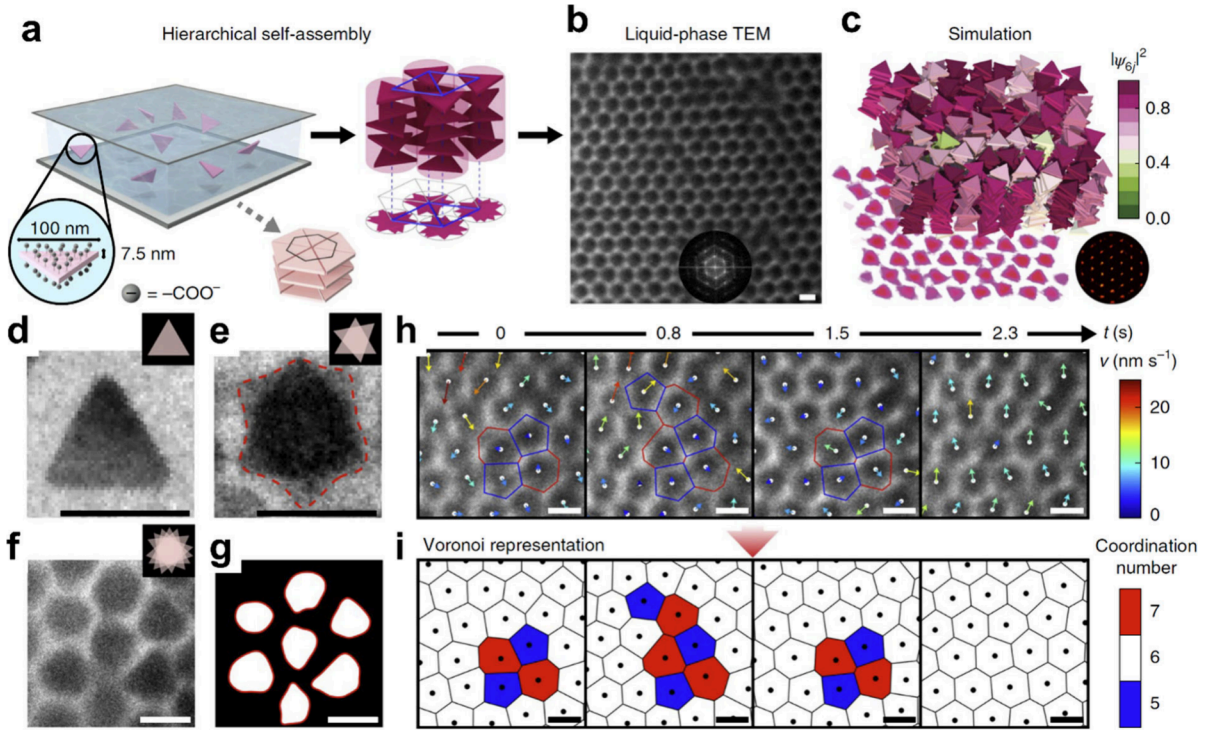

Figure 12. Kinetic pathways in the organization of 2D Au triangular nanoprisms that crystallize hierarchically in 3D to give an unexpected hexagonal lattice. (a–c) Illustration of the hierarchical crystallization process. (a) An aqueous suspension of nanoprisms sealed and sandwiched between two SiN_x chips. (b) Liquid-phase TEM and (inset) corresponding Fourier transform showing the highly ordered hexagonal lattice. (c) Monte Carlo simulations confirm the hexagonal lattice as the thermodynamically stable structure. (d–g) Liquid-phase TEM snapshots showing the stacking of misaligned prisms in top view: an individual prism sitting on the SiN_x chip (d), two prisms stacking with misalignment (e, polygonal projection contoured in dotted red line) and more prisms stacking into columns (f, g, and nearly circular projections contoured in solid red lines in the binary image). (h, i) Time-lapse liquid-phase TEM images (h) and corresponding Voronoi representations (i) of the lattice, showing the annealing of imperfectly coordinated sites. The color of each cell denotes the coordination number. The arrows in the top panel are colored by the magnitude of the instantaneous velocity of individual columns calculated from successive TEM images. Scale bars: 100 nm. Figures adapted with permission from ref 138. Copyright 2019 Spinger Nature.

between two neighboring plates in a single column, stabilizing the structure through a "lock-and-key"-type mechanism. Further increases in ligand bulk forced the nanoplates to shift from their positions, disrupting registry. These observations were explained by considering the radial distribution of ligands around the edges of nanoplates: bulkier ligands tend to point toward vertices, necessitating angular twists and lateral shifts to mitigate the local steric hindrance that results.

Shape complementarity can also be utilized to engineer the formation of exotic structures from 2D components. Murray and co-workers observed two different out-of-plane packings when LaF_3 triangular nanoplates were coassembled with Au nanospheres via solvent evaporation, depending on the relative size ratio of the two nanoparticles.[15] Above a threshold nanosphere size, the highly symmetrical hexagonal alternating structure was disrupted, and instead, a coassembly of spheres and angled dimers of plates was produced. Shape complementarity has also been exploited to program in-plane arrangements. Paik and Murray reported an exceptionally stable coassembly of rhombic and tripodal nanoplates that organizes into a long columnar surface-bound superlattice (Figure 11e–g).[55] When the edge lengths of the rhombic plates match the radial lengths of the tripodal plates, a local 2D tessellation of the two shapes propagates into a thin film with long-range in-plane order. This tessellation did not propagate in all directions, and therefore, only a monolayer of a lamellar structure was observed as the main product. Nevertheless, the observation that the interactions between the thin edges of nanoplates can drive such a system toward a stable coassembly outcome emphasizes the importance of shape complementarity as a driving force for colloidal organization.

3.3.3. Understanding Kinetic Assembly Pathways. Although the final assembly outcomes of 2D nanoplates are generally predictable, the kinetic pathways that define assembly remain elusive: do nanoplates go through a stepwise assembly process via discrete columnar structures or does crystallization occur cooperatively and lead directly to the hierarchically assembled superlattices? Recent studies by Chen and co-workers provide some insight into these questions. They utilized depletion forces to tune the hierarchical assembly of nanoplates with nanoscale to microscale thickness.[131,138] Since depletion forces are relatively weak, the nanoplates rotated even when they were already stacked in a long column. In fact, when relatively small triangular nanoprisms (~100 nm wide and 7.5 nm thick) are assembled, they do not always exhibit strict facet registration (Figure 12). Instead, columnar stacks assemble even though their constituent nanoplates are still misaligned or even rotating. This phenomenon was thoroughly studied through *in situ* electron microscopy (EM), and an unexpected and intriguing aspect of hierarchical self-organization was revealed. This kinetic pathway was further confirmed using MD simulations, providing a fresh perspective for experimentalists to consider when designing colloidal superlattices.[138] In addition, the study of micron-sized plates

https://doi.org/10.1021/acs.chemrev.4c00299
Chem. Rev. 2024, 124, 11063–11107

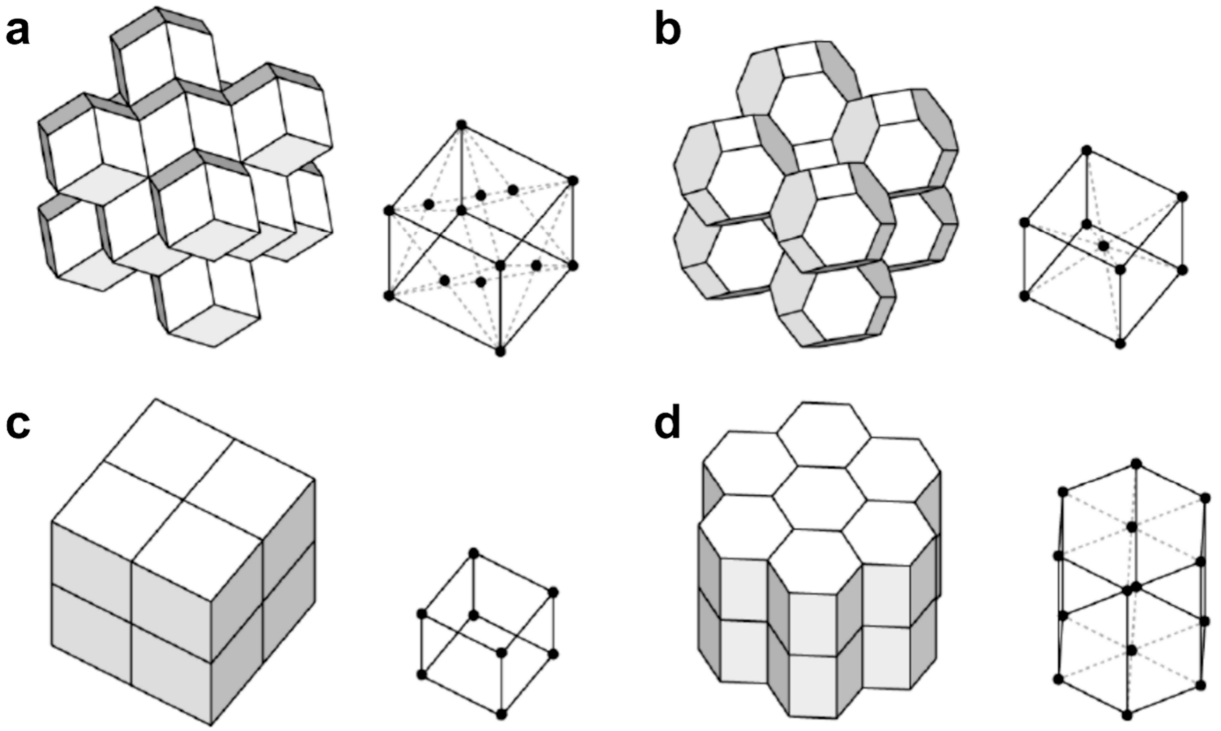

Figure 13. Assembly of space-filling 3D polyhedra into their corresponding space-filling configurations. (a–d) Schematic illustration of *fcc* (a), *bcc* (b), *sc* (c), and *sh* (d) lattices composed of RD, truncated octahedra, cubes, and hexagonal prisms, respectively. Figures adapted with permission from ref 143. Copyright 2018 E3S Web of Conferences.

under a similar experimental setup demonstrated the role of tip truncation on the secondary packing symmetries of columns: while triangular plates assemble into *honeycomb* lattices (as noted above), more truncated shapes instead form hexagonal lattices.[131] Geometrically, this result indicates that it is important to consider how close the shape of a nanoplate is to that of a regular triangle or hexagon in predicting the final assembly outcome.

3.4. Three-Dimensional (3D) Building Blocks

Most nanoparticles are 3D building blocks and most are polyhedral in nature. It is inherently difficult to pack 3D shapes in space analytically; one of the greatest unsolved mathematical challenges is determining the densest packing of a given polyhedra. The densest packing arrangement of only the simplest shapes, such as cubes and a small fraction of convex polyhedral shapes, have been determined, mostly through brute-force computation.[75,77,79] Indeed, solutions exist for an even smaller fraction of concave polyhedra, and a unified theory to predict the packing of hollow polyhedral particles does not exist.

In this section, important insights gained from a critical analysis of known experimental and computational works on this topic are highlighted. Due to differences in their packing behaviors, 3D building blocks can be categorized as convex, concave, or hollow polyhedra; each of these groups of building blocks is discussed in turn.

3.4.1. Packing of Space-Filling Convex Polyhedra. Like with their 2D counterparts, face-to-face packing is favored in the organization of convex polyhedra: entropically, face-to-face packing is likely to reduce the total packing volume, which is beneficial from a space-filling perspective; enthalpically, face-to-face contact maximizes the attractive interactions of surface ligands, which are more stable as a result of neighbor affinity. While the challenge of solving the densest packing solutions of arbitrary polyhedral shapes was noted above, the prediction of the structural outcome via colloidal crystallization is even more challenging due to the additional enthalpic considerations. In particular, the ligand distributions on polyhedral nanoparticles may not be uniform, resulting in affinities between certain areas beyond those predicted by shape alone. Furthermore, although the number of different types of polyhedra is infinite, the number of ordered lattices, otherwise known as space groups, is finite. Therefore, one way to rationalize the packing behaviors of convex polyhedra is to compare the shape of the building blocks (at their crystallized positions and orientations) with the space within the lattice that they occupy, formalized as the Voronoi cells of a lattice.[139] Through this lens, each symmetry can be viewed as a unique way of dividing 3D space, with a corresponding Voronoi cell shape that is also unique.

The packings of Voronoi cells into their corresponding symmetries are the most stable and straightforward packing solutions for polyhedral shapes: cubes into *sc*, truncated octahedra into *bcc*, rhombic dodecahedra into *fcc*, and hexagonal prisms into *sh* lattices (Figure 13). These lattices can infinitely fill 3D space; however, this fact also hinders particles with these shapes from packing into other symmetries if the single-component organization of hard polyhedral particles is considered alone. Indeed, the superlattices formed from polyhedral nanoparticles with these space-filling shapes are observed frequently because of the tendency of such shapes to tessellate and minimize the total volume.

When polyhedral metal nanoparticles are very large (edge length >200 nm), they will naturally assemble due to gravity. A series of silver particles with different degrees of truncation, from cubes to truncated octahedra, were assembled through a

https://doi.org/10.1021/acs.chemrev.4c00299
Chem. Rev. 2024, 124, 11063–11107

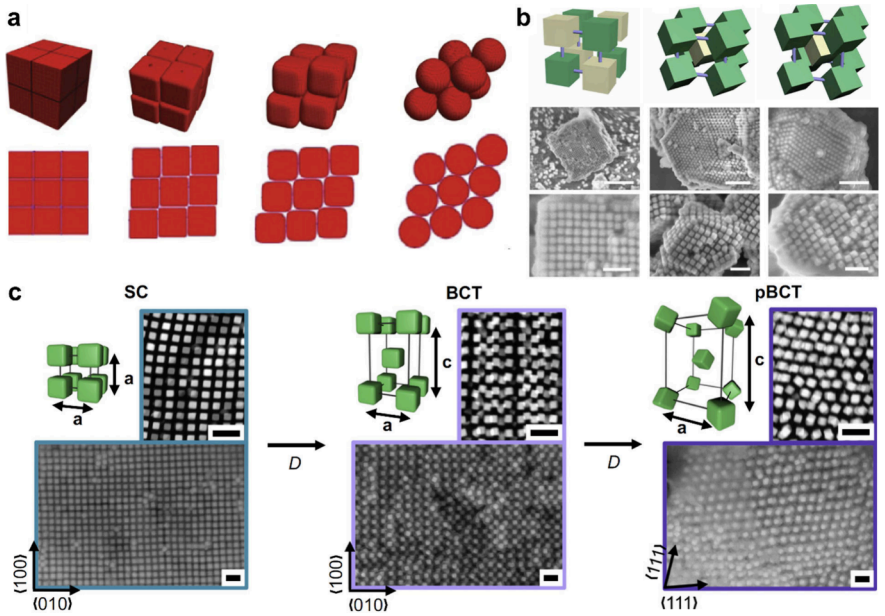

Figure 14. Organization of cubic building blocks into low symmetry lattices. (a) 3D (top) and 2D (bottom) illustrations of a phase transformation from *sc* to *fcc* due to the evolution of effective particle shape from a cube to a sphere using the "superball" model. Figures adapted with permission from ref 81. Copyright 2011 American Physical Society. (b) The assembly behavior of soft-shell gold nanocubes as a function of DNA linker length. Low- (top) and high- (bottom) magnification SEM images of silica-encapsulated lattices using DNA linkers of length 30-bp (left), 70-bp (middle), and 120-bp (right). Scale bars: left, 1 μm (top) 200 nm (bottom); middle and right, 500 nm (top) and 200 nm (bottom). Figures adapted with permission from ref 24. Copyright 2019 American Association for the Advancement of Science. (c) Experimental investigation into cube crystallization behavior shows two continuous phase transitions as a function of the DNA length (D) and cube edge length (L). As D increases for a given cube size (shown here as L = 57 nm), cubes organize into (left to right) *sc* (crystalline), *bct* (crystalline), and *fcc* (plastic) symmetries. Next to each unit cell is a TEM image of sectioned silica-embedded lattices. Below each unit cell is an SEM image of silica-embedded lattices with the lattice vectors indicated. Scale bars: 200 nm. Figures adapted with permission from ref 144. Copyright 2016 National Academy of Sciences.

gravity-driven method.[33] Unsurprisingly, cubes and truncated octahedra undergo type I assembly into their corresponding tessellated lattices, *sc* and *bcc*. A similar study explored the entropy-driven assembly of these silver nanocrystals via a solvent evaporation process. Though different exposed facets were found in two different microenvironments (the top and bottom of a droplet), the same packing symmetries for cubes and truncated octahedra were observed.[140] With much smaller particles (<100 nm), cubic and RD Au nanoparticles were subjected to a slow evaporation process, resulting in a series of macroscale surface-bound structures.[141] Both cubes and RDs were assembled into high-quality space-filling superlattices. This concept also holds for 2D particles with substantial thickness: beveled triangular nanoprisms assemble into a planar honeycomb (*ph*, higher symmetry) lattice when subject to a small depletion force, whereas when subject to a large depletion force, a more stable, space-filling interlocking honeycomb (*ih*, lower symmetry) structure with a hexagonal rod crystal habit is observed (Figure 11a).[52] These results demonstrate the robustness of space-filling (tessellation) as a determinant of entropy-driven assembly outcomes for convex polyhedra.

As noted for 1D and 2D building blocks, entropic and enthalpic driving forces often favor the same structural outcome. This principle is also true for the assembly of convex polyhedra under certain conditions, namely, that the surface ligands providing the enthalpic driving force occupy a negligible volume within the lattice and do not affect how the shape of the particle is presented during packing. Indeed, in a regime where these conditions are valid, referred to as the "zone of anisotropy,"[25] DNA-functionalized cubes and RDs assemble into colloidal crystals with *sc* and *fcc* symmetries and cubic and octahedral crystal habits.[23,25,142]

However, one cannot always ignore the fact that surface ligands occupy a portion of the lattice volume. When the volume occupied by surface ligands is not negligible, results from experiments and simulations deviate because the ideal hard particle systems used in most simulations no longer closely approximate the experimental systems. When the ligands are relatively rigid, the observed crystal symmetries transition from *sc*, through *bct*, and finally into *fcc* as ligand length increases (Figure 14c). Such behavior was experimentally explored using a series of nanocubes functionalized with double-stranded DNA (dsDNA) and crystallized through a slow-cooling process.[25] MD simulations revealed that unexpectedly, when longer dsDNA was used, symmetry breaking processes occurred. In another example, when Au nanocubes were functionalized with complementary, flexible, single-stranded DNA (ssDNA), a transition from *sc* to *bct* to *bcc* crystal symmetries was observed (Figure 14b; *bcc* is the preferred packing of complementary DNA-functionalized spheres).[24] Soft-shelled cubes, on the other hand, present a distinct, continuous transition from *sc* to *fcc* via a rhombohedral symmetry (Figure 14a).[81] When dodecanethiol-ligated Pd nanocube cubes assemble with their native shapes, they organize into a classic *sc* lattice. As ligand adsorption is increased, the cubes are effectively more rounded and organize into an intermediate rhombohedral phase with a gradually decreasing lattice angle that is dependent on the degree of rounding. Once enough ligands are adsorbed such that the shape anisotropy of the underlying cube is completely obscured, the system adopts a *fcc* packing arrangement.

https://doi.org/10.1021/acs.chemrev.4c00299
Chem. Rev. 2024, 124, 11063−11107

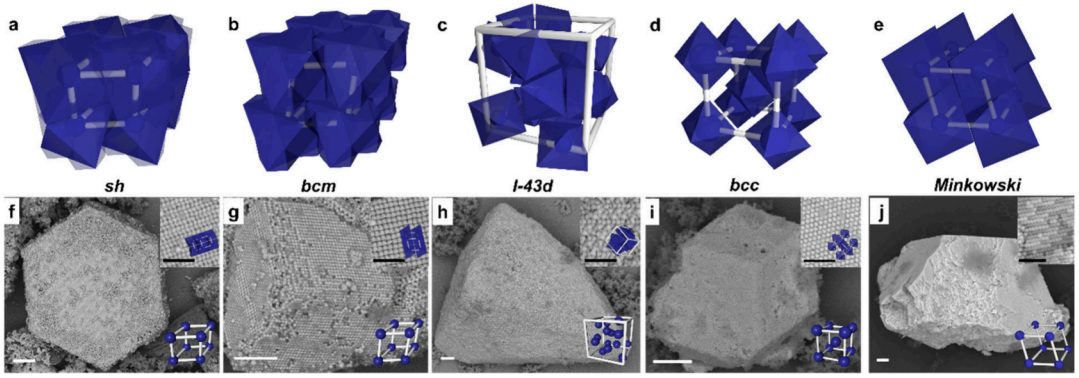

Figure 15. Polymorphic organization of octahedral building blocks. (a–d, f–i) Crystallization of octahedral NCs with different edge lengths (L) mediated by flexible, short DNA. (a–d), Schematic illustrations of *sh* (a), *bcm* (b), *I*43*d* (c), *bcc* (d) and *Minkowski* (e) lattices packed from octahedra. (f–j), SEM images of colloidal crystals with *sh* (f), *bcm* (g), *I*43*d* (h), and *bcc* (i) symmetries formed from octahedral NCs (L = 95, 82, 65, 39, 78 nm, respectively). Identifiable crystal habits are hexagonal prisms (f), triakis tetrahedra (h), and RDs (i). Scale bars: 2 μm; inset scale bars: 500 nm. Figures adapted with permission from ref 80. Copyright 2024 The American Association for the Advancement of Science.

Dipoles in magnetic nanoparticles also provide additional design handles for tuning organization outcomes. When a strong magnetic field is present, the assembly outcome of magnetite nanocubes results from a delicate balance between their local packing and their alignment to the field via their local ensemble dipole axes (the body diagonal direction for a single cube).[34] This complex organizational environment results in unique helical superstructures composed of magnetite cubes after slow-drying.[36]

3.4.2. Packing of Non-Space-Filling Convex Polyhedra. Most uniform polyhedra cannot fill 3D space perfectly; therefore, the entropic and enthalpic factors that dictate assembly outcome compete, and a single assembly outcome is not favored. For nonspace-filling shapes, the outcome of complex organizational processes results from an interplay between packing density, ligand interactions, and steric hindrance. The assembly of four such shapes—octahedra, cuboctahedra, tetrahedra, and decahedra—is focused on here.

Octahedra exhibit rich polymorphism in their assemblies, which include *bcc*, *I*43*d*, body-centered monoclinic (*bcm*), *sh*, and rhombohedral (Minkowski phase) symmetries.[33,141] *bcc* lattices are mostly observed for assemblies of small octahedra mediated by long ligands, where a large interparticle distance is stabilized and a low packing density of ∼30% is maintained (e.g., in the assembly of octahedral Pt_3Ni nanoparticles ∼10 nm in size).[145] Entropically, the outline of ligand-functionalized octahedra can be viewed as truncated octahedra, and there is a strong tendency toward *bcc* packing. If grown slowly, these colloidal crystals exhibit RD crystal habits.[142,146,147] However, if evaporation is conducted more quickly, for instance, at an elevated temperature (90 °C), then octahedral or hexapod crystal habits also emerge. This outcome results from the growth of a higher-index facet, and such outcomes are also seen in the synthesis of polyhedral nanoparticles with different shapes.[146] Interestingly, for enthalpy-driven crystallization methods, such as DNA-mediated assembly, *bcc* superlattices with RD crystal habits are also realized for octahedral nanoparticles with a certain ligand-to-particle edge length ratio, although the facets between neighboring octahedra cannot achieve perfect registration (2/3 of their area is shared, Figure 15d).[23,25,142] In this case, the octahedrally extended dsDNA strands define specific bonding directions that guide the formation of superlattices. This result is supported by the observation of a similar *bcc* colloidal crystal in the coassembly of octahedra and circular nanodisks functionalized with complementary DNA.[43]

Increasing the rigidity of the ligand shell on octahedral nanocrystals leads to other types of structures. At a minimum rigidity, a colloidal crystal with *I*43*d* symmetry was observed, in which each cubic unit cell contains 16 octahedra with different orientations (Figure 15c). Increasing rigidity leads to the generation of a *sh* superlattice, where octahedra are arranged into a hexagonal close packed layer, sharing half of their interparticle facet area, and stacked vertically in an alternating ABAB fashion (Figure 15a). This superlattice is distinct, because it features alternating pillars of octahedra. In some cases, hexagonal layers will grow differently in the vertical direction, shifting themselves by half of an octahedron, sharing half of their facet area (Figure 15b). This superlattice features octahedra hexagonally close packed with the same orientation. In the most rigid ligand form, octahedra pack into their densest known packing, the Minkowski phase, which is a rhombohedral superlattice in which all octahedra adopt the same orientation to achieve a packing density of 95% (Figure 15e).

Cuboctahedra, which are a truncated variant of octahedra, are also interesting in the context of colloidal crystallization due to their distinctively bifurcate crystallization behaviors when they have different dimensions. When they are less than 10 nm in size, cuboctahedral quantum dots (QDs) assemble into *sc* lattices via the registration of their square (100) facets.[148,149] This tendency for specific facet registration was utilized to produce single-crystalline sintered networks of QDs, where the (100) facets of QDs are postsynthetically fused to form a single, continuous, nanoscale crystalline network.[150] Cuboctahedral nanoparticles of larger sizes (>50 nm) instead assemble into a *bct* lattice (Figure 16).[33,140] Compared to the highly symmetrical *sc* lattice, where the (100) facets of particles are registered both in-plane and out-of-plane, the *bct* lattice presents a lower symmetry structure, where (100) facets reside in the hollow square patterns defined by adjacent layers. This behavior can be rationalized by considering the driving force for assembly. In type I assembly processes, at play for the smaller cuboctahedra, packing efficiency seeks to increase and therefore the *bct* lattice is favored because its out-of-plane distortion partially embeds square facets and decreases interplane distances. In contrast, *sc* lattices result from type II assembly processes, where the ligand and atomic affinities stabilize a less densely packed arrangement (Figure 16b–d).

https://doi.org/10.1021/acs.chemrev.4c00299
Chem. Rev. 2024, 124, 11063–11107

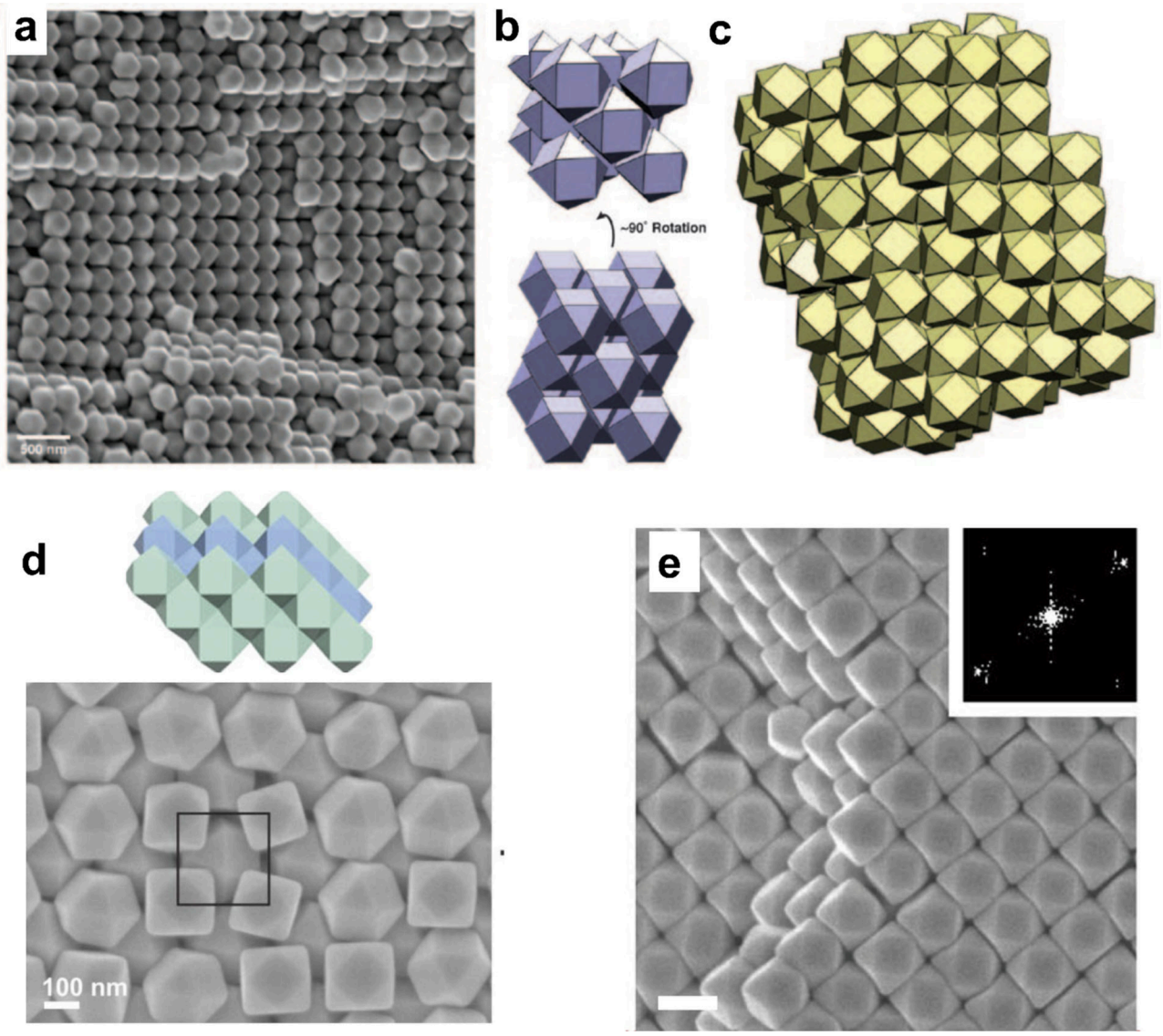

Figure 16. Organization of cuboctahedral building blocks. (a−c) Crystallization of uniform cuboctahedral silver nanoparticles into their densest packings. (a) SEM micrographs show a face-centered tetragonal (*fct*, equivalent to *bct*) lattice, with (b) unit cell and (c) lattice illustrated. Scale bar: 500 nm. Figures adapted with permission from ref 33. Copyright 2011 Spinger Nature. (d, e) Cuboctahedral silver nanoparticles assembled in dual microenvironments, dried on a substrate. Both show the same *bct* structure as illustrated in (d). Scale bar in (e): 200 nm. Figures adapted with permission from ref 140. Copyright 2018 Spinger Nature.

Tetrahedra are one of the most intriguing convex polyhedra useful in colloidal crystal engineering; because of their tetrahedral symmetry and pronounced anisotropy, they cannot fill 3D space,[78] and because they are challenging to synthesize in high quality, their assembly has been underexplored. Recent experimental efforts have mainly focused on assembling tetrahedral QDs ∼ 10 nm in size. Through a slow-drying process, tetrahedral CdSe QDs functionalized with C_{18}-length ligands were observed to assemble into a *sh* superlattice with a hexagonal crystal habit.[54] Each unit cell contains two tetrahedra organized in opposite orientations. In plane, these QDs arrange into a honeycomb layer perpendicular to their 3-fold axes (Figure 17a, d). However, the entire superlattice has an estimated packing fraction of only ∼59%.

The surfaces of tetrahedral nanoparticles have been asymmetrically functionalized to increase their structural sophistication. Chen and co-workers utilized CdSe-CdS core−shell tetrahedra where the three (1011) facets are capped with oleic acid, and the remaining (0002) facet was capped with octadecylphosphonic acid (ODPA).[18,19] Interestingly, this ligand arrangement results in a strong interaction between the ODPA-capped facets. This chemical affinity breaks the symmetry of the tetrahedral core and enables a hierarchical organization of tetrahedra. Specifically, two tetrahedra can interact via their ODPA-capped facets to generate a bitetrahedral secondary building unit (SBU), which subsequently assembles into larger tertiary building units (TBUs) composed of 36 individual tetrahedra. This TBU is a four-layered polyhedron that closely resembles a truncated octahedron and organizes in a *bcc* superlattice (Figure 17b, e), for which the truncated octahedron is the Voronoi cell. Within the four-layered TBU, the first and fourth layers are compose of three bitetrahedra, while the second and third layers are 12-member ring structures. A dodecagonal quasicrystal approximant structure was also identified under the same assembly conditions via the formation of a distinct TBU (Figure 17c,

https://doi.org/10.1021/acs.chemrev.4c00299
Chem. Rev. 2024, 124, 11063−11107

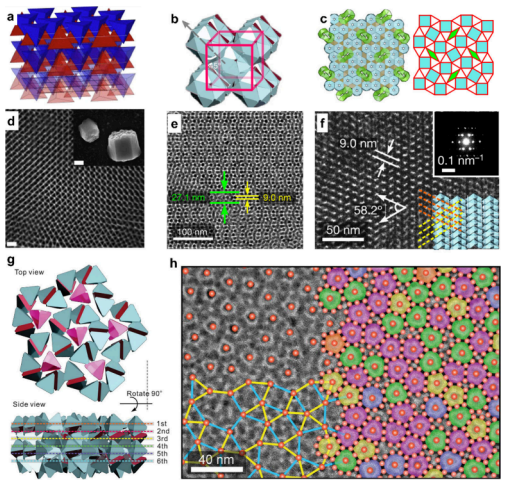

Figure 17. Organization of tetrahedral and truncated tetrahedral QDs. (a, d) Assembly of tetrahedral 10 nm CdSe NCs with C_{18}-length ligands. (a) Crystal structure and (d) TEM image of a large-area superlattice. Inset in (d): SEM image of hexagonal prism-shaped 3D crystals. Scale bar: 20 nm; inset, 1 μm. Figures adapted with permission from ref 54. Copyright 2014 American Chemical Society. (b) Unit cell model and (e) TEM image along the [110] *bcc* projection of 3D cluster-based *bcc* supercrystals assembled from truncated tetrahedral QDs. (c, f) 2D superlattice with a tentative quasicrystal-approximant superstructure from truncated tetrahedral QDs. (c) Computer-generated illustration of the 2D superlattice (left) and tiling (right). (f) TEM image of the side view of the assembly. Figures adapted with permission from ref 18. Copyright 2018 Springer Nature. (g, h) 10-fold quasicrystalline superlattice (QC-SL) assembled from truncated tetrahedral quantum dots. (g) A computer-generated model of a double-decker QC-SL with six interconnected decagon-derivative units shown from a top view and a side view. The centers of each polygon unit are labeled in magenta. (h) TEM image of the flexible polygon tiling. Larger orange spheres at top left indicate the centers of each polygon; the yellow and blue lines connect the polygon centers with the nearest and second nearest interpolygon center distance, respectively; the right side of the image is tiled by color-coded flexible polygons. Figures adapted with permission from ref 19. Copyright 2018 The American Association for the Advancement of Science.

f).[18] Bitetrahedral SBUs favored a 5-fold ring structure when attached to a flat surface, with an additional tetrahedron located at the center (Figure 17g, h).[19] The resulting TBU has a rather flexible decagonal form, which further propagates in-plane to give an aperiodic structure with strong 10-fold symmetry. This surface-bound superlattice was identified as a decagonal quasicrystal (DQC) constructed through a newly proposed flexible tiling rule.

Three recent reports were published in which the slow evaporation of colloidal solutions containing CTAB- or CTAC-stabilized tetrahedral gold NPs were investigated.[50,151,152] When dried on a substrate, tetrahedral NPs form bilayers of hexagonal lattices (Figure 18a, b). Interestingly, as tetrahedra size increases, a planar chirality emerges. In such symmetry-broken structures, every NP rotates toward the same direction, either clockwise or counterclockwise, with no apparent preference. When nucleated in solution, three types of 3D superlattices with monoclinic, cubic diamond, and hexagonal diamond symmetries are attained (Figure 18c–e).

Tetrahedral symmetry is ubiquitous in organic chemistry and in nature (e.g., the structure of diamond). Atomic diamond exhibits unprecedented strength, and colloidal diamond had long been targeted for its exotic photonic properties. Pine and co-workers realized this structure using clusters of microspheres as a pseudotetrahedral building block (Figure 19a–e).[153] This work, which highlights an example of DNA-mediated type II assembly, exemplifies two essential criteria for the preparation of a cubic diamond lattice: 1) a tetrahedral bonding environment between building blocks, achieved by functionalizing only an exposed portion of the central particle (light blue in Figure 19a) with self-complementary DNA; and 2) staggered bonding between neighboring building blocks, achieved via the steric hindrance between unfunctionalized particles (Figure 19a). Notably, the packing efficiency of this colloidal diamond lattice is as high as 68% (Figure 19c, d), approaching that of the densest packing of spheres (74%). The entropic favorability underlying this dense packing arises from the similarity between the outline shapes of these tetrahedral clusters and a truncated triakis tetrahedron, which is the Voronoi cell shape of a cubic diamond lattice and therefore can fill space with 100% efficiency.

The organization of two related shapes—the truncated tetrahedron and the trigonal bipyramid—has also been explored. Specifically, asymmetrically truncated tetrahedral CdTe QDs with sub-5 nm sizes have been studied.[154] These QDs initially assembled into free-floating sheets with hexagonal symmetry, corresponding to the expected honeycomb packing of truncated tetrahedra. Upon illumination with visible light, the photooxidation of CdS induced a build-up of mechanical shear stress, which was relieved by a structural distortion to form a twisted ribbon structure.

Tetrahedra can be related to trigonal bipyramids (TBPs) through the construction of a SBU in which the polar tips of four TBPs locally fill space to form a triakis tetrahedron, one of the Catalan solids (Figure 19b). Two triakis tetrahedral SBUs can further assemble by sharing one TBP, which leads to four types of TBUs that all geometrically resemble Frank–Kasper polyhedra that also can subsequently organize. This behavior was explored experimentally using large Au TBP nanoparticles and long dsDNA with self-complementary sticky ends, and three types of clathrate structures were obtained: clathrate I, II, and IV (Figure 19f, g, h).[71] This work emphasizes the geometric relationship between tetrahedra and Frank–Kasper polyhedra, opening new possibilities for exploring libraries of structurally complex, yet highly ordered, colloidal crystals.

Regular decahedra, which are a subset of pentagonal bipyramids in which all 10 faces are equilateral triangles (Figure 20a), have been computationally suggested to pack into a rhombohedral lattice when only entropy factors are considered.[77] However, the 5-fold symmetry of decahedra may prohibit the formation of periodic lattices without at least some degree of randomness, since 5-fold symmetries are forbidden for periodic arrays. Interestingly, a recent experiment reveals that, upon slow-drying, decahedra pack into a lattice with triclinic symmetry, which has the lowest symmetry among the 14 Bravais lattices. More intriguingly, when decahedra are assembled through DNA-mediated crystallization, a dodecagonal quasicrystal (DDQC) is the primary product (Figure 20).[61] This single-component colloidal DDQC is the first to be formed from a uniform constituent (that is, from structures with uniform shape and surface ligands). Computational investigations have resolved this apparent discrepancy: under a type I assembly regime, decahedra assemble into triclinic

https://doi.org/10.1021/acs.chemrev.4c00299
Chem. Rev. 2024, 124, 11063–11107

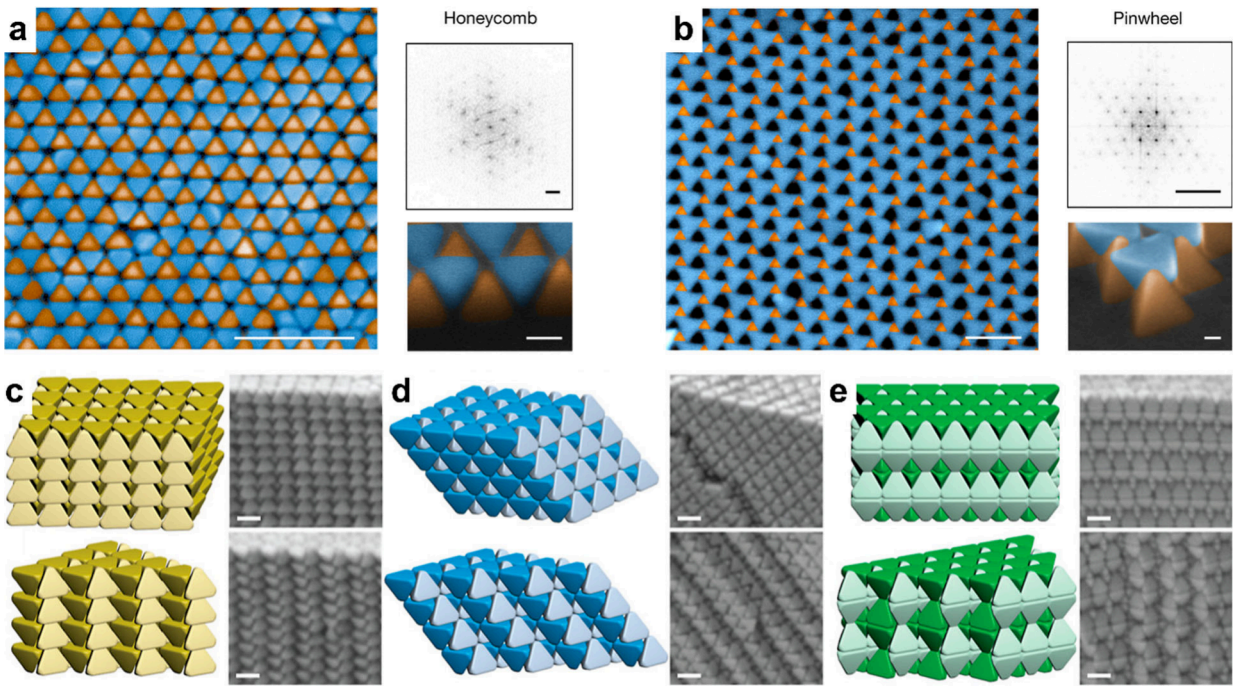

Figure 18. Organization of tetrahedral gold NPs. (a, b) SEM images (left), FFT (top right) and tilted SEM images (bottom right) of the large-scale extended corner-sharing lattice (a) and pinwheel lattice (b) formed by tetrahedral building blocks on substrates. Scale bars: 200 nm (top view), 20 nm (tilted view) and 10 nm^{-1} (FFT). Figures adapted with permission from ref 152. Copyright 2022 Spinger Nature. (c−e) Three regions of distinct superstructures, namely, monoclinic (yellow), cubic diamond (blue), and hexagonal diamond (green) lattices, are color-coded accordingly. Scale bars: 50 nm. Figures adapted with permission from ref 151. Copyright 2022 American Chemical Society.

lattices because they have the highest packing efficiencies among all of the periodic and aperiodic packing possibilities, while the DDQC packing has the highest facet−facet contact area and is therefore preferred in type II assembly regimes. This finding highlights the ability of DNA to stabilize colloidal organizations that are otherwise unstable and also reiterates the importance of enthalpy in colloidal systems. Indeed, the pursuit of low-symmetry colloidal superlattices via the enthalpy-driven colloidal crystallization of low-symmetry building blocks is a nascent field and there are many more systems that can be explored.

3.4.3. Packing of Mixtures of Convex Polyhedra. The rich assembly behavior discussed thus far has focused on systems with a single type of convex polyhedron. By comparison, the coassembly of two or more convex polyhedra is less well-understood. Computationally, it is significantly more challenging to determine the most favorable copacking of multiple polyhedral species than of a single one. Experimentally, however, it is not significantly different to study the crystallization process with multiple species than of a single species, if the nanoparticles of the desired shapes and dimensions can be prepared. Either way, the overarching challenge is predetermining which shapes will coassemble rather than undergo single-component phase separation.

This challenge was recently addressed by considering the shape complementarity of mixtures of polyhedra. Two exemplary pairs of shapes that can fill the space cooperatively and with 100% efficiency were identified: cuboctahedra with octahedra and octahedra with tetrahedra (Figure 21).[80] To align the enthalpic driving force for assembly with this entropic driving force, the particles were functionalized with self-complementary DNA such that every particle had an attractive interaction for every other particle. Within a single assembly, the shape complementarity of the two polyhedra ensures that, in their corresponding space-filling configurations, the most densely packed arrangement is obtained via the maximization of facet registration and DNA hybridization. As predicted, experimental assemblies of cuboctahedra and octahedra with the same edge lengths generated a *CsCl*-type lattice (Figure 21a), while octahedra and tetrahedra with the same edge lengths assembled into a *ccp* lattice (Figure 21b). These results emphasize that the structural outcomes of densely packed assemblies can be designed by maximizing DNA hybridization through shape complementarity.

To develop this concept further, a compartmentalization strategy was employed to reduce the symmetry of cocrystallized structures while maintaining shape complementarity.[80] Specifically, bitetrahedra and decahedra were reimagined as compounds of two and five face-sharing tetrahedra, respectively. Octahedral and bitetrahedral nanoparticles with the same edge lengths crystallized into a new lattice with reduced symmetry (hexagonal rather than cubic) while maintaining 100% space-filling efficiency (Figure 21c). Intriguingly, octahedral and decahedral nanoparticles with the same edge lengths crystallized into a quasi-space-filling layered configuration, where each layer was composed of edge-sharing decahedra, connected by octahedra. The symmetry of these lattices conforms to the quasi-periodic Penrose P1 tiling, but it is repeated infinitely out-of-plane (Figure 21d). It is important to identify interspecies shape complementarity because it can drive purely shape-driven colloidal crystallization toward a predesigned structure.

In addition to purely geometric packing, enthalpy-driven assembly offers opportunities for forcing the coassembly of different species. For example, concave and convex cubes can be assembled in an alternating fashion, the most stable

https://doi.org/10.1021/acs.chemrev.4c00299
Chem. Rev. 2024, 124, 11063−11107

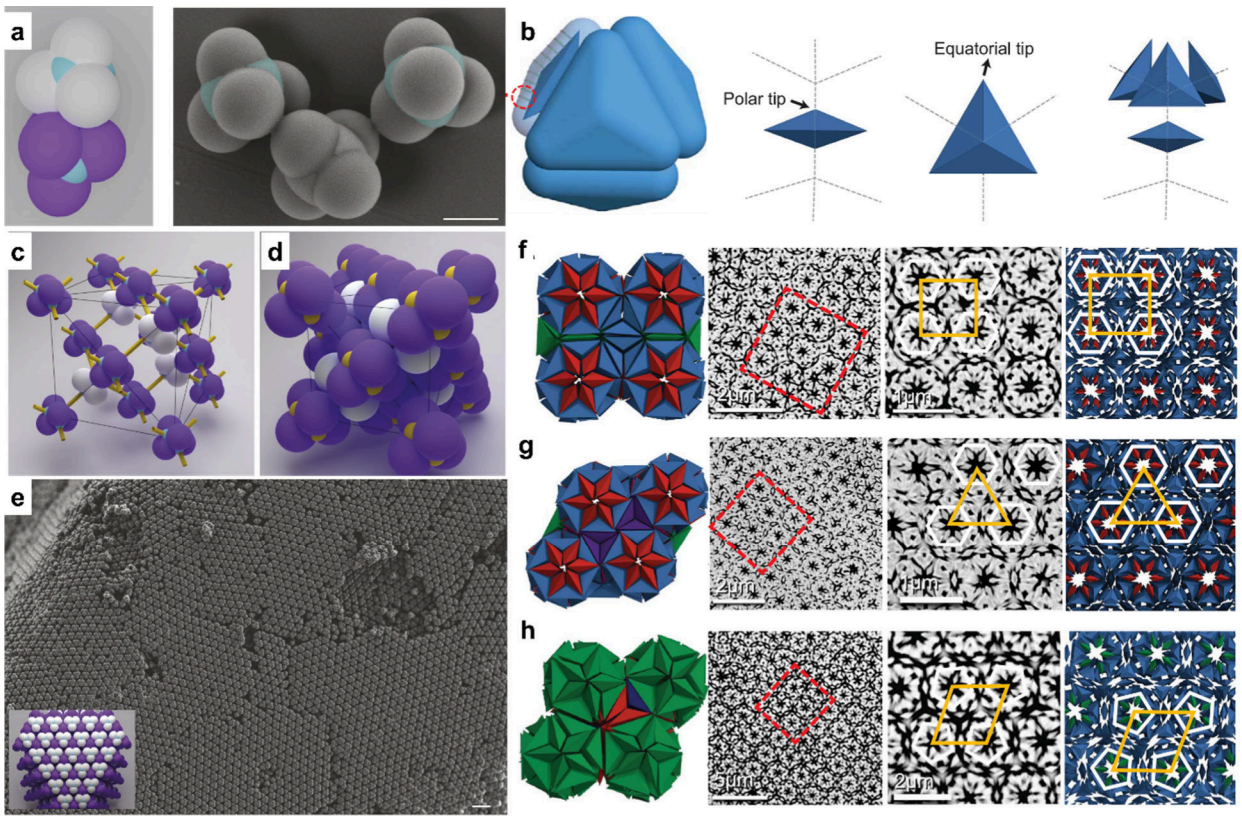

Figure 19. Organization of building blocks related to tetrahedra. (a, c–e) Colloidal cubic diamond lattice assembled from DNA-modified compressed tetrahedral patchy clusters. (a) Model (left) and SEM image (right) of compressed tetrahedral clusters. Some patches are highlighted in light blue. Scale bar: 1 μm. (c, d) Unit cell of a cubic diamond crystal of patchy cluster. In (c), clusters have been shrunk to make the bonding between patches visible, while in (d) the clusters are the correct size. (e) SEM images of the {111} plane of colloidal diamond crystals. Inset, a computer-generated image of the {111} plane. Figures adapted with permission from ref 153. Copyright 2020 Springer Nature. (b, f–h) Clathrate colloidal crystals assembled from DNA-functionalized blunt TBP Au nanoparticles. (b) Schematic illustrations of the blunt TBP and tetrahedral clusters of TBPs. (f–h) Colloidal crystal analogues of clathrate I oriented along [100] (f), clathrate IV oriented along [0001] (g), and clathrate II oriented along [110] (h). Figures adapted with permission from ref 71. Copyright 2017 The American Association for the Advancement of Science.

outcome among all two-component combinations of flat, concave, and convex cubes.[43] Similarly, flat cubes and small nanodisks can be assembled into an alternating lattice with *sc* symmetry, while larger disks force the structure to adopt a linear form, rather than a 3D network due to steric hindrance.[43] Compared with spherical cocrystallization, the study of the cocrystallization of multiple polyhedral shapes is still in its infancy. Numerous reasonable designs can be implemented and more parameters (including shape, size, and stoichiometry) can be explored to enhance this exciting new area of colloidal crystal engineering and increase its complexity.

3.4.4. Packing of Concave Polyhedra. The discussion of the type II assembly of 3D particles has focused on face-to-face contact, which is the dominant mode of interaction for convex polyhedra. However, additional interaction modes, such as edge-sharing or corner-sharing, become relevant in the context of the assembly of concave polyhedra. For example, upon slow-drying, the assembly of arrow-shaped Au nanoparticles on surfaces resulted in two competing local motifs: face-sharing packing, which produces a relatively loose structure, and interlocked packing, which allows for a denser structure.[155−157] These nanoarrows tend to pack via their (111) facet when assembled as a monolayer, likely due to their structural similarity to extended octahedra. This organization leads to two structures, purely driven by face-to-face packing, that mirror the *cmm* and *pgg* arrangements discussed previously for tessellating rhombic plates in 2D (Section 3.3.2). More complex packings involving different degrees of interlocking also arise and were identified as Zipper, Weave-I, and Weave-II structures (Figure 22).[156] When packed in 3D, a rhombohedral structure (Figure 22f, g) with a clearly identifiable rhombohedral crystal habit was observed as the dominant product. This rhombohedral packing of nanoarrows is an elongated version of the *bcc* packing of octahedra. Interestingly, a unique *monoclinic* structure that relies on the packing of residual (100) facets and results in a square in-plane packing was also discovered (Figure 22h). The propagation of the square 2D pattern via out-of-plane (111) facet interactions leads to an oblique stacking angle and is responsible for the observed monoclinic symmetry.

Highly branched shapes commonly noted as tetrapods and octopods are another distinct class of concave NCs (Figure 23). Although they deviate substantially from their convex forms, the assembly of these shapes still follows volume and energy minimization rules. Three possible local interactions exist when tetra- and octopods assemble: 1) tip-to-tip, 2) edge-to-edge, and 3) interlocked edge contacts. In any given system, the relative contributions of each of these interactions in the formation of the overall structure can be tuned via the assembly conditions because no interaction is necessarily dominate.

https://doi.org/10.1021/acs.chemrev.4c00299
Chem. Rev. 2024, 124, 11063−11107

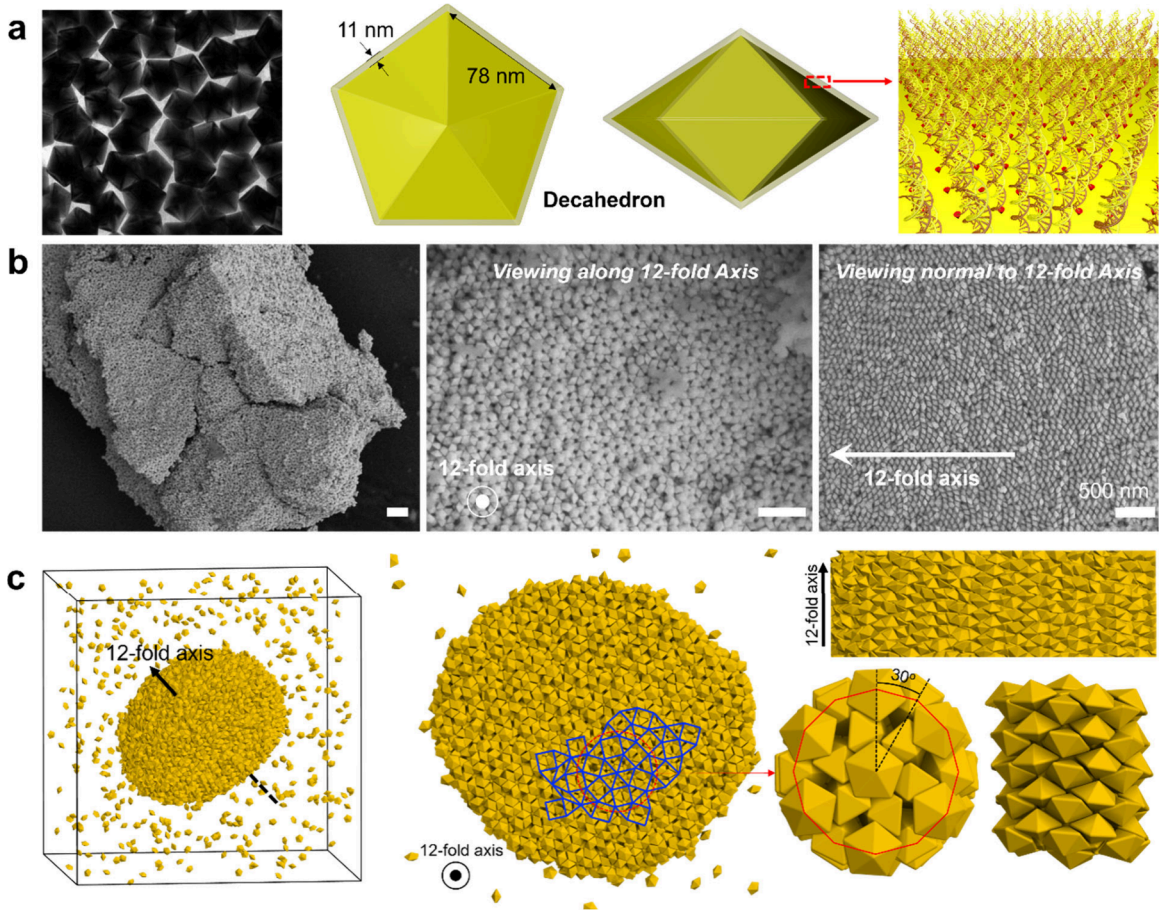

Figure 20. Organization of decahedral building blocks. (a–c) Schematic illustrations of experimental and simulated dodecagonal quasicrystals (DDQCs) assembled from DNA-functionalized decahedral NCs (edge length = 80 nm). (a) Schematic illustrations of decahedral NCs functionalized with short, flexible DNA strands. (b) SEM images of DDQCs assembled from DNA-functionalized decahedral NCs. Scale bars: 500 nm. (c) MD simulation results of DDQCs assembled from decahedral particles. Figures adapted with permission from ref 61. Copyright 2023 Springer Nature.

Tetrapods have relatively few assembly modes due to their low symmetry and number of branches. The most classic packing fashion—the monolayer—is driven by tip-to-tip interactions. In this case, only three of the four branches of each tetrapod are used for assembly, resulting in a triangular close-packed 2D structure (honeycomb) in which tetrapods are equally likely to adopt two different orientations (Figure 23a).[158] If assembly is instead driven only by edge-sharing interactions, two types of assemblies are possible: 1D chains that share four edges between each of two neighboring tetrapods and 2D nets that share two edges between each pair of neighboring tetrapods.[159] The 1D structure can grow infinitely, but it does not easily pack into a 3D lattice because its direction of propagation does not align with any rotational axis of the tetrapod building blocks. In contrast, the 2D structure does not have long-range order, and tetrapods instead form a tiling of a mixture of pentagons and hexagons (Figure 23b, c). Both pentagonal and hexagonal SBU can be formed because the edge angle of tetrapods (109.5°) lies between that of regular pentagons (108°) and hexagons (120°). A honeycomb net (relying on 6-fold symmetry) can be observed as one of the 2D tessellation products, but due to the mismatch-induced structural strain (109.5° < 120°), they do not extend over large areas. These pentagons and hexagons are not always flat shapes, so additional strain could result in structural instabilities during the propagation of 2D nets and also hinder the possibility for 3D structures.

The organization of octopods, distinct from their tetrapodal analogues, often results in highly ordered structures in 1-, 2-, and 3D.[160−163] Unlike tetrapods, octopods form one predominant 1D structure under most circumstances. These long, interlocked chains have two alternating repeating units, which involve four tip-to-tip connections between two so-called "muscle" octopods in two neighboring unit cells,[161] and one "skeleton" octopod that interlocks with both neighboring muscle octopods. Therefore, the tips of the muscle octopods are in contact with other tips, and all of their edges are interlocked by the skeleton octopods. However, the tips and edges of the skeleton octopods remain available for interaction, allowing these 1D chains to propagate to form a 3D superlattice in which skeleton octopods interact with each other by edge-sharing motifs. In this case, a 2D net of edge-sharing crosses (with 72° angles, Figure 23e) is produced. This propagation can happen simultaneously in two perpendicular directions, generating a network through which each skeleton octopod shares its four edges (Figure 23d). The resulting hierarchical superlattice has an overall tetragonal symmetry.

Although edge-to-edge and tip-to-tip packings of 3D nanoparticles usually arise from their concavity, favorable edge-sharing or tip-to-tip interactions can also be observed for

https://doi.org/10.1021/acs.chemrev.4c00299
Chem. Rev. 2024, 124, 11063−11107

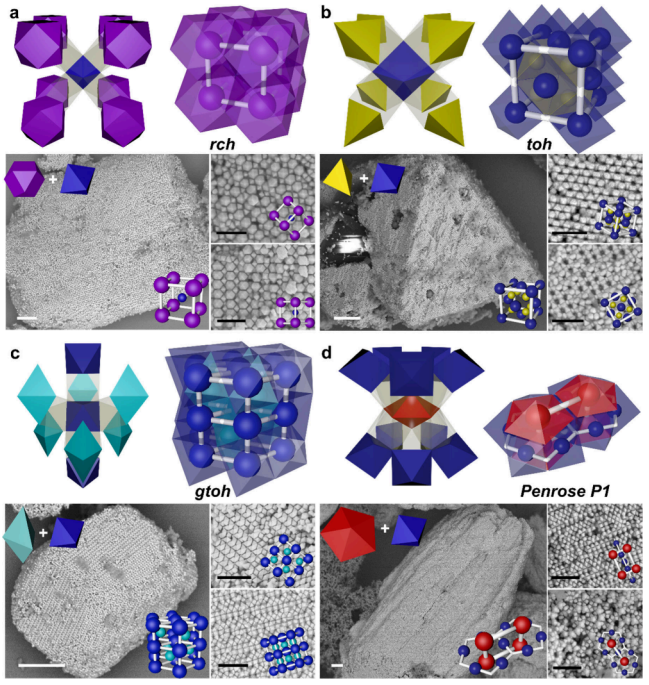

Figure 21. Co-crystallization of polyhedral building blocks based on shape complementarity. (a–d) Schematic illustration and SEM images of space-filling configurations with (a) rectified cubic honeycomb (*rch*) structure formed from cuboctahedra and octahedra (edge length, L = 95 nm), (b) tetra-octa honeycomb (*toh*) structure formed from tetrahedra and octahedra (L = 82 nm), (c) gyrated tetra-octa honeycomb (*gtoh*) structure formed from bitetrahedra and octahedra (L = 78 nm), and (d) Penrose P1-like quasi-space-filling structure formed from decahedra and octahedra (L = 85 nm). Scale bars: 2 μm; inset scale bars: 500 nm. Figures adapted with permission from ref 80. Copyright 2024 The American Association for the Advancement of Science.

convex particles due to heavy ligand functionalization or spatial confinement. The functionalization of nanocubes with long, rigid ligands can result in tip-to-tip assembly, which can be understood as a symmetry reduction process that favors the corners of cubes over their facets (as noted in Section 2.3.1). Confined spaces, on the other hand, give rise to a much more complicated range of assembly outcomes. For example, when octahedral nanoparticles are slowly dried on a surface, recent studies have revealed that edge-sharing packing motifs can be realized, resulting in one of two superlattices, hexagonal or cubic, depending on whether the facets or vertices are touching the substrate.[164] When the assembly of octahedra is confined to circular cavities on surfaces, a series of exotic arrangements result depending on the relative cavity size.[165] These clusters are often highly symmetrical, with two-, three-, four-, five-, and six-fold symmetries observed when different template sizes were employed.

3.4.5. Packing of Hollow Polyhedra. Hollow nanoparticles, such as nanoframes and nanocages, are a distinct class of colloidal building blocks where the internal volume is deliberately etched away. The etching process removes some or all of the particle's facets: nanoframes are particles from which all facets have been removed, leaving only the edges of a polyhedron, whereas nanocages retain some of the facets. The absence of facets strongly impacts the crystallization behavior predicted by the type II assembly processes, where face-to-face interactions dominate the assembly outcome. Our laboratory recently addressed the DNA-programmed assembly of hollow nanoparticles and discovered that the enthalpy-driven crystallization of porous nanoframes relies on an "edge-tiling" mode of assembly,[62] which is distinct from that typically seen in assemblies of solid polyhedra. In contrast, the organization of nanocages, with their partial facets, is still dominated by facet–facet attractions, like is seen with solid polyhedra.

The edge-tiling assembly outcome observed for nanoframes of convex polyhedra depends on the outline shape of the original structure from which it was derived: if the polyhedral shape is space-filling, edge-tiling will produce the same space-filling configurations, that is, cubic nanoframes assemble into *sc* lattices and truncated octahedral nanoframes assemble into *bcc* lattices (Figure 24). If, however, the polyhedral shape is nonspace-filling, edge-tiling produces a cospace-filling configuration, whereby the absent, complementary polyhedra are defined as structural voids. For example, it was noted earlier

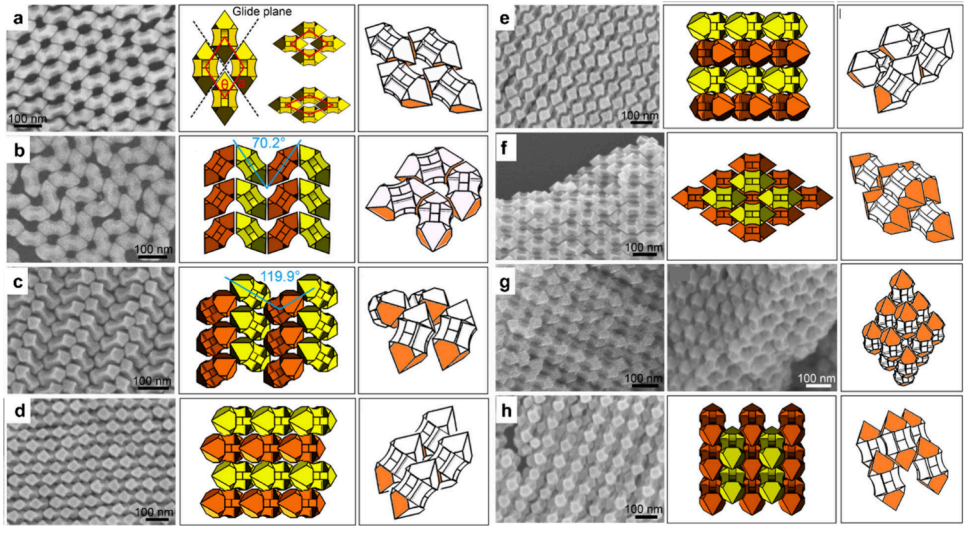

Figure 22. Surface-bound, organization of concave polyhedral nanoarrows to form (a–e) 2D and (f–h) 3D superlattices upon slow-drying. SEM images and geometric models of Net-I (a), Net-II (b), Zipper (c), Weave-I (d), Weave-II (e), Net-III (f, g), and Weave-III (h) structures. Scale bars: 100 nm. Figures adapted with permission from ref 156. Copyright 2017, The American Association for the Advancement of Science.

https://doi.org/10.1021/acs.chemrev.4c00299
Chem. Rev. 2024, 124, 11063–11107

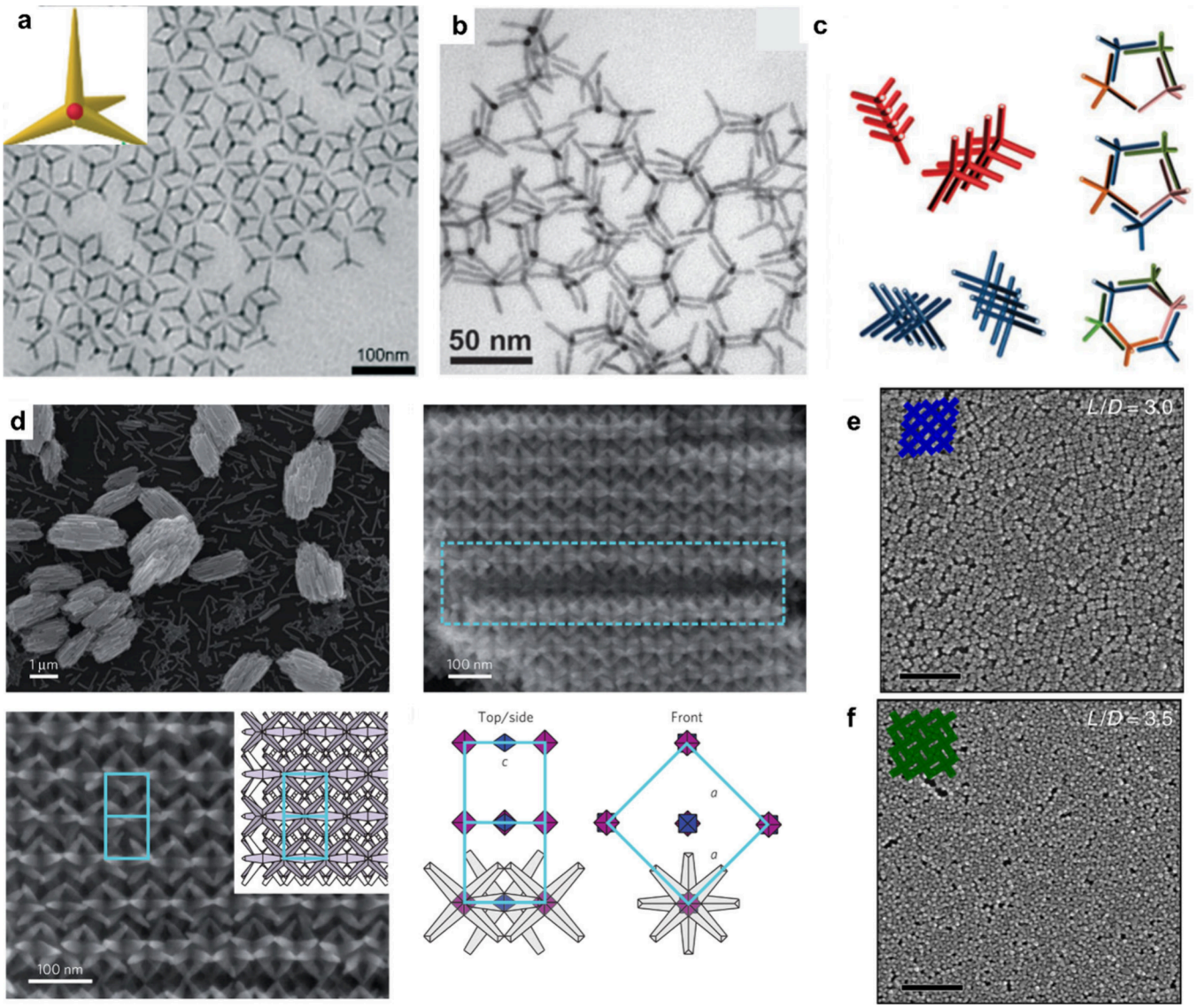

Figure 23. Organization of branched building blocks. (a) TEM images of an assembled monolayer of uniform CdSe@CdS tetrapods. Figures adapted with permission from ref 158. Copyright 2017 Royal Society of Chemistry. (b, c) Assemblies of ZnTe/CdTe tetrapods into honeycomb-like networks (b), formed with poly(methyl methacrylate) (PMMA) present in solution. Models of the various assemblies are sketched in (c). Figures adapted with permission from ref 159. Copyright 2011 Royal Society of Chemistry. (d) SEM images and models illustrating hierarchically assembled CdSe octopods into tetragonal superlattices. After the addition of acetonitrile to an aged solution of octopods in toluene, 3D clusters are formed, as revealed by SEM after deposition on a silicon substrate. Figures adapted with permission from ref 161. Copyright 2011 Springer Nature. (e, f) High-resolution SEM images of surface-assembled planar superlattices of octopods with different ARs. Octopods with a small AR stand on four pods in square lattice domains (f). Scale bars: 200 nm. Figures adapted with permission from ref 162. Copyright 2018 Springer Nature.

that solid octahedra and tetrahedra coassemble into a space-filling configuration (Figure 21b). Accordingly, octahedral nanoframes assemble into *cubic close packed* (*ccp*) lattices, leaving two sets of tetrahedral voids in alternating orientations. Similarly, cuboctahedral nanoframes assemble into *bct* lattices, leaving two sets of square pyramidal voids in alternating orientations. Notably, the registry of neighboring nanoframes creates large open channels inside the colloidal crystals, which can then be used to accommodate colloidal guest species.

The assembly of nanocages is like that of solid polyhedral nanoparticles, in that selective facet registration is the primary driving force. Truncated octahedral nanocages that retain their (100) facets assemble into *bcc* lattices, allowing registry of all remaining facets; likewise, truncated cubic nanocages with retained (100) facets assemble into *sc* lattices with full facet registry. Although the symmetries are often the same as the very "open" assemblies of the corresponding nanoframes, superlattices composed of nanocages are much more "closed." This route enables the rational tuning of the macro-porosity of these open channel superlattices (Figure 24).

3.5. Organization of Proteins

Proteins are a distinct class of nanoparticle that, at first glance, may seem to have little in common with their inorganic nanoparticle counterparts: proteins are typically smaller (1−20 nm vs 30−1000 nm), less chemically robust, and unable to support the same high ligand densities that inorganic nanoparticles can.[166] The surface of a protein is inherently chemically anisotropic, with each surface amino acid exhibiting different properties based on its chemical composition and local environment. This rich chemistry allows proteins to

https://doi.org/10.1021/acs.chemrev.4c00299
Chem. Rev. 2024, 124, 11063−11107

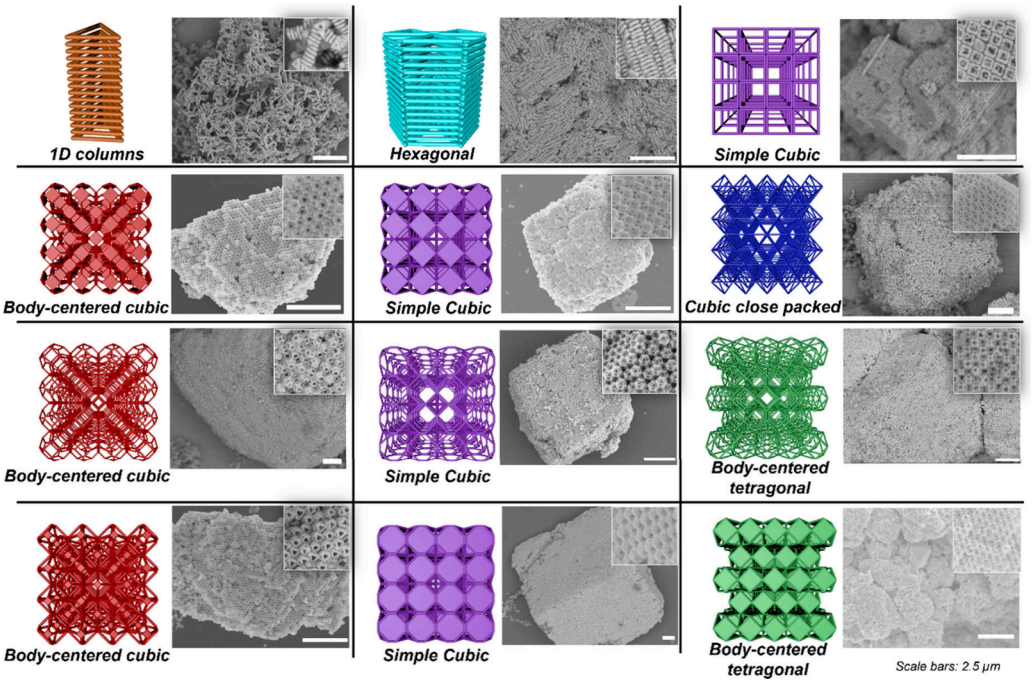

Figure 24. Organization of hollow polyhedral building blocks, including nanoframes and nanocages, into open channel superlattices through DNA-mediated crystallization. Figures adapted with permission from ref 62. Copyright 2022 Springer Nature.

interact with other species in a variety of ways, including through the hydrophobic effect, ion-pairing, disulfide linkages, and hydrogen bonds, leading to a surfeit of native protein−protein interactions. Therefore, to direct assembly toward desired anisotropic outcomes, favorable enthalpic interactions must be introduced that override a protein's inherent desire to assemble (or not). Thus, many of the concepts articulated already in this review are applicable to proteins and their assembly into larger collections of structures. Therefore, rather than comprehensively surveying this field, as was recently done by Tezcan and co-workers,[167] this section highlights how the concepts listed in Section 2, such as shape complementarity and valency, have been applied, understood, and developed in the context of protein-based materials.

3.5.1. Symmetry-Based Protein Assembly. Shape complementarity is a powerful means to predict and design the packing of anisotropic objects (as noted in Section 2.3). Implicit in this approach is the requirement that the objects' symmetries are compatible with tiling a 2D plane (in one of 17 plane groups) or filling a 3D volume (in one of 230 space groups). Consequently, shape complementarity may equivalently be considered a requirement for compatible symmetries.

Symmetry is a ubiquitous feature of naturally occurring proteins, many of which exist as dimers, trimers, or larger oligomers defined by a C_n rotation axis. In 2001, Yeates and co-workers recognized that the inherent tendency of such proteins to self-associate into specific oligomers could be harnessed to design extended protein arrays.[171] Specifically, it was proposed that two protein monomers with different oligomer symmetries could be tethered to produce a fusion protein that forms larger assemblies (Figure 25a). Yeates and co-workers articulated "construction rules" that predict the geometric outcome of assembly based on the symmetry elements of the protein oligomers and the relative placement of those symmetry elements in 3D space (most commonly, the angle between two

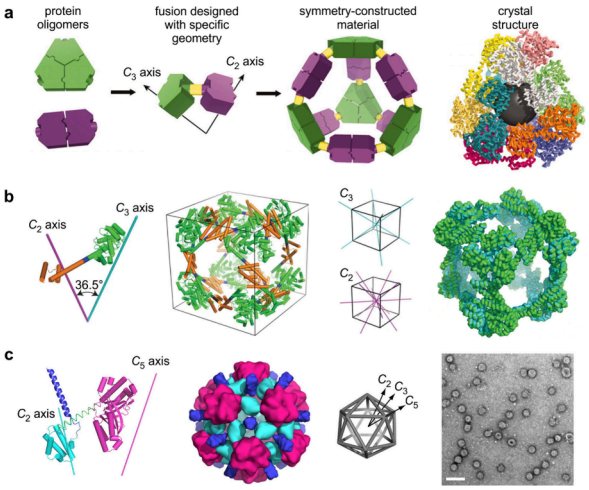

Figure 25. Symmetry-based protein fusions for protein cage design. (a) Protein fusions constructed from individual monomers that naturally form C_n-symmetric oligomers assembly into protein cages. (Right) The 50 Å void in the center of the designed tetrahedron is depicted as a black sphere. Figure adapted with permission from ref 168. Copyright 2012 The American Association for the Advancement of Science. (b) Controlling the angle between symmetry axes programmed assembly into a cube-like structure with O symmetry. The crystal structure (right, green ribbon) closely reproduces the design model (right, cyan ribbon). Figure adapted with permission from ref 169. Copyright 2014 Springer Nature. (c) Sixty copies of a protein fusion containing three components assemble into an isocahedral cage, visualizable by TEM. Scale bar: 100 nm. Figure adapted with permission from ref 170. Copyright 2020 American Chemical Society.

C_n axes, Figure 25). Using this strategy, a tetrahedron was constructed from 12 protein fusions, each comprising a trimer-forming protein fused to a dimer-forming protein via a short helical peptide. Assemblies larger and smaller than 12 subunits

https://doi.org/10.1021/acs.chemrev.4c00299
Chem. Rev. 2024, 124, 11063−11107

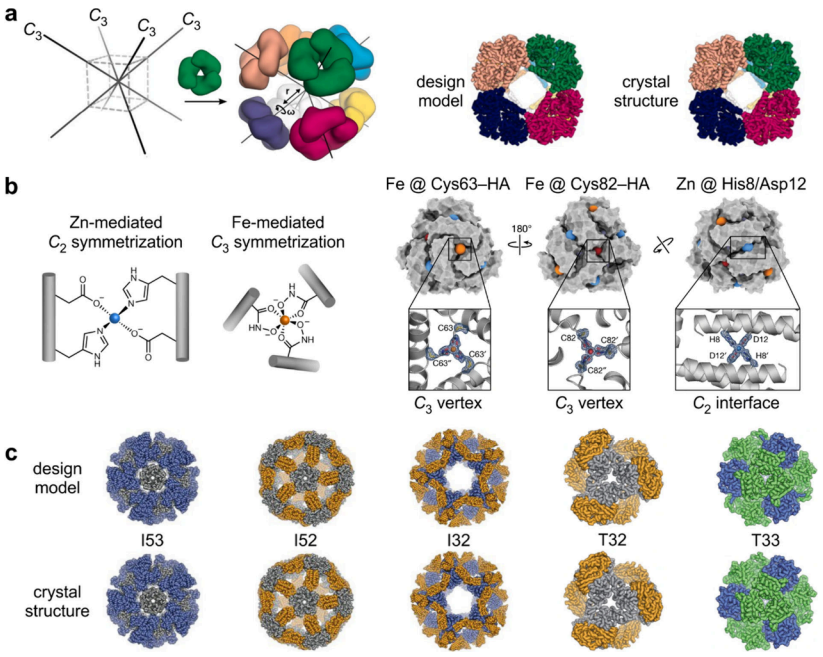

Figure 26. Designed interactions for protein cage assembly. (a) An octahedron constructed from trimers positioned at each C_3-axis of a cube. Figure adapted with permission from ref 175. Copyright 2012 the American Association For The Advancement Of Science. (b) Metal-mediated symmetrization generates C_3 vertices and C_2 interfaces. Figure adapted with permission from ref 174. Copyright 2020 Springer Nature. (c) Icosahedra (I*xx*) and tetrahedra (T*xx*) realized through computational design, where *x* denotes the C_n symmetry of each polyhedron's constituent oligomers. Figures adapted with permission from ref 176. Copyright 2016 The American Association for the Advancement of Science.

were also observed and were attributed to polymorphism induced by flexibility in the helical linker. Subsequent studies employed a more rigid linker to deliberately orient the two proteins with an intersymmetry axis angle of 54.7° (i.e., approximately half the ideal angle for a tetrahedral geometry (109.5°)).[168] The fusion protein assembled into a 12-subunit tetrahedron whose structure could be solved by single-crystal X-ray crystallography (Figure 25a, right). Reducing the angle further to 36.5° (i.e., approximately equal to the angle of intersection (35.3°) between the C_2- and C_3-axes in octahedral symmetry, O), yielded a cube with O symmetry (Figure 25b).[169] Subsequently, a three-component fusion, containing a dimer-forming, a trimer-forming, and a pentamer-forming protein, assembled into a 60-subunit icosahedron (Figure 25c).[170] Recently, Laniado and Yeates elaborated a "complete multiplication table" for such symmetry-combination material that articulates a roadmap for designing specific 2D and 3D structures from symmetry principles.[172]

This symmetry-based approach to generating protein polyhedra has proven to be equally powerful when coupled with computational design. In an early example, Baker, Yeates, and colleagues constructed protein tetrahedra and octahedra by first "docking" trimeric proteins on the C_3-axes of each polyhedron and subsequently optimizing the protein sequence to introduce favorable protein−protein interactions between adjacent trimers (Figure 26a, left).[172] Crystal structures of the resultant single-component 12-meric tetrahedron and 24-meric octahedron showed excellent agreement with the computationally designed models (Figure 26a, right). A similar approach was used with 20 trimers to generate a 60-subunit icosahedron (Figure 26).[173]

While the examples mentioned above depend on using protein oligomers with inherent C_n symmetry, the Tezcan group reported an alternative strategy to program C_n-symmetric assembly possibilities into an otherwise non-assembling protein monomer using metal-coordination (Figure 26b).[174] Using site-directed mutagenesis and chemical modification, two sets of metal-binding sites were engineered onto the protein surface: C_2-symmetric Zn^{2+}-binding sites via histidine and aspartic acid and C_3-symmetric Fe^{3+}-binding sites via hydroxamate-capped cysteine. The metal-induced assembly of different protein mutants produced cages with either six- or 12-subunits.

The high degree of symmetry and homomeric design of single-component protein cages produce structures that, overall, are only weakly anisotropic. Later work by the Baker lab, where two-component cages were used, showed how two proteins with different oligomerization geometries could be designed to coassemble. This method directly parallels the fusion approach of the Yeates group except that, rather than being tethered by a short peptide linker, the two self-associating proteins interact through an additional, computationally optimized protein−protein interaction (Figure 26c). Geometries that have been realized include tetrahedra (from a mixture of trimers and dimers)[177] and icosahedra (from either pentamers and trimers or pentamers and dimers, Figure 26).[176] The assembly process for icosahedra was found to be highly cooperative.[178]

Though shape complementarity (or symmetry compatibility) is a reliable design approach, a recent protein cage based on the Archimedean snub cube highlights that geometric constructions that are mathematically imperfect may still be physically plausible. Heddle and co-workers discovered that an 11-meric protein toroid in which each monomer is mutated to bear a single cysteine surface residue, assembles into a snub cube protein cage mediated by S−Au−S interactions (Figure 27).[179] The authors describe this structure as a "paradoxical cage" due to the inability of C_{11}-symmetric objects to assemble

https://doi.org/10.1021/acs.chemrev.4c00299
Chem. Rev. 2024, 124, 11063−11107

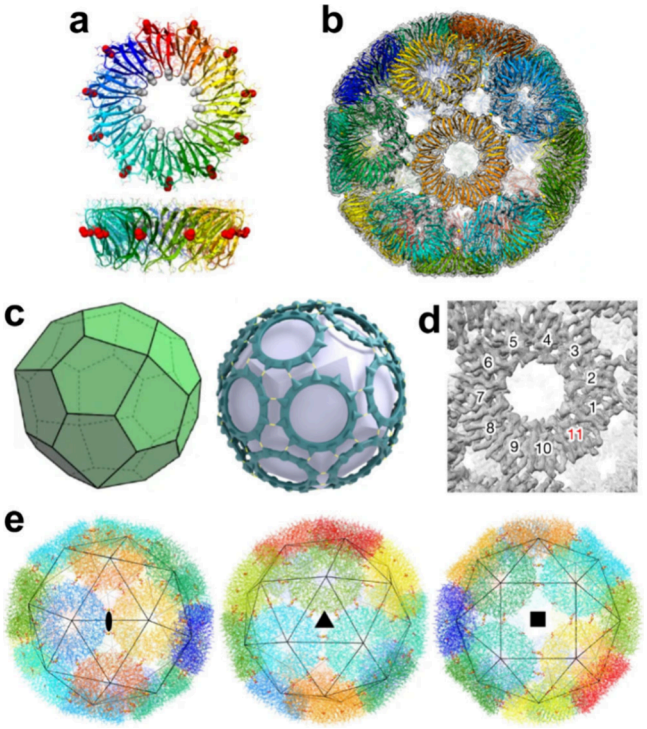

Figure 27. Assembly of a snub cube. (a) Cysteine mutations (red) on an 11-meric toroidal TRAP oligomer. (b) Left-handed cage assembled from 24 TRAP oligomers. (c) Snub cube (left) and overlay of C_{11}-symmetric protein rings on the surface of a snub cube (right). (d) Ten of 11 cysteine residues on each TRAP ring are able to participate in S−Au−S interactions. (e) Model of left-handed cage with each TRAP oligomer positioned on the vertex of a snub cube (black wire model). Figure adapted with permission from ref 179. Copyright 2019 Springer Nature.

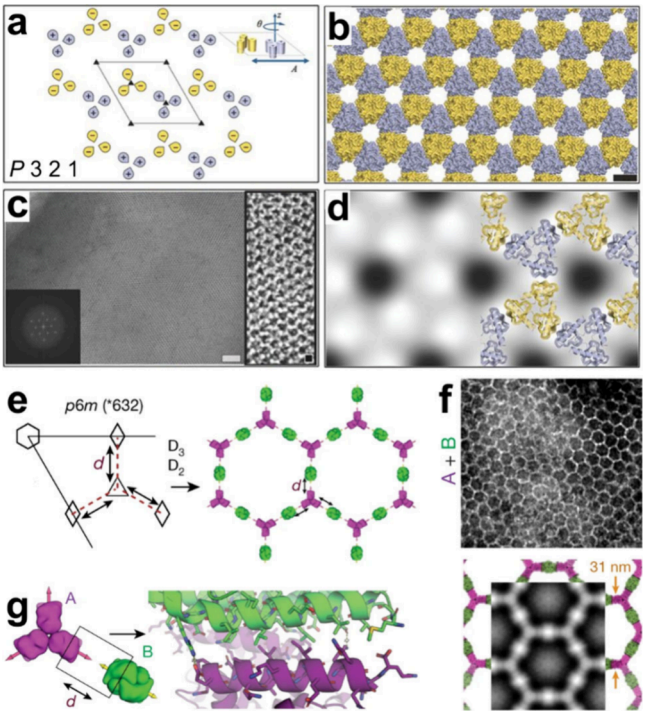

Figure 28. Computational design of 2D protein arrays. (a) *P*321 unit cell. (b) Model single-component protein array. Scale bar: 5 nm. (c) TEM images of protein array prepared in *E. coli*. FFT shown on right. Scale bar: 50 nm. (d) Calculated projection of the electron density map. Design model shown as an overlay. (a−d) Figures adapted with permission from ref 181. Copyright 2015 The American Association for the Advancement of Science. (e) Design strategy for a *p6m* 2D array from D_3 and D_2 oligomers. (f) TEM images of protein array prepared in *E. coli*. (g) Designed heterointerface. (e−g) Figures adapted from ref 182. Copyright 2021 Springer Nature.

into regular convex polyhedra. However, this apparently paradoxical structure can be rationalized by considering the dual shape of the snub cube, the pentagonal icositetrahedron, which is formed from 24 identical irregular pentagonal faces (Figure 27c). The 11-sided polygon circumscribed by the toroidal protein coincides almost perfectly with the irregular pentagon on the icositetrahedron's surface, permitting 10 of the 11 pendant cysteines on each toroid to participate in Au-mediated cross-links between proteins (Figure 27d). This result demonstrates that geometric imperfections can be tolerated with a sufficient enthalpic driving force.

In their original 2001 paper,[171] Yeates and colleagues proposed how their symmetry-based approach could be applied to extended 2D structures as well as finite assemblies such as protein cages (Figure 25). However, extended structures could not be realized at that time due to the challenge of making the connection between the two proteins within a fusion rigid enough to prevent alternative assembly pathways. This challenge was overcome by Noble and co-workers, who employed more highly symmetric building blocks as components for the fusion protein.[180] This higher degree of symmetry allowed a greater number of connections to be made between the two proteins within the protein fusion, thereby rigidifying the protein−protein bond, forcing the two symmetry axes to be parallel and directing the assembly of planar, 2D structures (Figure 28).

It has proven fruitful to combine computational methods with symmetry-based approaches for the design of extended protein arrays as it has been for discrete protein cages. The Baker lab designed ordered 2D protein structures by matching the internal point symmetry of cyclic oligomeric proteins with six different plane groups (Figure 28a−d),[181] selected because they were compatible with cyclic point symmetry and contained only two unique interfaces, one of which is the protein−protein interface within the oligomer. When this concept was expanded to include two different proteins (forming trimers and dimers, respectively), *p6m* lattices were the assembly outcome (Figure 28e−g).[182] The two components were differentially functionalized, leading to 2D materials that could modulate the clustering of receptors on cell membranes. Most recently, the symmetry-based approach was applied to design and prepare 3D protein assemblies, isolated as single crystals solved in the $F4_132$ and $I432$ space groups.[183] The $I432$ space group, constructed from protein trimers and tetramers, had been identified previously as a "potentially privileged" symmetry construction due to a lack of other plausible polymorphs accessible from these building blocks.[172]

3.5.2. Valency-Controlled Protein Assembly in 1D.

Valency is a foundational concept in chemistry that has inspired the design of increasingly sophisticated colloidal architectures (see Section 2.2). The preparation of these complex structures has relied on the ability to define the placement of interacting motifs at specific locations on the surface of a nanoparticle (see Figure 5 and Figure 8). Proteins offer a distinct advantage over inorganic nanocrystals in this

https://doi.org/10.1021/acs.chemrev.4c00299
Chem. Rev. 2024, 124, 11063−11107

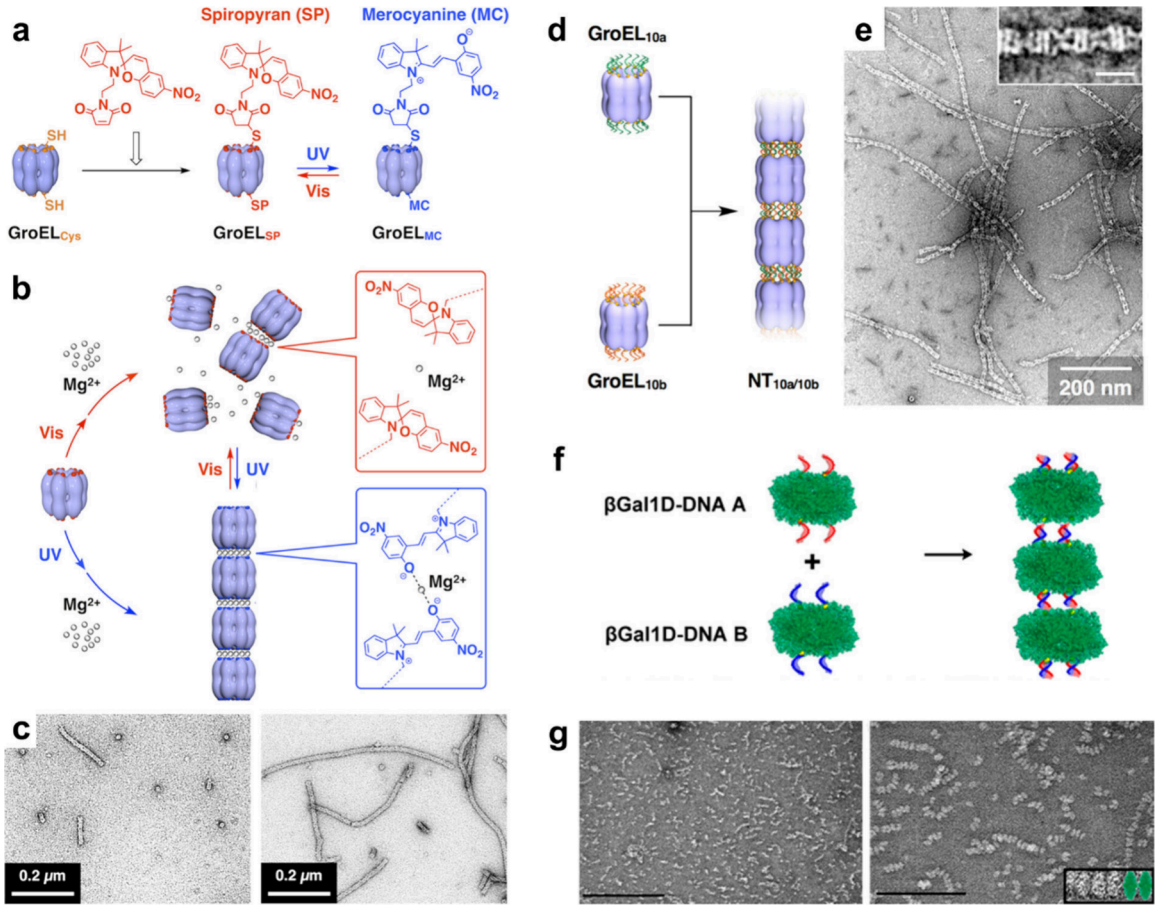

Figure 29. Ligand-directed formation of 1D protein assemblies. (a) GroEL functionalized with a photoresponsive ligand. (b) Irradiation of GroEL$_{SP}$ with UV light isomerizes the ligand to form a merocyanine capable of binding Mg^{2+}, inducing nanotube formation. (c) TEM of GroEL$_{SP}$ after a 15 min irradiation step with visible light (left) and after a 15 min irradiation step with UV light (right). (a–c) Figures adapted with permission from ref 185. Copyright 2013 American Chemical Society. (d) GroEL functionalized with complementary DNA forms nanotubes, visualized by TEM (e). (d, e) Figures adapted with permission from ref 186. Copyright 2018 American Chemical Society. (f) Two oligonucleotides on one face of a βGal monomer are sufficient to direct 1D assembly. (g) TEM images of βGal assemblies. Scale bars: 500 nm (left), 200 nm (right). (f, g) Figures adapted with permission from ref 187. Copyright 2018 American Chemical Society.

regard because the former are inherently chemically heterogeneous, permitting site-specific chemical functionalization via mutagenesis and/or chemical ligation. This synthetic capability has facilitated the exploration of bond number, directionality, and flexibility (see Section 2.2) in protein-based systems.

Many studies into ligand-based valency in protein-based systems have focused on homomeric protein oligomers because a single mutation to the amino acid sequence of one monomer is replicated multiple times due to the highly symmetric structure of the oligomer. Mougous and colleagues observed that the toroidal protein Hcp1, which is composed of six identical subunits, stacks in the solid state to form extended columns (Figure 29).[184] By mutating two amino acid residues on each monomer to cysteine residues, the researchers were able to induce the spontaneous formation of 1D Hcp1 nanotubes due to disulfide bond formation (Figure 29). The anisotropic distribution of sulfhydryl groups, which were confined to the top and bottom faces of the protein toroid, was sufficient to achieve highly directional assembly into nanotubes. Another Hcp1 variant with only one mutation, that is, displaying cysteine residues on only one face, was used as a chain-capping agent to control the length of the Hcp1 nanotubes (Figure 29).

The Aida group coupled site-specific mutagenesis with photoacid ligands to achieve photoresponsive nanotube formation (Figure 29a).[185] GroEL, a D_7-symmetric toroidal protein, was mutated to display cysteine residues on its top and bottom faces, which were functionalized with spiropyran molecules. Upon irradiation with UV light, spiropyran isomerizes to form merocyanine, which contains an anionic oxygen atom capable of binding metal cations. Consequently, UV irradiation of a solution containing spiropyran-functionalized GroEL and Mg^{2+} ions induced nanotube formation, which could be reversed by irradiation with visible light (Figure 29b, c). Length control could also be achieved in this system using a cyclic, but nondihedral, chain-capping protein.[188]

The unique properties of DNA that have enabled unprecedented control over colloidal crystallization have also been explored in the context of protein assembly. The Mirkin and Aida groups independently investigated how the site-specific attachment of DNA molecules onto the surface of proteins could be used to affect directional nanotube formation. Both groups showed that protein assembly proceeds when proteins are functionalized with complementary DNA sequences. The Aida group further explored how the strength of the DNA–DNA interaction affected the stability of protein

https://doi.org/10.1021/acs.chemrev.4c00299
Chem. Rev. 2024, 124, 11063–11107

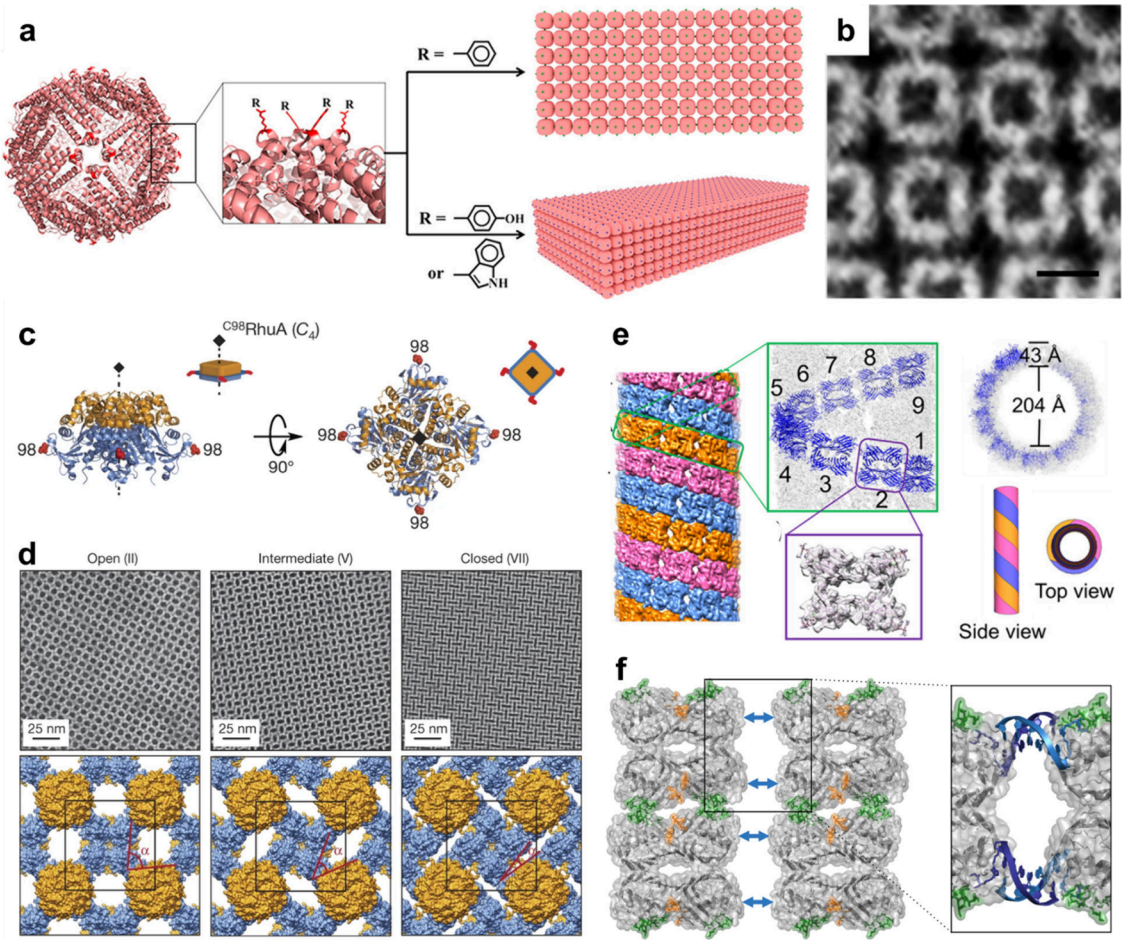

Figure 30. Protein organization into 2- and 3D materials via surface chemistry. (a) Ferritin cages crystallize into 2- and 3D arrays depending on the identity of the aromatic amino acids introduced around the C_4 axes of the protein cage. (b) Constructed electron density map from inverse FFT of a TEM image. Scale bar: 10 nm. (a, b) Figures adapted with permission from ref 189. Copyright 2018 American Chemical Society. (c) Tetrameric RhuA with a C98 mutation maintains C_4 symmetry and assembles into (d) auxetic materials that undergo continuous, collective movement between open and closed porous 2D structures. (c, d) Figures adapted with permission from ref 190. Copyright 2016 Springer Nature. (e) Soybean agglutinin assembles into helical nanotubes programmed by noncovalent RhB glycoconjugates. Figure adapted with permission from ref 191. Copyright 2016 American Chemical Society. (f) Quasi-tetrahedral ConA proteins bound to DNA glycoconjugates crystallize into layered structures (left), enabling DNA-programmable structural anisotropy along a single crystallographic axis (right). Figure adapted with permission from ref 192. Copyright 2021 American Chemical Society.

assemblies (Figure 29d, e).[186] A GroEL mutant functionalized with 15-bp DNA strands was coassembled with another GroEL mutant with either 10- or 15-bp DNA strands capable of either partial or full hybridization to the original 15-bp strand, respectively. Upon challenge with fully complementary15-bp DNA, the nanotubes assembled via 10-bp duplexes disassembled, whereas those held together by 15-bp duplexes persisted. In contrast, the Mirkin group sought to understand how many oligonucleotides are needed to define an anisotropic interaction.[187] Surprisingly, two DNA strands on a single face of β-galactose (βGal) were sufficient to define a cooperative protein−protein interface that led to specific, directional 1D assembly (Figure 29f, g).

3.5.3. Valency-Controlled Protein Assembly in 2- and 3D. The examples of 1D protein assembly discussed in the previous subsection were aided by the natural shape of the protein, which provided a contiguous, near-planar surface on which ligands or amino acid residues could interact. Programming the assembly of proteins into 2- and 3D structures would be severely limited if the same, plane-like surfaces were required for each interaction. Instead, approaches to program multidimensional protein assembly typically rely on small interacting patches, or point valency, analogous to the "patchy" particles discussed in Section 3.1.2. These patchy particles introduce another design parameter, bond flexibility (see Section 2.2.3), which can assist or hinder efforts to direct assembly toward specific outcomes, as will be discussed in this section.

One strategy to reduce bond flexibility is to use interacting motifs that are small with respect to the size of the protein being assembled. Zhao and co-workers deployed this approach to control the organization of 24-meric ferritin cages into 2- and 3D protein arrays (Figure 30a, b).[189] By mutating a single residue per protein monomer along the C_4 symmetry axes of the protein cage, the authors defined six multivalent patches on the protein surface, each comprising four aromatic amino acid residues. The assembly of 2D superlattices with strictly square planar packing was induced via substitution with phenylalanine residues, while the assembly of 3D superlattices with well-defined cubic packing were yielded when tyrosine or tryptophan were substituted. The dependence on amino acid

https://doi.org/10.1021/acs.chemrev.4c00299
Chem. Rev. 2024, 124, 11063−11107

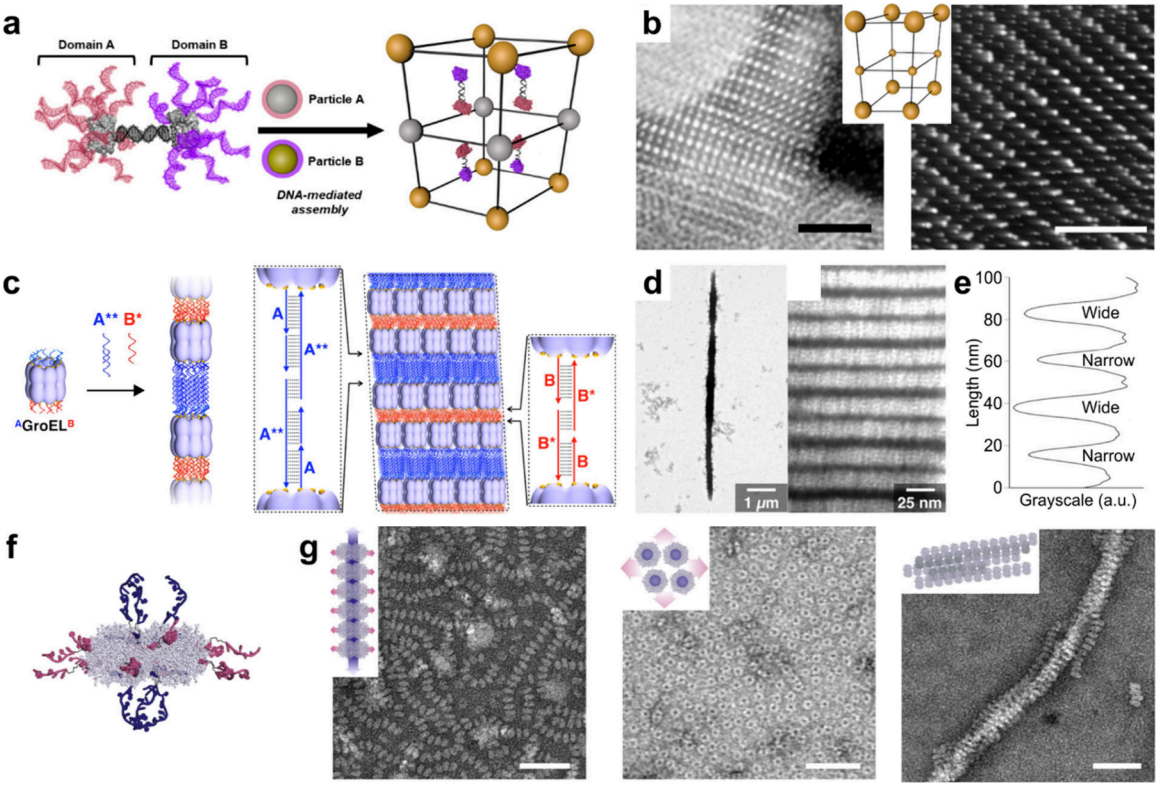

Figure 31. Protein structures programmed by anisotropic ligand functionalization. (a) A protein Janus nanoparticle decorated with two orthogonal DNA sequences interacts with two particles with respectively complementary DNA to form layered structures. (b) TEM images of thin (~60 nm) sections of a superlattice prepared from Janus proteins, 5 nm gold NPs and 10 nm gold NPs. Scale bars: 150 nm. (a, b) Figures adapted with permission from ref 195. Copyright 2018 American Chemical Society. (c) Janus GroEL, functionalized with two DNA sequences, assembles into dual-periodic lamellar structures in the presence of appropriate linker DNA strands. (d) TEM shows the periodic lamellar structure with (e) alternating wide and narrow dark regions (DNA). (c–e) Figures adapted with permission from ref 196. Copyright 2020 American Chemical Society. (f) DNA is spatially encoded on the surface of a toroidal homomeric protein, SP1, defining two directions (axial, purple; equatorial, pink). (g) TEM images of SP1–DNA conjugates with different DNA sequences. Left to right: axial only, equatorial only, strong axial-weak equatorial. Scale bars: 50 nm. (f, g) Figures adapted with permission from ref 197. Copyright 2021 National Academy of Sciences.

side chain was attributed to the different geometries of the $\pi-\pi$ interactions between aromatic groups.

In a similar vein, Tezcan and co-workers found that a single cysteine mutation to the surface of the C_4-symmetric tetramer rhamulose-1-phosphate aldolase (RhuA) effected 2D protein assembly mediated by cysteine-cysteine disulfide linkages in an orientation-specific fashion (Figure 30c).[190] The resultant 2D crystals of RhuA were essentially defect-free (defect frequency of 1 in ~9,000), which the authors attributed to the reversible nature of disulfide bond formation and the unexpected flexibility of the disulfide linkage, which contains five rotatable bonds. Remarkably, this disulfide flexibility also endowed the assemblies with dynamic, auxetic behavior, whereby a collective motion across the entire lattice converted the open, porous 2D lattice to a closed form (Figure 30d). These lattices were the first experimentally realized materials to exhibit a Poisson's ratio of −1, the thermodynamic limit for an isotropic 2D material. Later studies with glutamate-containing mutants introduced metal-induced structure switching,[193] and furthermore, variants harnessing dipolar interactions underwent hierarchical assembly on mica substrates.[194]

The examples by Tezcan and Zhao highlight how short interacting motifs, such as individual amino acid residues, can be used to program specific anisotropic assembly outcomes. This mirrors the enthalpically driven behavior of inorganic nanoparticles functionalized with ligands that are short compared to the size of the nanoparticle (see Section 3.4.1). Furthermore, these assembly outcomes imply that any native interactions between protein surfaces are dominated by the designed interactions, due to their strength and geometric inflexibility. In contrast, proteins functionalized with a small number of longer, more flexible ligands provide an opportunity for both native protein–protein and designed interactions to direct assembly outcomes. The Jiang group reported the formation of helical microtubule-like protein nanotubes constructed from a tetrameric lectin (sugar-binding protein), soybean agglutinin (SBA), and a synthetic conjugate containing *N*-acetyl-α-D-galactosamine (GalNAc) and a hydrophobic dye, rhodamine B (RhB).[191] Two supramolecular interactions—sugar-lectin binding and hydrophobic RhB-RhB dimerization—led to the formation of extended protofilaments that subsequently associated to form helical nanotubes (Figure 30e). Computational modeling suggests that the symmetry of the four sugar binding sites on the lectin were well-conserved in the filament structures. In contrast, the Mirkin group explored the use of DNA-mannose glycoconjugates to program the crystallization outcome of a tetrameric lectin, concanavalin A (ConA, Figure 30Figure 30f).[192] Single crystals of ConA bound to four DNA glycoconjugates with complementary DNA sequences could be obtained with sufficient resolution to visualize the DNA duplexes within the crystal lattice. Unexpectedly, changing the length of the DNA glycoconju-

https://doi.org/10.1021/acs.chemrev.4c00299
Chem. Rev. 2024, 124, 11063–11107

gates led to a change to the unit cell length along a single crystallographic axis, despite the quasi-tetrahedral symmetry of ConA. This observation was rationalized to be a result of the formation of emergent, non-native protein−protein interfaces and demonstrates that the relationship between valency defined at the molecular (protein) scale and anisotropy observed at the materials (crystal) scale may be a rich area for further exploration.

3.5.4. Programming Anisotropy via Ligand Design. Unlike their inorganic counterparts, proteins have surfaces that are inherently chemically anisotropic, providing additional opportunities to program anisotropy into protein assembly via multiple, orthogonally interacting ligands. DNA is particularly powerful because it binds in a sequence-specific manner. Mirkin and co-workers harnessed this property to create protein Janus nanoparticles in which orthogonal DNA sequences were grafted onto each half of a protein dimer (Figure 31a).[195] These Janus particles were assembled with mixtures of inorganic nanoparticles, each bearing a DNA sequence complementary to that on only one-half of the Janus particle. With this method, simple hexagonal lattices containing alternating layers of silver and gold nanoparticles or 5 and 10 nm gold nanoparticles (Figure 31b) were realized. Such structures had been previously inaccessible.

In a follow-up to their initial 1D nanotube studies the involved GroEL (Figure 29),[186] the Aida group utilized a similar Janus-type protein design to engineer 1D protein nanotubes with a dual-periodic sequence (Figure 31c).[196] Key to this approach was the preparation of a GroEL oligomer with different, complementary DNA sequences attached to its two faces, prepared via GroEL ring exchange and multiple runs of size exclusion chromatography. This asymmetry afforded a periodic lamellar structure to be generated with two alternating interlayer spacings throughout the lattice (Figure 31d, e).

Researchers in the Mirkin group utilized site-specific mutagenesis and two orthogonal biocompatible "click" reactions to attach multiple DNA strands to the surface of a toroidal protein, SP1 (Figure 31f, g).[197] The resultant one-pot DNA functionalization method enabled rapid access to proteins with spatially encoded patches of two different oligonucleotides. By varying the relative length and interaction energy of the two DNA sequences, the researchers programmed protein assembly via different hierarchical pathways, resulting in a variety of fibrillar and lamellar morphologies.

4. STRATEGIES TO ACHIEVE DESIGNER SUPERLATTICES

Assembly processes involving colloidal building blocks inherently aim to restrict the number of possible organized arrangements within a complex system via reversible interactions and shape complementarities. In isotropic systems, interaction strengths and sphere packing result in assembly outcomes that require substantial fine-tuning to be differentiated. The examples discussed in Section 3 highlight the major advantages of introducing anisotropy into a system and defining the directions and strengths of local interactions in organization processes (Figure 32). In this section, the key points of those case studies are synthesized and presented as an inverse design strategy, based on geometric considerations, to enable the synthesis of target colloidal superlattices on demand.

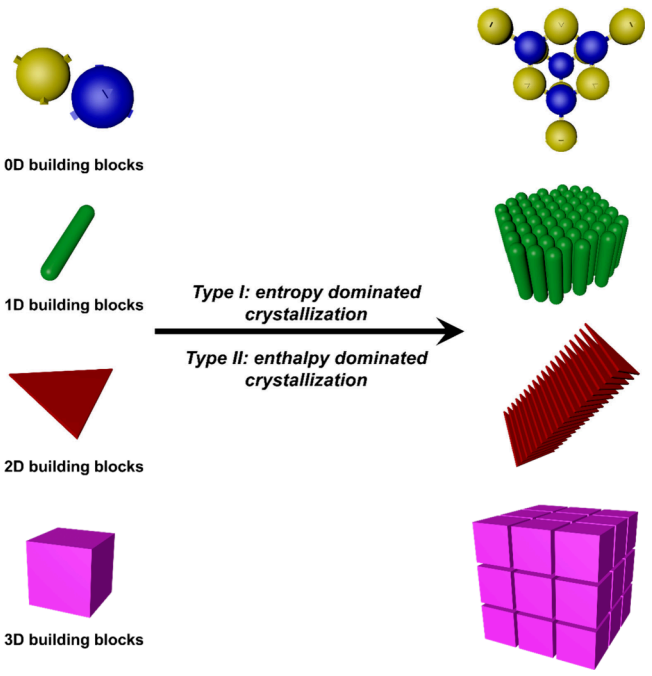

Figure 32. Graphical summary of the organization of building blocks over multiple dimensions.

4.1. Understanding and Deriving the Local Shape Complementarities of Polyhedra

Though it is known that space-filling polyhedra pack readily into their corresponding lattices, the vast majority of synthetically accessible colloidal building blocks do not fill space with 100% efficiency. Moreover, a general methodology to design or predict ideal packing arrangements based on geometric arguments has not yet been established. In this section, a new approach for the design of superlattices from nonspace-filling polyhedral nanoparticles based on the shapes of the building blocks is presented. This discussion is confined to the five Platonic solids: tetrahedra, cubes, octahedra, dodecahedra, and icosahedra because these represent exemplary case studies.

Clusters of polyhedra are first considered in which a central polyhedron enjoys perfect facet registry with the neighboring particles. These clusters necessarily adopt the symmetry of their dual shapes. Of the five Platonic solids, only the cluster of seven cubes (one central cube with six surrounding cubes bound to its six faces) can fill space perfectly, that is, propagate without introducing spatial voids. If periodic voids are allowed, there is another valid packing solution: a *CsCl* lattice formed by a single octahedron surrounded by clusters of nine octahedra (Figure 33). In this case, the periodic voids are stabilized by many toroidal tilings of eight octahedra (Figure 33b, c). However, even when voids are permitted, ordered propagations cannot be achieved through the perfect facet registration of single-component Platonic polyhedra. If, at this point, imperfect yet parallel facet registration (that is, incomplete registration) is allowed, a series of superlattices formed by tetrahedra, cubes, and octahedra would also be permissible. Clearly, ideal facet registration is not the sole consideration in such systems.

In the tessellation of 2D shapes (Section 3.3.2), shape complementarity does not arise from in-plane facet registration but rather is derived from the *plane* angles at the vertices of the

https://doi.org/10.1021/acs.chemrev.4c00299
Chem. Rev. 2024, 124, 11063−11107

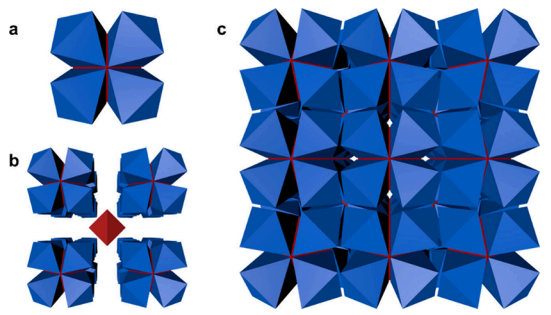

Figure 33. A CsCl-like 3D superlattice constructed from face-sharing octahedra. (a) A cluster of nine face-sharing octahedra, the center one colored in red. (b) One octahedron (red) surrounded by eight octahedral clusters (a), when compressed, eight clusters and one center octahedron will register their triangular faces. (c) A CsCl superlattice formed based on the construction method illustrated in (b).

nanoplates, specifically, the interior angles between the two edges. For example, three regular hexagons (interior plane angle = 120°), four squares (90°), or six equilateral triangles (60°) occupy a full 360° around a single point and can therefore tessellate with no gaps. Similarly, in 3D tessellations, the shape complementarity must derive from the 3D analogue of the plane angle, the *solid* angle, which is the interior angle bound by the *faces* around a polyhedral vertex. Given that a sphere has a solid angle of 4π steradians, solid angles will here be defined by their fraction of 4π steradians for ease of calculation. Therefore, a sphere has a solid angle of 1, and it follows that, for example, the vertex solid angle, Ω, of a cube is 1/8 because eight cubes arranged around a single vertex fill all of the space around that point (Figure 34a).

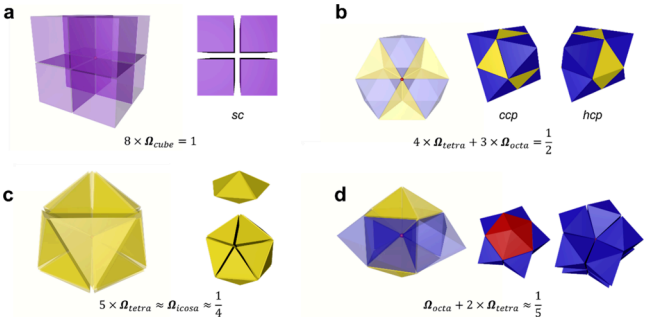

Figure 34. Shape complementarity relationships between platonic solids deduced from a corner solid angle perspective. In each case, space-filling is focused on the red dot at the center of the cluster (left). Schematic illustrations of (a) eight corner-sharing cubes locally filling all space, (b) four corner-sharing tetrahedra and three corner-sharing octahedra locally filling half of the space, (c) five corner-sharing tetrahedra approximately filling one-quarter of the space, and (d) one octahedron and two corner-sharing tetrahedra approximately filling one-fifth of the space.

To start, the vertex solid angles of Platonic solids are considered: Ω_{tetra} = 0.04387, Ω_{cube} = 0.125, Ω_{octa} = 0.10817, Ω_{dodeca} = 0.23569, Ω_{icosa} = 0.20965. By rounding these exact values, one can generate several instructive approximations:

$$8 \times \Omega_{cube} = 1 \tag{1}$$

$$4 \times \Omega_{tetra} + 3 \times \Omega_{octa} = \frac{1}{2} \tag{2}$$

$$5 \times \Omega_{tetra} \approx \Omega_{icosa} \approx \frac{1}{4} \tag{3}$$

$$\Omega_{octa} + 2 \times \Omega_{tetra} \approx \frac{1}{5} \tag{4}$$

In geometric terms, it follows from these approximations that 1) eight vertex-sharing corners of cubes can fill the space without gaps (Figure 34a); 2) four vertex-sharing corners of tetrahedra plus three vertex-sharing corners of octahedra can fill half of the space without gaps (Figure 34b); 3) five vertex-sharing corners of tetrahedra approximately equal to one corner of an icosahedron (Figure 34c); and 4) five vertex-sharing corners of octahedra plus ten vertex-sharing corners of tetrahedra can approximately fill the space (Figure 34d). Importantly, approximation (2) highlights the perfect shape complementarity between tetrahedra and octahedra (that is, they can coassemble in a specific ratio to fill space). This property can be utilized to generate various space-filling pairs: tetrahedra with octahedra, tetrahedra with truncated tetrahedra, and octahedra with truncated cubes, among others. Approximation (3) explains the ubiquitous existence of penta-twinned crystals in *fcc* symmetries and, together with approximation (4), helps to explain the stabilization and formation of atomic DQCs.

In addition to the solid angles at vertices, the *face* solid angles, ω, of the Platonic solids are also instructive. The solid angle of a face subtended from the center of a Platonic solid is simply the solid angle of a full sphere (here, 1) divided by the number of faces, because the Platonic solids are highly symmetric. Therefore, it is deduced that $\omega_{tetra} = \frac{1}{4}$, $\omega_{cube} = \frac{1}{6}$, $\omega_{octa} = \frac{1}{8}$, $\omega_{dodeca} = \frac{1}{12}$, and $\omega_{icosa} = \frac{1}{20}$ (Figure 35). These

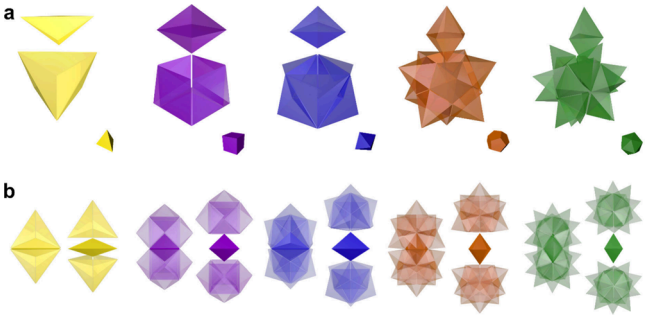

Figure 35. Shape complementarity relationships between Platonic solids deduced from a face solid angle perspective. In each case, one Platonic solid is converted into several bipyramidal shapes, using its center as the axial vertex, and its face as the mirror plane (a). Such a bipyramidal conversion strategy allow one to bridge two solids via one bipyramid, while having perfect local shape complementarity (b).

values indicate a series of additional, local shape complementarities whereby the face of each Platonic solid represents the base of a pyramid and the tips of those pyramids fill space at the center of a cluster. Therefore, four Catalan trigonal pyramids, six square pyramids, eight right pyramids, or 12 pentagonal pyramids can form a dense cluster without gaps. Notably, in the icosahedral case, it follows that a dense cluster should form from 20 trigonal pyramids that approximate tetrahedra.

https://doi.org/10.1021/acs.chemrev.4c00299
Chem. Rev. 2024, 124, 11063−11107

4.2. Extending Local Shape Complementarities to Ordered Superlattices

Having established geometric rules for the local space-filling of polyhedra, one can arrange Platonic solids into ordered superlattices. There are two main ways to propagate structures into ordered 3D superlattices, using radial or dihedral symmetries. In these scenarios, the geometric construction of a superlattice is achieved either by adding layers around a smaller space-filling construction (radial method) or by stacking 2D layers of a space-filling structure (dihedral method).

4.2.1. Extending Superlattices through Radial Symmetries. This approach can be applied to structures with symmetries, such as tetrahedral (Figure 36a), octahedral (Figure 36b), and icosahedral (Figure 36c) ones, where 1/4, 1/8, or 1/20 of the superlattices are constructed and extended radially. For example, a truncated tetrahedron and a face-sharing tetrahedron can construct a repeating unit that can fill 1/4 of space around a single point. Repeating this structure to fill the remaining 3/4 of the space and then extending this motif in all directions builds a diamond lattice containing an equal number of each building block (Figure 36a). Likewise, one face-sharing octahedron and one tetrahedron can construct a repeating unit that fills 1/8 of the space. By further extending this unit structure to fill the other 7/8 of the space, a space-filling *fcc* structure containing octahedra and tetrahedra in the ratio 1:2 can be constructed. Similarly, the *CsCl* lattice of cuboctahedra and octahedra (1:1) can also be constructed (Figure 36b). Indeed, this is a general result: if local structures can propagate in 1/8 of the space (irrespective of symmetry), a crystalline structure can be constructed. Finally, the *fcc* packing of spheres is known to form a tetrahedral habit, which is approximately equivalent to 1/20 of the icosahedral space. Therefore, radially repeating such tetrahedra to fill the remaining 19/20 of the space generates a 20-fold twinned *fcc* lattice. However, due to the approximate nature of this equivalency, a radially distributed strain will always exist, therefore hindering the infinite propagation of such a structure. Indeed, it is generally observed that icosahedral nanoparticles or superlattices cannot grow very large. There are, of course, methods to construct icosahedrally ordered structures without strain, mostly with icosahedral quasicrystals, but at least two types of building blocks are needed.

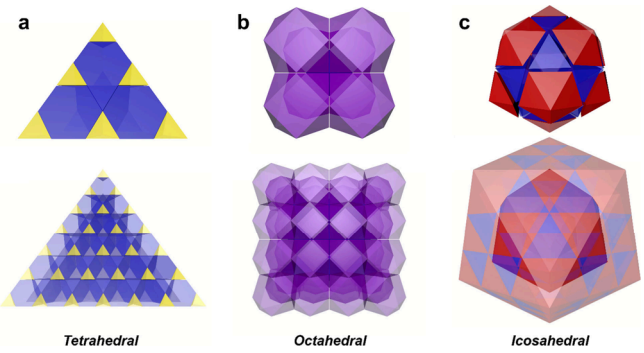

Figure 36. Three typical radial construction methods to expand local shape complementarity to extended ordered lattices. (a) A tetrahedral expansion of tetrahedra (yellow) and truncated tetrahedra (blue). (b) An octahedral expansion of octahedra (blue) and cuboctahedra (purple). (c) An icosahedral expansion of octahedra (blue) and compounds of face-sharing tetrahedra (red, including tetrahedra, bitetrahedra, and decahedra).

4.2.2. Extending Superlattices through Dihedral Symmetries. Although superlattices constructed through dihedral symmetries are sometimes equivalent to those constructed by radial symmetries, the dihedral ones do provide some unique insights. Dihedral ones can be constructed by employing a 2D space-filling pattern first and then layering it to produce a 3D superlattice (Figure 37). To ensure a good 2D tessellation, only triangular, square, and hexagonal projections are allowed. For example, octahedra and tetrahedra in the ratio 1:2 can form a honeycomb pattern, with triangular projections (Figure 37a). This lattice can be extended out-of-plane in two ways. In the first, tetrahedra interact with octahedra via facet−facet interactions, leading to the *fcc* lattice derived by the radial method (Figure 37b). The second construction instead uses tetrahedra-tetrahedra facet−facet interactions to generate a new *hcp* lattice (Figure 37c, also Figure 34b). In principle, the same honeycomb lattice could be layered with a distinct 2D lattice with the same projection of triangular facets. Analogously, the construction of cubes and hexagonal prisms are good examples of 2D tessellations of squares and hexagons.

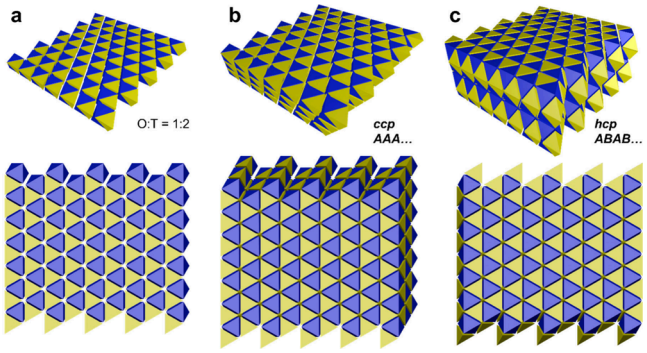

Figure 37. Dihedral construction method to expand local shape complementarity to extended, ordered lattices. (a) A monolayer constructed using octahedra (blue) and tetrahedra (yellow) in a 1:2 ratio. (b) A *ccp* 3D lattice (tetra-octa honeycomb) constructed by stacking monolayers (a) in the same orientation, with each layer shifted by a constant distance to register triangular faces. (c) An *hcp* 3D lattice (gyrated tetra-octa honeycomb) constructed by stacking monolayers (a) in an alternating orientation. Figures adapted with permission from ref 80. Copyright 2024 The American Association for the Advancement of Science.

In addition to crystalline 2D tessellations, quasicrystalline tilings can also be extended in 3D. For example, DDQCs and their approximants can be constructed by repeating layers of cubes and triangular prisms. A DQC can be constructed using approximation (4) from Section 4.1, due to the similarity between the vertical projection angle of edge-up octahedra (equal to the dihedral angle of tetrahedra, ~70.53°) and the fat rhombus angle in a Penrose tiling (72°). These edge-up octahedra layers can then be connected by the tips of icosahedra or decahedra (Johnson solid J13), forming a decagonal quasicrystalline 3D tessellation (Figure 38).[80]

The superlattices discussed here are a small selection of the geometrically plausible constructions, many of which have not even been considered yet due to the huge effort required to complete a combinatorial screening process. These methodologies are provided in the hope that these highly plausible target structures will inform efforts to find new packings by

https://doi.org/10.1021/acs.chemrev.4c00299
Chem. Rev. 2024, 124, 11063−11107

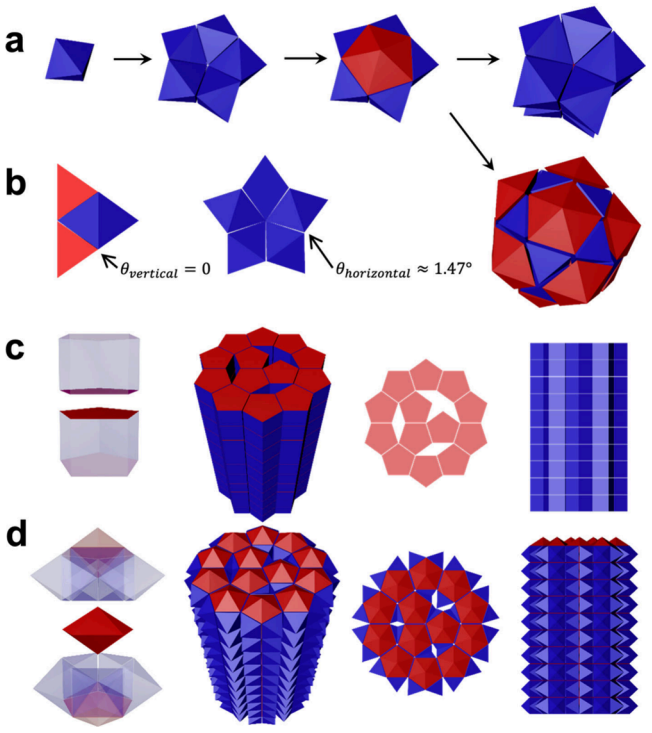

Figure 38. Schematic illustrations of geometric relationships between tetrahedra, octahedra, and decahedra. (a) Structural evolution of clusters formed from octahedra and decahedra. (b) An octahedra-decahedra cluster viewed from the side and top directions. (c) A Penrose-tiling-like quasi-space-filling configuration formed from face-sharing pentagonal prisms. (d) A Penrose-tiling-like quasi-space-filling configuration formed from face-sharing octahedra and decahedra. Note that (d) is a direct geometric transformation result from (c), therefore some octahedra partially overlap with neighboring ones. Figures adapted with permission from ref 80. Copyright 2024 American Association for the Advancement of Science.

narrowing the screening range, despite the vast number and stoichiometries of potential building blocks. When designing experiments or interpreting characterization data, it would be useful to evaluate the feasibility of different geometries by using the considerations presented here.

4.3. Inverse Design of Anisotropic Building Blocks

In addition to exploring how to organize known building blocks into ever more sophisticated structures, an alternative strategy is to inversely design new building blocks to realize specific target lattices. This approach is particularly important in the context of discovering structure−function relationships with nanoparticle assemblies that are as-of-yet largely under-explored in the field of colloid chemistry. Where these studies have been conducted, even the simplest colloidal crystals have been found to have interesting properties: *fcc* crystals of spherical nanoparticles exhibit deep, strong light-matter coupling effects,[198] while *sc* crystals of cubic nanoparticles display abnormally high refractive indices.[199] Moreover, nature and traditional synthetic chemistry, especially the framework community, already offer many ordered lattices that can be considered and are likely to have unexpected properties.

With this in mind, researchers can consider developing a platform whereby colloidal superlattices with specific symmetries can be synthesized on demand. There are some caveats: 1) colloidal organization is a rare, cooperative result of both local preferred clustering and accessible kinetic pathways, and therefore a specific colloidal building block will not always arrange into the desired lattice; 2) many geometrically reasonable approximations of a target building block may lead to the same organization outcome; and 3) a certain ensemble of building blocks may arrange into many similarly reasonable superlattices, especially when the degree of freedom of valency-endowed particles is high (for example, bivalent patchy particles can form 1D chains or Kagome lattices[72]) or when multiple coassembled structures compete in a multi-component system (consider a system containing tetrahedral, bitetrahedral, and octahedral nanoparticles with identical edge lengths). Notwithstanding these complications, geometric strategies are presented that will spur the development of the field in this direction, focusing initially on discrete clusters and building toward the inverse design of 3D superlattices.

4.3.1. Inverse Design of Colloidal Molecules. Discrete colloidal clusters, or colloidal molecules (CMs), were introduced in Section 3.1.1. The design of CMs generally follows one of two approaches: either the steric hindrance of polyhedral shapes or building blocks with specific, designed valencies are used. The first strategy is conceptually more straightforward: by connecting six building blocks to a cube, one on each face, an octahedral cluster will form, and by connecting eight building blocks to an octahedron, one on each face, a cubic cluster will form. Generally, clusters of the dual shapes of the central polyhedral nanoparticle can be designed simply by adding one building block to every face of that central polyhedron (Figure 1, bottom right panel). Geometry-induced local packing is arguably the most reliable strategy for building colloidal molecules or clusters. The second strategy requires a more sophisticated synthetic expertise but may lead to more highly controllable product outcomes. For example, arbitrary clustered arrangements of nanoparticles can be realized through certain DNA origami-based designs, where each nanoparticle is guided into a desired position through specific DNA interactions.[200]

However, thinking beyond the current scope of the field, one can articulate an inverse-design strategy that is based purely on geometric considerations and that would allow for any uniform polyhedral-shaped colloidal clusters to be constructed from valency-defined nanoparticles. Each uniform polyhedron is considered to be a frame enclosed by edges and vertices. The optimum valency needed to construct that polyhedron can be extracted by considering the arrangement of edges around a vertex (Figure 39). For example, a trivalent building block with three bonding directions set 60° apart from one another will naturally form a tetrahedral cluster (Figure 39a), a tetravalent building block with four bonding directions each set 60° apart from its neighboring ones will naturally form an octahedral cluster (Figure 39b), and so on. This strategy suggests that all uniform, convex polyhedral clusters can be constructed by defining the directions of a single component comprising a tri-, tetra-, or pentavalent patchy particle.

The main challenge of designing arbitrary molecular clusters is arguably a synthetic one rather than a conceptual one. An alternative geometric approach treats the polyhedral cluster as a shell enclosed by faces. In this context, taking the center of each face as the central point for a valency-defined building block, the optimum valency can be determined in two ways: either by connecting the face center to the midpoints of its bounding edges (Figure 39c) or by connecting the face center to its surrounding vertices (Figure 39d). For example, square planar tetravalent patchy particles with an appropriate degree

https://doi.org/10.1021/acs.chemrev.4c00299
Chem. Rev. 2024, 124, 11063−11107

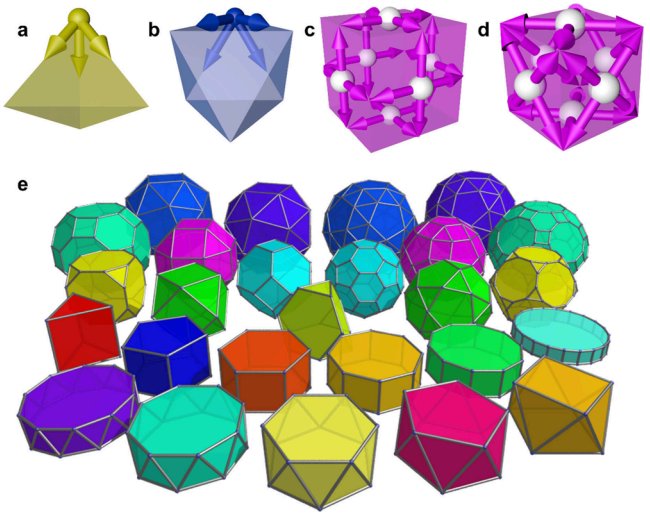

Figure 39. Inverse design of anisotropic building blocks for constructing colloidal clusters. (a) A trivalent patchy building block with 60° between each valent direction, extracted from the corner of a tetrahedron. (b) A quadvalent patchy building block with 60° between neighboring valent directions, extracted from the corner of an octahedron. (c, d) A cube-templated cluster of six square planar tetravalent building blocks via (c) edge midpoints or (d) vertices. (e) A library of uniform polyhedra that could be used to generate space-configurations of clusters.

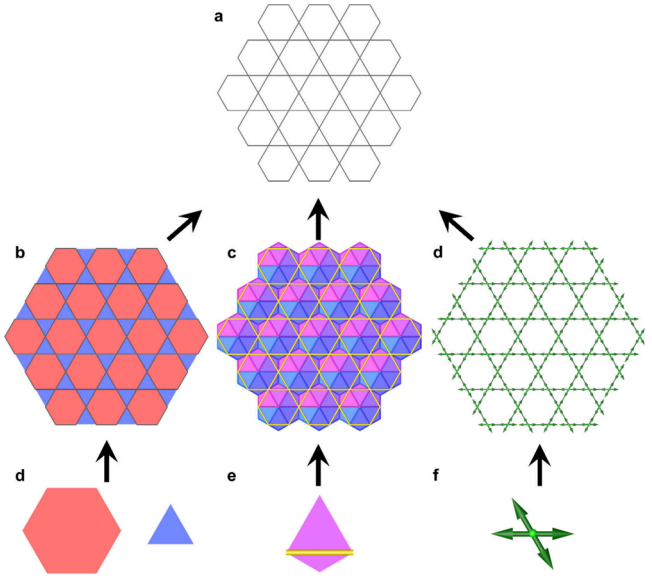

Figure 40. Inverse design of building blocks for 2D ordered lattices. (a) An exemplary 2D ordered lattice, the Kagome lattice. This lattice can be deconstructed via multiple strategies: (b, d) *area tiling*, with building blocks in (d); (c, e) *edge tiling*, with building blocks in (e); (d, f) *vertex tiling*, with building blocks in (f).

of freedom at their connection points are predicted to assemble into cubic clusters. This concept was validated by Heddle and co-workers, in which undecavalent (11-fold) protein building blocks assembled into pentagonal icositetrahedra (the dual shape of snub cubes).[201] Target polyhedral clusters can be deconstructed in three ways if this approach is expanded to allow for two types of building blocks: vertices and edges, vertices and face centers, and face centers and edges. This strategy has been beautifully demonstrated in the *de novo* design of symmetric protein cages by Baker and co-workers.[173,176,202] Both of these examples highlight the potentially fruitful role of using designed proteins as building blocks with defined valency for colloidal assembly.

4.3.2. Inverse Design of 2D Crystalline Structures. Any 2D lattice, whether periodic or aperiodic, can be converted to a 2D tessellation such as the eight Archimedean tessellations or the Penrose tiling. Intuitively, the shapes that are used in these tessellations are the most ideal building blocks for each specific 2D lattice due to the native shape complementarities at their corners and edges. As a result, if colloids are synthesized with the shape of individual tiles or a tessellating local combination thereof (*area tiling*, Figure 40b), the desired 2D tessellation is likely to be an outcome of colloidal organization. However, it is difficult to preserve the anisotropy of polygonal colloids with more than six edges, which instead behave like circular or less anisotropic building blocks.

Therefore, an alternative strategy, analogous to the method presented in the previous subsection for 1D clusters, is to view the 2D tessellation as a network of local coordination environments defined by the arrangement of edges about each vertex (*vertex tiling*, Figure 40d). This deconstruction strategy, which coincidentally is more relevant to valence-defined colloids, can be used to convert all Archimedean tessellations into a single type of coordination environment (joint). For example, Archimedean tessellation is formalized as *3.6.3.6* (Figure 40a), where each number indicates the *n*-sided polygons surrounding the vertex during a single 360° rotation. Each vertex in this tessellation is circumscribed by a triangle (three-sided regular polygon), hexagon (six-sided), another triangle, and another hexagon; hence, the notation *3.6.3.6* (Figure 40a). Consequently, a building block with valent directions defined with the corresponding interior angles (for *3.6.3.6*, four directions with separations 60°, 120°, 60°, and 120°) should organize into the corresponding tessellations, since all edges in semiregular tessellations are the same, which means the distances between any pair of neighboring particles are equal. This vertex tiling strategy can be further extended to more complex or aperiodic tessellations, such as quasicrystalline tilings. Despite their aperiodicity, quasiperiodic tessellations are still composed of only a few coordination types. For example, a DDQC can be deconstructed as three types of joints: *3.3.4.3.4* (σ), *3.3.3.4.4* (H), and *3.3.3.3.3.3* (Z). Though never realized experimentally, molecular systems have been designed to assemble into a Penrose tiling using this approach.[203,204]

Finally, *edge tiling* (Figure 40c) can also serve as a deconstruction strategy when the complementarity of each type of edge is predetermined. For example, bivalent segmented spherical particles can arrange into Kagome lattices due to the local shape complementarity between three spheres (densest packing of circles).[72] However, edge tiling requires narrowly defined degrees of freedom at the bonding sites, thereby significantly limiting the generalizability of this approach.

4.3.3. Inverse Design of 3D Crystalline Structures. When extended to 3D, deconstruction methods similar to those employed for 2D tessellations (*vide supra*) can be applied to 3D tessellations (that is, ordered lattices). It is worth noting that the deconstruction strategy is not limited to only tessellation-based geometries. For example, 3D lattices can also be constructed using 2D units via edge-sharing or vertex-

https://doi.org/10.1021/acs.chemrev.4c00299
Chem. Rev. 2024, 124, 11063−11107

sharing (Figure 41). The 3D equivalent of area tiling in 2D is *volume tiling* (Figure 42b), with the simplest example being the

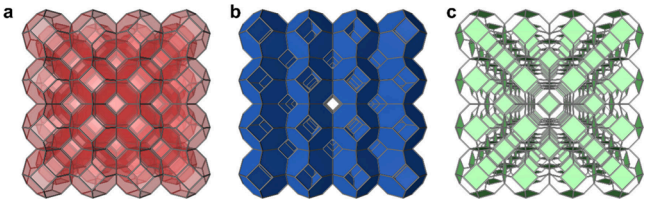

Figure 41. Inverse design of 2D building blocks for 3D ordered lattices. (a) An exemplary 3D ordered lattice, the *bcc* lattice. This lattice can be demonstrated as (b) edge-sharing hexagons or (c) vertex-sharing squares.

assembly of Voronoi polyhedral-shaped building blocks into their corresponding 3D lattices. *Vertex tiling* still requires the extraction of vertices with bonding directions arranged along edges: a *sc* lattice (dense packing of cubes) has a hexavalent 3D joint (4^8, denoting eight 90° (=360°/4) angles between the six directions), an *sh* lattice (dense packing of hexagonal prisms) has a pentavalent 3D joint ($4^3.6^3.4^3$), and a *bcc* lattice (dense packing of truncated octahedra) has a tetravalent 3D joint (4.6.4.6). *Edge tiling* requires shape complementarity to be predetermined in 3D, but simple analogies can still be made. For example, if bivalent spherical building blocks are to be assembled in 3D, while still following the spherical dense packing local arrangement (tetrahedral arrangement) at the connection joints, a diamond lattice is the preferred outcome.

Other than volume tiling, vertex tiling, and edge tiling, a new deconstruction method, *face tiling* (Figure 42c) is now available in 3D. Since 3D tessellations rely entirely on face-to-face registration, one can use a polyhedral face as a mirror plane to convert existing Voronoi polyhedra into new ones. Like the pyramidal conversion of Platonic solids (see Section 4.1), this strategy converts the regular polyhedra in 3D tessellations into their pyramidal forms: each cube in a *sc* tiling can be converted into six square pyramids, which can be combined with square pyramids in neighboring cubes, using the cubic faces as mirror planes to generate square bipyramids. Similarly, each hexagonal prism within a *sh* tiling can be converted into two hexagonal pyramids and six square pyramids, while each truncated octahedron from a *bcc* tiling can be converted into eight hexagonal pyramids and six square pyramids.

Through these deconstruction strategies, even without generating new ordered lattices, superlattices with target symmetries can be converted to multiple distinct forms, most of which have not yet been realized. Though illustrated in the packing of Platonic solids, these principles are general and can provide diverse routes to the synthesis of any given crystalline superlattice. Thus, these strategies serve as inspiration for colloid chemists designing and preparing their own building blocks (Figure 42).

5. OUTLOOK

Ultimate goals of studying organized nanoscale matter include unveiling the fundamental principles through which nature synthesizes materials on scales beyond our reach and establishing methods to prepare materials with similar or even enhanced structural complexity by design. Through this lens, the importance of anisotropy cannot be overemphasized: nature exploits anisotropy routinely and effortlessly as a

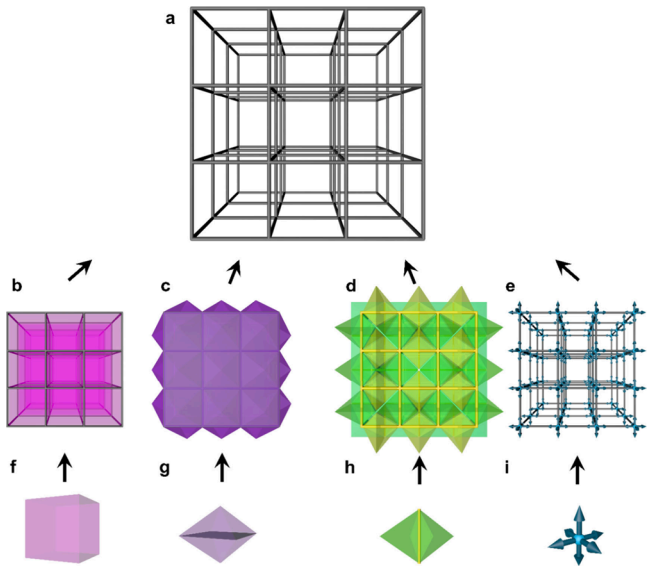

Figure 42. Inverse design of building blocks for 3D ordered lattices. (a) An exemplary 3D ordered lattice, the *sc* lattice. This lattice can be deconstructed via multiple strategies: (b, f) *volume tiling*, with the building block in (f); (c, g) *face tiling*, with the building block in (g); (d, h) *edge tiling*, with the building block in (h); (e, i) *vertex tiling*, with the building block in (i).

prerequisite to achieve complex systems that function in sophisticated ways. The ideas discussed herein represent the state-of-the-art in our understanding of how to control anisotropy using essential concepts such as enthalpy, entropy, valency, and shape complementarity. These themes connect the efforts of many researchers that have worked to control nanoscale structures in materials across length scales. We have also proposed a polyhedra-derived geometric construction strategy to push the envelope of structural sophistication in colloidal superlattices and discussed how they might be constructed by design. With this blueprint in hand, we encourage the community to devote ever more effort to exploring the *functions* of such highly engineered materials as well, recognizing that a cycle between structural design and resultant properties measurement will continue to propel this field forward. However, although the guidelines discussed herein are significant for moving the field forward, one should not conclude that our understanding is complete. Natural systems harness imperfections and defects to their benefit, yet the fate of colloidal systems with defects—such as the rounding or truncation of vertices—remains difficult to predict because such structures may deviate substantially from their intended designs. Indeed, there exists a wealth of knowledge with which to design functional devices, but a vast landscape of fundamental structural questions still needs to be explored. In short, this is an exciting time to be a colloid chemist.

AUTHOR INFORMATION

Corresponding Author

Chad A. Mirkin − *International Institute for Nanotechnology, Northwestern University, Evanston, Illinois 60208, United States; Department of Chemistry and Department of Chemical and Biological Engineering, Northwestern University, Evanston, Illinois 60208, United States;* orcid.org/0000-0002-6634-7627; Email: chadnano@northwestern.edu

https://doi.org/10.1021/acs.chemrev.4c00299
Chem. Rev. 2024, 124, 11063−11107

Authors

Wenjie Zhou − *International Institute for Nanotechnology, Northwestern University, Evanston, Illinois 60208, United States; Department of Chemistry, Northwestern University, Evanston, Illinois 60208, United States;* orcid.org/0000-0002-7626-4032

Yuanwei Li − *International Institute for Nanotechnology, Northwestern University, Evanston, Illinois 60208, United States; Department of Chemical and Biological Engineering, Northwestern University, Evanston, Illinois 60208, United States;* orcid.org/0000-0002-0338-5335

Benjamin E. Partridge − *International Institute for Nanotechnology, Northwestern University, Evanston, Illinois 60208, United States; Department of Chemistry, Northwestern University, Evanston, Illinois 60208, United States;* orcid.org/0000-0003-2359-1280

Complete contact information is available at: https://pubs.acs.org/10.1021/acs.chemrev.4c00299

Author Contributions

¶W.Z. and Y.L. contributed equally to this work. CRediT: **Wenjie Zhou** conceptualization, formal analysis, writing - original draft, writing - review & editing; **Yuanwei Li** conceptualization, formal analysis, writing - original draft, writing - review & editing; **Benjamin E. Partridge** conceptualization, formal analysis, writing - original draft, writing - review & editing; **Chad A. Mirkin** conceptualization, formal analysis, funding acquisition, investigation, project administration, resources, supervision, writing - original draft, writing - review & editing.

Notes

The authors declare no competing financial interest.

Biographies

Wenjie Zhou received his Ph.D. in Chemistry from Northwestern University in 2022. He is currently a postdoctoral scholar associate in the Department of Mechanical and Civil Engineering at the California Institute of Technology. His research interests include leveraging geometry, topology, and computational design to synthesize and manufacture architected materials across various length scales, and to understand the emerging behaviors in optical and mechanical metamaterial systems.

Yuanwei Li is a Stanford Science Fellow in Materials Science and Engineering at Stanford University. Yuanwei received her Ph.D. in Chemical and Biological Engineering from Northwestern University in 2023, where she designed and synthesized functional colloidal crystals through geometry-inspired design principles. She is passionate about designing customized nanoarchitected materials for improved sustainability and health monitoring.

Benjamin Partridge received his Ph.D. in Chemistry from the University of Pennsylvania in 2018, after which he moved to Northwestern University as an International Institute for Nanotechnology Postdoctoral Fellow with Chad Mirkin. In 2022, Ben launched his independent career at the University of Rochester, where he is an Assistant Professor of Chemistry. His research focuses on leveraging the noncovalent bond to advance the supramolecular synthesis of materials that mimic and manipulate biological systems.

Chad Mirkin is the Director of the International Institute for Nanotechnology and Rathmann Professor of Chemistry, MSE, BME, CBE, and Medicine at Northwestern University. He invented and has developed spherical nucleic acids and various nanopatterning and materials discovery methodologies. He has authored over 880 papers and over 1,200 patents (>430 issued) and founded 10 companies. Mirkin has been recognized with over 250 awards, including the Kavli Prize, and has been elected to all three US National Academies. He served for eight years on PCAST. He has given over 900 invited lectures and educated over 340 graduate students and postdocs (>140 are faculty members worldwide).

ACKNOWLEDGMENTS

This material is based upon work supported by the following awards: Air Force Office of Scientific Research FA9550-22-1-0300 and FA9550-17-1-0348, National Science Foundation DMR-2104353, and the Center for Bio-Inspired Energy Science, an Energy Frontier Research Center funded by the U.S. Department of Energy, Office of Science, Basic Energy Sciences DE-SC0000989.

REFERENCES

(1) Niizato, T.; Gunji, Y. Consistent Concepts of Self-Organization and Self-Assembly. *Complexity* **2011**, *16*, 10−21.
(2) Parrend, P.; Collet, P. A Review on Complex System Engineering. *J. Syst. Sci. Complex.* **2020**, *33*, 1755−1784.
(3) Baker, J.; Kudrolli, A. Maximum and Minimum Stable Random Packings of Platonic Solids. *Phys. Rev. E* **2010**, *82*, 061304.
(4) Bollen, J.; ten Thij, M.; Breithaupt, F.; Barron, A. T. J.; Rutter, L. A.; Lorenzo-Luaces, L.; Scheffer, M. Historical Language Records Reveal a Surge of Cognitive Distortions in Recent Decades. *Proc. Natl. Acad. Sci. U. S. A.* **2021**, *118*, No. e2102061118.
(5) Schweisguth, F.; Corson, F. Self-Organization in Pattern Formation. *Dev. Cell* **2019**, *49*, 659−677.
(6) Song, Q.; Cheng, Z.; Kariuki, M.; Hall, S. C. L.; Hill, S. K.; Rho, J. Y.; Perrier, S. Molecular Self-Assembly and Supramolecular Chemistry of Cyclic Peptides. *Chem. Rev.* **2021**, *121*, 13936−13995.
(7) Michaelides, E. E. Brownian Movement and Thermophoresis of Nanoparticles in Liquids. *Int. J. Heat Mass Transfer* **2015**, *81*, 179−187.
(8) Whitesides, G. M.; Grzybowski, B. Self-Assembly at All Scales. *Science* **2002**, *295*, 2418−2421.
(9) Isaacoff, B. P.; Brown, K. A. Progress in Top-down Control of Bottom-up Assembly. *Nano Lett.* **2017**, *17*, 6508−6510.
(10) Lin, Q.-Y.; Mason, J. A.; Li, Z.; Zhou, W.; O'Brien, M. N.; Brown, K. A.; Jones, M. R.; Butun, S.; Lee, B.; Dravid, V. P.; et al. Building Superlattices from Individual Nanoparticles via Template-Confined DNA-Mediated Assembly. *Science* **2018**, *359*, 669−672.
(11) Zhou, W.; Liu, Z.; Huang, Z.; Lin, H.; Samanta, D.; Lin, Q. Y.; Aydin, K.; Mirkin, C. A. Device-Quality, Reconfigurable Metamaterials from Shape-Directed Nanocrystal Assembly. *Proc. Natl. Acad. Sci. U. S. A.* **2020**, *117*, 21052−21057.
(12) Zheng, C. Y.; Palacios, E.; Zhou, W.; Hadibrata, W.; Sun, L.; Huang, Z.; Schatz, G. C.; Aydin, K.; Mirkin, C. A. Tunable Fluorescence from Dye-Modified DNA-Assembled Plasmonic Nanocube Arrays. *Adv. Mater.* **2019**, *31*, 1904448.
(13) Boles, M. A.; Engel, M.; Talapin, D. V. Self-Assembly of Colloidal Nanocrystals: From Intricate Structures to Functional Materials. *Chem. Rev.* **2016**, *116*, 11220−11289.
(14) Dshemuchadse, J.; Damasceno, P. F.; Phillips, C. L.; Engel, M.; Glotzer, S. C. Moving beyond the Constraints of Chemistry via Crystal Structure Discovery with Isotropic Multiwell Pair Potentials. *Proc. Natl. Acad. Sci. U. S. A.* **2021**, *118*. DOI: 10.1073/pnas.2024034118.
(15) Shevchenko, E. V.; Talapin, D. V.; Kotov, N. A.; O'Brien, S.; Murray, C. B. Structural Diversity in Binary Nanoparticle Superlattices. *Nature* **2006**, *439*, 55−59.
(16) Macfarlane, R. J.; Lee, B.; Jones, M. R.; Harris, N.; Schatz, G. C.; Mirkin, C. A. Nanoparticle Superlattice Engineering with DNA. *Science* **2011**, *334*, 204−208.

(17) Coropceanu, I.; Boles, M. A.; Talapin, D. V. Systematic Mapping of Binary Nanocrystal Superlattices: The Role of Topology in Phase Selection. *J. Am. Chem. Soc.* **2019**, *141*, 5728−5740.
(18) Nagaoka, Y.; Tan, R.; Li, R.; Zhu, H.; Eggert, D.; Wu, Y. A.; Liu, Y.; Wang, Z.; Chen, O. Superstructures Generated from Truncated Tetrahedral Quantum Dots. *Nature* **2018**, *561*, 378−382.
(19) Nagaoka, Y.; Zhu, H.; Eggert, D.; Chen, O. Single-Component Quasicrystalline Nanocrystal Superlattices through Flexible Polygon Tiling Rule. *Science* **2018**, *362*, 1396−1400.
(20) Shi, Y.; Lyu, Z.; Zhao, M.; Chen, R.; Nguyen, Q. N.; Xia, Y. Noble-Metal Nanocrystals with Controlled Shapes for Catalytic and Electrocatalytic Applications. *Chem. Rev.* **2021**, *121*, 649−735.
(21) Grzelczak, M.; Pérez-Juste, J.; Mulvaney, P.; Liz-Marzán, L. M. Shape Control in Gold Nanoparticle Synthesis. *Chem. Soc. Rev.* **2008**, *37*, 1783−1791.
(22) Wu, Z.; Yang, S.; Wu, W. Shape Control of Inorganic Nanoparticles from Solution. *Nanoscale* **2016**, *8*, 1237−1259.
(23) Jones, M. R.; Macfarlane, R. J.; Lee, B.; Zhang, J.; Young, K. L.; Senesi, A. J.; Mirkin, C. A. DNA-Nanoparticle Superlattices Formed from Anisotropic Building Blocks. *Nat. Mater.* **2010**, *9*, 913−917.
(24) Lu, F.; Vo, T.; Zhang, Y.; Frenkel, A.; Yager, K. G.; Kumar, S.; Gang, O. Unusual Packing of Soft-Shelled Nanocubes. *Sci. Adv.* **2019**, *5*, No. eaaw2399.
(25) O'Brien, M. N.; Girard, M.; Lin, H.-X.; Millan, J. A.; Olvera de la Cruz, M.; Lee, B.; Mirkin, C. A. Exploring the Zone of Anisotropy and Broken Symmetries in DNA-Mediated Nanoparticle Crystallization. *Proc. Natl. Acad. Sci. U. S. A.* **2016**, *113*, 10485−10490.
(26) Kwon, T.; Jun, M.; Lee, K. Catalytic Nanoframes and Beyond. *Adv. Mater.* **2020**, *32*, 1−30.
(27) Li, Y.; Lin, H.; Zhou, W.; Sun, L.; Samanta, D.; Mirkin, C. A. Corner-, Edge-, and Facet-Controlled Growth of Nanocrystals. *Sci. Adv.* **2021**, *7*, No. eabf1410.
(28) Smith, J. D.; Scanlan, M. M.; Chen, A. N.; Ashberry, H. M.; Skrabalak, S. E. Kinetically Controlled Sequential Seeded Growth: A General Route to Crystals with Different Hierarchies. *ACS Nano* **2020**, *14*, 15953−15961.
(29) Deng, K.; Luo, Z.; Tan, L.; Quan, Z. Self-Assembly of Anisotropic Nanoparticles into Functional Superstructures. *Chem. Soc. Rev.* **2020**, *49*, 6002−6038.
(30) Boles, M. A.; Talapin, D. V. Many-Body Effects in Nanocrystal Superlattices: Departure from Sphere Packing Explains Stability of Binary Phases. *J. Am. Chem. Soc.* **2015**, *137*, 4494−4502.
(31) Elbert, K. C.; Vo, T.; Krook, N. M.; Zygmunt, W.; Park, J.; Yager, K. G.; Composto, R. J.; Glotzer, S. C.; Murray, C. B. Dendrimer Ligand Directed Nanoplate Assembly. *ACS Nano* **2019**, *13*, 14241−14251.
(32) Rupich, S. M.; Shevchenko, E. V.; Bodnarchuk, M. I.; Lee, B.; Talapin, D. V. Size-Dependent Multiple Twinning in Nanocrystal Superlattices. *J. Am. Chem. Soc.* **2010**, *132*, 289−296.
(33) Henzie, J.; Grünwald, M.; Widmer-Cooper, A.; Geissler, P. L.; Yang, P. Self-Assembly of Uniform Polyhedral Silver Nanocrystals into Densest Packings and Exotic Superlattices. *Nat. Mater.* **2012**, *11*, 131−137.
(34) Urbach, Z. J.; Park, S. S.; Weigand, S. L.; Rix, J. E.; Lee, B.; Mirkin, C. A. Probing the Consequences of Cubic Particle Shape and Applied Field on Colloidal Crystal Engineering with DNA. *Angew. Chem. Int. Ed.* **2021**, *60*, 4065−4069.
(35) Park, S. S.; Urbach, Z. J.; Brisbois, C. A.; Parker, K. A.; Partridge, B. E.; Oh, T.; Dravid, V. P.; Olvera de la Cruz, M.; Mirkin, C. A. DNA-and Field-Mediated Assembly of Magnetic Nanoparticles into High-Aspect Ratio Crystals. *Adv. Mater.* **2020**, *32*, 1906626.
(36) Singh, G.; Chan, H.; Baskin, A.; Gelman, E.; Repnin, N.; Král, P.; Klajn, R. Self-Assembly of Magnetite Nanocubes into Helical Superstructures. *Science* **2014**, *345*, 1149−1153.
(37) Wang, T.; La Montagne, D.; Lynch, J.; Zhuang, J.; Cao, Y. C. Colloidal Superparticles from Nanoparticle Assembly. *Chem. Soc. Rev.* **2013**, *42*, 2804−2823.
(38) Cong, H.; Yu, B.; Tang, J.; Li, Z.; Liu, X. Current Status and Future Developments in Preparation and Application of Colloidal Crystals. *Chem. Soc. Rev.* **2013**, *42*, 7774−7800.
(39) Wang, Y.; Santos, P. J.; Kubiak, J. M.; Guo, X.; Lee, M. S.; Macfarlane, R. J. Multistimuli Responsive Nanocomposite Tectons for Pathway Dependent Self-Assembly and Acceleration of Covalent Bond Formation. *J. Am. Chem. Soc.* **2019**, *141*, 13234−13243.
(40) Zhang, J.; Santos, P. J.; Gabrys, P. A.; Lee, S.; Liu, C.; Macfarlane, R. J. Self-Assembling Nanocomposite Tectons. *J. Am. Chem. Soc.* **2016**, *138*, 16228−16231.
(41) Laramy, C. R.; O'Brien, M. N.; Mirkin, C. A. Crystal Engineering with DNA. *Nat. Rev. Mater.* **2019**, *4*, 201−224.
(42) Gabrys, P. A.; Zornberg, L. Z.; Macfarlane, R. J. Programmable Atom Equivalents: Atomic Crystallization as a Framework for Synthesizing Nanoparticle Superlattices. *Small* **2019**, *15*, 1805424.
(43) O'Brien, M. N.; Jones, M. R.; Lee, B.; Mirkin, C. A. Anisotropic Nanoparticle Complementarity in DNA-Mediated Co-Crystallization. *Nat. Mater.* **2015**, *14*, 833−839.
(44) Jones, M. R.; Macfarlane, R. J.; Prigodich, A. E.; Patel, P. C.; Mirkin, C. A. Nanoparticle Shape Anisotropy Dictates the Collective Behavior of Surface-Bound Ligands. *J. Am. Chem. Soc.* **2011**, *133*, 18865−18869.
(45) Shao, L.; Ma, J.; Prelesnik, J. L.; Zhou, Y.; Nguyen, M.; Zhao, M.; Jenekhe, S. A.; Kalinin, S. V.; Ferguson, A. L.; Pfaendtner, J.; et al. Hierarchical Materials from High Information Content Macromolecular Building Blocks: Construction, Dynamic Interventions, and Prediction. *Chem. Rev.* **2022**, *122*, 17397−17478.
(46) Zhang, X.; Dai, X.; Gao, L.; Xu, D.; Wan, H.; Wang, Y.; Yan, L.-T. The Entropy-Controlled Strategy in Self-Assembling Systems. *Chem. Soc. Rev.* **2023**, *52*, 6806.
(47) Macfarlane, R. J.; Lee, B.; Hill, H. D.; Senesi, A. J.; Seifert, S.; Mirkin, C. A. Assembly and Organization Processes in DNA-Directed Colloidal Crystallization. *Proc. Natl. Acad. Sci. U. S. A.* **2009**, *106*, 10493−10498.
(48) Yang, S.; Murray, C. B. A Snapshot Review of Dynamic Colloidal Nanoparticle Superlattices. *MRS Adv.* **2024**, *9*, 1077.
(49) Maassen, S. J.; Huskens, J.; Cornelissen, J. J. L. M. Elucidating the Thermodynamic Driving Forces of Polyanion-Templated Virus-like Particle Assembly. *J. Phys. Chem. B* **2019**, *123*, 9733−9741.
(50) Cheng, Z.; Jones, M. R. Assembly of Planar Chiral Superlattices from Achiral Building Blocks. *Nat. Commun.* **2022**, *13*, 4207.
(51) Wang, Y.; Chen, J.; Li, R.; Götz, A.; Drobek, D.; Przybilla, T.; Hübner, S.; Pelz, P.; Yang, L.; Apeleo Zubiri, B.; et al. Controlled Self-Assembly of Gold Nanotetrahedra into Quasicrystals and Complex Periodic Supracrystals. *J. Am. Chem. Soc.* **2023**, *145*, 17902−17911.
(52) Kim, J.; Song, X.; Ji, F.; Luo, B.; Ice, N. F.; Liu, Q.; Zhang, Q.; Chen, Q. Polymorphic Assembly from Beveled Gold Triangular Nanoprisms. *Nano Lett.* **2017**, *17*, 3270−3275.
(53) Li, Y.; Tanriover, I.; Zhou, W.; Hadibrata, W.; Dereshgi, S. A.; Samanta, D.; Aydin, K.; Mirkin, C. A. Monolayer Plasmonic Nanoframes as Large-Area, Broadband Metasurface Absorbers. *Small* **2022**, *18*, 2201171.
(54) Boles, M. A.; Talapin, D. V. Self-Assembly of Tetrahedral CdSe Nanocrystals: Effective "Patchiness" via Anisotropic Steric Interaction. *J. Am. Chem. Soc.* **2014**, *136*, 5868−5871.
(55) Paik, T.; Murray, C. B. Shape-Directed Binary Assembly of Anisotropic Nanoplates: A Nanocrystal Puzzle with Shape-Complementary Building Blocks. *Nano Lett.* **2013**, *13*, 2952−2956.
(56) Santos, P. J.; Gabrys, P. A.; Zornberg, L. Z.; Lee, M. S.; Macfarlane, R. J. Macroscopic Materials Assembled from Nanoparticle Superlattices. *Nature* **2021**, *591*, 586.
(57) Akcora, P.; Liu, H.; Kumar, S. K.; Moll, J.; Li, Y.; Benicewicz, B. C.; Schadler, L. S.; Acehan, D.; Panagiotopoulos, A. Z.; Pryamitsyn, V.; et al. Anisotropic Self-Assembly of Spherical Polymer-Grafted Nanoparticles. *Nat. Mater.* **2009**, *8*, 354−359.
(58) Ning, Y.; Liu, Z.; Yang, S.; Morimitsu, Y.; Osuji, C. O.; Murray, C. B. Design of Dendritic Promesogenic Ligands for Liquid Crystal-Nanoparticle Hybrid Systems. *Chem. Mater.* **2023**, *35*, 3532.

https://doi.org/10.1021/acs.chemrev.4c00299
Chem. Rev. 2024, 124, 11063−11107

(59) Zhu, E.; Yan, X.; Wang, S.; Xu, M.; Wang, C.; Liu, H.; Huang, J.; Xue, W.; Cai, J.; Heinz, H.; et al. Peptide-Assisted 2-D Assembly toward Free-Floating Ultrathin Platinum Nanoplates as Effective Electrocatalysts. *Nano Lett.* **2019**, *19*, 3730−3736.
(60) Merg, A. D.; Boatz, J. C.; Mandal, A.; Zhao, G.; Mokashi-Punekar, S.; Liu, C.; Wang, X.; Zhang, P.; van der Wel, P. C. A.; Rosi, N. L. Peptide-Directed Assembly of Single-Helical Gold Nanoparticle Superstructures Exhibiting Intense Chiroptical Activity. *J. Am. Chem. Soc.* **2016**, *138*, 13655−13663.
(61) Zhou, W.; Lim, Y.; Lin, H.; Lee, S.; Li, Y.; Huang, Z.; Du, J. S.; Lee, B.; Wang, S.; Sánchez-Iglesias, A.; et al. Colloidal Quasicrystals Engineered with DNA. *Nat. Mater.* **2024**, *23*, 424−428.
(62) Li, Y.; Zhou, W.; Tanriover, I.; Hadibrata, W.; Partridge, B. E.; Lin, H.; Hu, X.; Lee, B.; Liu, J.; Dravid, V. P.; et al. Open-Channel Metal Particle Superlattices. *Nature* **2022**, *611*, 695−701.
(63) Gillespie, R. J. The Valence-Shell Electron-Pair Repulsion (VSEPR) Theory of Directed Valency. *J. Chem. Educ.* **1963**, *40*, 295.
(64) Wang, S.; Lee, S.; Du, J. S.; Partridge, B. E.; Cheng, H. F.; Zhou, W.; Dravid, V. P.; Lee, B.; Glotzer, S. C.; Mirkin, C. A. The Emergence of Valency in Colloidal Crystals through Electron Equivalents. *Nat. Mater.* **2022**, *21*, 580−587.
(65) Cheng, H. F.; Distler, M. E.; Lee, B.; Zhou, W.; Weigand, S.; Mirkin, C. A. Nanoparticle Superlattices through Template-Encoded DNA Dendrimers. *J. Am. Chem. Soc.* **2021**, *143*, 17170−17179.
(66) Hueckel, T.; Hocky, G. M.; Sacanna, S. Total Synthesis of Colloidal Matter. *Nat. Rev. Mater.* **2021**, *6*, 1053−1069.
(67) Su, K.; Wang, W.; Du, S.; Ji, C.; Zhou, M.; Yuan, D. Reticular Chemistry in the Construction of Porous Organic Cages. *J. Am. Chem. Soc.* **2020**, *142*, 18060−18072.
(68) Xu, W.; Tu, B.; Liu, Q.; Shu, Y.; Liang, C. C.; Diercks, C. S.; Yaghi, O. M.; Zhang, Y. B.; Deng, H.; Li, Q. Anisotropic Reticular Chemistry. *Nat. Rev. Mater.* **2020**, *5*, 764−779.
(69) Jiang, H.; Alezi, D.; Eddaoudi, M. A Reticular Chemistry Guide for the Design of Periodic Solids. *Nat. Rev. Mater.* **2021**, *6*, 466−487.
(70) Uniform Polyhedra. *Philos. Trans. R. Soc. London. Ser. A, Math. Phys. Sci.* **1954**, *246*, 401−450.
(71) Lin, H.; Lee, S.; Sun, L.; Spellings, M.; Engel, M.; Glotzer, S. C.; Mirkin, C. A. Clathrate Colloidal Crystals. *Science* **2017**, *355*, 931−935.
(72) Chen, Q.; Bae, S. C.; Granick, S. Directed Self-Assembly of a Colloidal Kagome Lattice. *Nature* **2011**, *469*, 381−384.
(73) Mao, X.; Chen, Q.; Granick, S. Entropy Favours Open Colloidal Lattices. *Nat. Mater.* **2013**, *12*, 217−222.
(74) Girard, M.; Wang, S.; Du, J. S.; Das, A.; Huang, Z.; Dravid, V. P.; Lee, B.; Mirkin, C. A.; Olvera de la Cruz, M. Particle Analogs of Electrons in Colloidal Crystals. *Science* **2019**, *364*, 1174−1178.
(75) Teich, E. G.; van Anders, G.; Klotsa, D.; Dshemuchadse, J.; Glotzer, S. C. Clusters of Polyhedra in Spherical Confinement. *Proc. Natl. Acad. Sci. U. S. A.* **2016**, *113*, No. E669-E678.
(76) Lee, S.; Teich, E. G.; Engel, M.; Glotzer, S. C. Entropic Colloidal Crystallization Pathways via Fluid-Fluid Transitions and Multidimensional Prenucleation Motifs. *Proc. Natl. Acad. Sci. U. S. A.* **2019**, *116*, 14843−14851.
(77) Damasceno, P. F.; Engel, M.; Glotzer, S. C. Predictive Self-Assembly of Polyhedra into Complex Structures. *Science* **2012**, *337*, 453−457.
(78) Torquato, S.; Jiao, Y. Dense Packings of the Platonic and Archimedean Solids. *Nature* **2009**, *460*, 876−879.
(79) Chen, E. R.; Engel, M.; Glotzer, S. C. Dense Crystalline Dimer Packings of Regular Tetrahedra. *Discret. Comput. Geom.* **2010**, *44*, 253−280.
(80) Zhou, W.; Li, Y.; Je, K.; Vo, T.; Lin, H.; Partridge, B. E.; Huang, Z.; Glotzer, S. C.; Mirkin, C. A. Space-Tiled Colloidal Crystals from DNA-Forced Shape-Complementary Polyhedra Pairing. *Science* **2024**, *383*, 312−319.
(81) Zhang, Y.; Lu, F.; van der Lelie, D.; Gang, O. Continuous Phase Transformation in Nanocube Assemblies. *Phys. Rev. Lett.* **2011**, *107*, 135701.
(82) O'Brien, M. N.; Jones, M. R.; Lee, B.; Mirkin, C. A. Anisotropic Nanoparticle Complementarity in DNA-Mediated Co-Crystallization. *Nat. Mater.* **2015**, *14*, 833−839.
(83) Pauling, L. The Principles Determining the Structure of Complex Ionic Crystals. *J. Am. Chem. Soc.* **1929**, *51*, 1010−1026.
(84) Pitzer, K. S. The Nature of the Chemical Bond and the Structure of Molecules and Crystals: An Introduction to Modern Structural Chemistry. *J. Am. Chem. Soc.* **1960**, *82*, 4121.
(85) Li, W.; Palis, H.; Mérindol, R.; Majimel, J.; Ravaine, S.; Duguet, E. Colloidal Molecules and Patchy Particles: Complementary Concepts, Synthesis and Self-Assembly. *Chem. Soc. Rev.* **2020**, *49*, 1955−1976.
(86) Zhang, T.; Lyu, D.; Xu, W.; Mu, Y.; Wang, Y. Programming Self-Assembled Materials With DNA-Coated Colloids. *Front. Phys.* **2021**, *9*, 1−17.
(87) Duguet, É.; Hubert, C.; Chomette, C.; Perro, A.; Ravaine, S. Patchy Colloidal Particles for Programmed Self-Assembly. *Comptes Rendus Chim.* **2016**, *19*, 173−182.
(88) Pawar, A. B.; Kretzschmar, I. Fabrication, Assembly, and Application of Patchy Particles. *Macromol. Rapid Commun.* **2010**, *31*, 150−168.
(89) Wang, Y.; Wang, Y.; Breed, D. R.; Manoharan, V. N.; Feng, L.; Hollingsworth, A. D.; Weck, M.; Pine, D. J. Colloids with Valence and Specific Directional Bonding. *Nature* **2012**, *491*, 51−55.
(90) Zheng, X.; Wang, Y.; Wang, Y.; Pine, D. J.; Weck, M. Thermal Regulation of Colloidal Materials Architecture through Orthogonal Functionalizable Patchy Particles. *Chem. Mater.* **2016**, *28*, 3984−3989.
(91) Diaz, J. A. A.; Oh, J. S.; Yi, G.-R. R.; Pine, D. J. Photo-Printing of Faceted DNA Patchy Particles. *Proc. Natl. Acad. Sci. U. S. A.* **2020**, *117*, 10645−10653.
(92) Sacanna, S.; Irvine, W. T. M. M.; Chaikin, P. M.; Pine, D. J. Lock and Key Colloids. *Nature* **2010**, *464*, 575−578.
(93) Wang, Y.; Wang, Y.; Zheng, X.; Yi, G.-R.; Sacanna, S.; Pine, D. J.; Weck, M. Three-Dimensional Lock and Key Colloids. *J. Am. Chem. Soc.* **2014**, *136*, 6866−6869.
(94) Rouet, P. E.; Chomette, C.; Duguet, E.; Ravaine, S. Colloidal Molecules from Valence-Endowed Nanoparticles by Covalent Chemistry. *Angew. Chem.Int. Ed.* **2018**, *57*, 15754−15757.
(95) Al Harraq, A.; Lee, J. G.; Bharti, B. Magnetic Field-Driven Assembly and Reconfiguration of Multicomponent Supraparticles. *Sci. Adv.* **2020**, *6*. DOI: 10.1126/sciadv.aba5337.
(96) Abelmann, L.; Hageman, T. A. G.; Löthman, P. A.; Mastrangeli, M.; Elwenspoek, M. C. Three-Dimensional Self-Assembly Using Dipolar Interaction. *Sci. Adv.* **2020**, *6*, 6−10.
(97) Liu, M.; Zheng, X.; Grebe, V.; Pine, D. J.; Weck, M. Tunable Assembly of Hybrid Colloids Induced by Regioselective Depletion. *Nat. Mater.* **2020**, *19*, 1354−1361.
(98) Zhang, Z.; Keys, A. S.; Chen, T.; Glotzer, S. C. Self-Assembly of Patchy Particles into Diamond Structures through Molecular Mimicry. *Langmuir* **2005**, *21*, 11547−11551.
(99) van Anders, G.; Ahmed, N. K.; Smith, R.; Engel, M.; Glotzer, S. C. Entropically Patchy Particles: Engineering Valence through Shape Entropy. *ACS Nano* **2014**, *8*, 931−940.
(100) Tracey, D. F.; Noya, E. G.; Doye, J. P. K. Programming Patchy Particles to Form Complex Periodic Structures. *J. Chem. Phys.* **2019**, *151*. DOI: 10.1063/1.5128902.
(101) Rao, A. B.; Shaw, J.; Neophytou, A.; Morphew, D.; Sciortino, F.; Johnston, R. L.; Chakrabarti, D. Leveraging Hierarchical Self-Assembly Pathways for Realizing Colloidal Photonic Crystals. *ACS Nano* **2020**, *14*, 5348−5359.
(102) Van Der Linden, M. N.; Doye, J. P. K.; Louis, A. A. Formation of Dodecagonal Quasicrystals in Two-Dimensional Systems of Patchy Particles. *J. Chem. Phys.* **2012**, *136*. DOI: 10.1063/1.3679653.
(103) Wang, Y.; Wang, Y.; Breed, D. R.; Manoharan, V. N.; Feng, L.; Hollingsworth, A. D.; Weck, M.; Pine, D. J. Colloids with Valence and Specific Directional Bonding. *Nature* **2012**, *491*, 51−55.
(104) Liu, M.; Zheng, X.; Grebe, V.; Pine, D. J.; Weck, M. Tunable Assembly of Hybrid Colloids Induced by Regioselective Depletion. *Nat. Mater.* **2020**, *19*, 1354−1361.

(105) Ma, N.; Minevich, B.; Liu, J.; Ji, M.; Tian, Y.; Gang, O. *Directional Assembly of Nanoparticles by DNA Shapes: Towards Designed Architectures and Functionality*; Springer International Publishing, 2020; Vol. *378*.
(106) Stearns, L. A.; Chhabra, R.; Sharma, J.; Liu, Y.; Petuskey, W. T.; Yan, H.; Chaput, J. C. Template-Directed Nucleation and Growth of Inorganic Nanoparticles on DNA Scaffolds. *Angew. Chem. Int. Ed.* **2009**, *48*, 8494−8496.
(107) Liu, W.; Halverson, J.; Tian, Y.; Tkachenko, A. V.; Gang, O. Self-Organized Architectures from Assorted DNA-Framed Nanoparticles. *Nat. Chem.* **2016**, *8*, 867−873.
(108) Tian, Y.; Lhermitte, J. R.; Bai, L.; Vo, T.; Xin, H. L.; Li, H.; Li, R.; Fukuto, M.; Yager, K. G.; Kahn, J. S.; et al. Ordered Three-Dimensional Nanomaterials Using DNA-Prescribed and Valence-Controlled Material Voxels. *Nat. Mater.* **2020**, *19*, 789−796.
(109) Liu, W.; Tagawa, M.; Xin, H. L.; Wang, T.; Emamy, H.; Li, H.; Yager, K. G.; Starr, F. W.; Tkachenko, A. V.; Gang, O. Diamond Family of Nanoparticle Superlattices. *Science* **2016**, *351*, 582−586.
(110) Ben Zion, M. Y.; He, X.; Maass, C. C.; Sha, R.; Seeman, N. C.; Chaikin, P. M. Self-Assembled Three-Dimensional Chiral Colloidal Architecture. *Science* **2017**, *358*, 633−636.
(111) Liu, W.; Tagawa, M.; Xin, H. L.; Wang, T.; Emamy, H.; Li, H.; Yager, K. G.; Starr, F. W.; Tkachenko, A. V.; Gang, O. Diamond Family of Nanoparticle Superlattices. *Science* **2016**, *351*, 582−586.
(112) Tian, Y.; Zhang, Y.; Wang, T.; Xin, H. L.; Li, H.; Gang, O. Lattice Engineering through Nanoparticle-DNA Frameworks. *Nat. Mater.* **2016**, *15*, 654−661.
(113) Zheng, J.; Cheng, X.; Zhang, H.; Bai, X.; Ai, R.; Shao, L.; Wang, J. Gold Nanorods: The Most Versatile Plasmonic Nanoparticles. *Chem. Rev.* **2021**, *121*, 13342.
(114) Chen, H.; Shao, L.; Li, Q.; Wang, J. Gold Nanorods and Their Plasmonic Properties. *Chem. Soc. Rev.* **2013**, *42*, 2679−2724.
(115) Liang, Y.; Xie, Y.; Chen, D.; Guo, C.; Hou, S.; Wen, T.; Yang, F.; Deng, K.; Wu, X.; Smalyukh, I. I.; et al. Symmetry Control of Nanorod Superlattice Driven by a Governing Force. *Nat. Commun.* **2017**, *8*, 1−8.
(116) Gómez-Graña, S.; Pérez-Juste, J.; Alvarez-Puebla, R. A.; Guerrero-Martínez, A.; Liz-Marzán, L. M. Self-Assembly of Au@Ag Nanorods Mediated by Gemini Surfactants for Highly Efficient SERS-Active Supercrystals. *Adv. Opt. Mater.* **2013**, *1*, 477−481.
(117) Pietrobon, B.; McEachran, M.; Kitaev, V. Synthesis of Size-Controlled Faceted Pentagonal Silver Nanorods with Tunable Plasmonic Properties and Self-Assembly of These Nanorods. *ACS Nano* **2009**, *3*, 21−26.
(118) Ye, X.; Millan, J. A.; Engel, M.; Chen, J.; Diroll, B. T.; Glotzer, S. C.; Murray, C. B. Shape Alloys of Nanorods and Nanospheres from Self-Assembly. *Nano Lett.* **2013**, *13*, 4980−4988.
(119) Lan, X.; Su, Z.; Zhou, Y.; Meyer, T.; Ke, Y.; Wang, Q.; Chiu, W.; Liu, N.; Zou, S.; Yan, H.; et al. Programmable Supra-Assembly of a DNA Surface Adapter for Tunable Chiral Directional Self-Assembly of Gold Nanorods. *Angew. Chem. Int. Ed.* **2017**, *129*, 14824−14828.
(120) Nie, Z.; Fava, D.; Kumacheva, E.; Zou, S.; Walker, G. C.; Rubinstein, M. Self-Assembly of Metal-Polymer Analogues of Amphiphilic Triblock Copolymers. *Nat. Mater.* **2007**, *6*, 609−614.
(121) Chen, G.; Gibson, K. J.; Liu, D.; Rees, H. C.; Lee, J. H.; Xia, W.; Lin, R.; Xin, H. L.; Gang, O.; Weizmann, Y. Regioselective Surface Encoding of Nanoparticles for Programmable Self-Assembly. *Nat. Mater.* **2019**, *18*, 169−174.
(122) Liu, Y.; Deng, K.; Yang, J.; Wu, X.; Fan, X.; Tang, M.; Quan, Z. Shape-Directed Self-Assembly of Nanodumbbells into Superstructure Polymorphs. *Chem. Sci.* **2020**, *11*, 4065−4073.
(123) Laramy, C. R.; Lopez-Rios, H.; O'Brien, M. N.; Girard, M.; Stawicki, R. J.; Lee, B.; de la Cruz, M. O.; Mirkin, C. A. Controlled Symmetry Breaking in Colloidal Crystal Engineering with DNA. *ACS Nano* **2018**, *13*, 1412−1420.
(124) Xu, L.; Ma, W.; Wang, L.; Xu, C.; Kuang, H.; Kotov, N. A. Nanoparticle Assemblies: Dimensional Transformation of Nanomaterials and Scalability. *Chem. Soc. Rev.* **2013**, *42*, 3114−3126.
(125) Wang, T.; Zhuang, J.; Lynch, J.; Chen, O.; Wang, Z.; Wang, X.; LaMontagne, D.; Wu, H.; Wang, Z.; Cao, Y. C. Self-Assembled Colloidal Superparticles from Nanorods. *Science* **2012**, *338*, 358−363.
(126) Singh, A.; Dickinson, C.; Ryan, K. M. Insight into the 3D Architecture and Quasicrystal Symmetry of Multilayer Nanorod Assemblies from Moiré Interference Patterns. *ACS Nano* **2012**, *6*, 3339−3345.
(127) Nimbalkar, A.; Kim, H. Opportunities and Challenges in Twisted Bilayer Graphene: A Review. *Nanomicro Lett.* **2020**, *12*. DOI: 10.1007/s40820-020-00464-8.
(128) Ahn, S. J.; Moon, P.; Kim, T. H.; Kim, H. W.; Shin, H. C.; Kim, E. H.; Cha, H. W.; Kahng, S. J.; Kim, P.; Koshino, M.; et al. Dirac Electrons in a Dodecagonal Graphene Quasicrystal. *Science* **2018**, *361*, 782−786.
(129) Jones, M. R.; Kohlstedt, K. L.; O'Brien, M. N.; Wu, J.; Schatz, G. C.; Mirkin, C. A. Deterministic Symmetry Breaking of Plasmonic Nanostructures Enabled by DNA-Programmable Assembly. *Nano Lett.* **2017**, *17*, 5830−5835.
(130) Young, K. L.; Jones, M. R.; Zhang, J.; Macfarlane, R. J.; Esquivel-Sirvent, R.; Nap, R. J.; Wu, J.; Schatz, G. C.; Lee, B.; Mirkin, C. A. Assembly of Reconfigurable One-Dimensional Colloidal Superlattices Due to a Synergy of Fundamental Nanoscale Forces. *Proc. Natl. Acad. Sci. U. S. A.* **2012**, *109*, 2240−2245.
(131) Luo, B.; Kim, A.; Smith, J. W.; Ou, Z.; Wu, Z.; Kim, J.; Chen, Q. Hierarchical Self-Assembly of 3D Lattices from Polydisperse Anisometric Colloids. *Nat. Commun.* **2019**, *10*, 1−9.
(132) Wu, H.; Chen, W. Synthesis and Reaction Temperature-Tailored Self-Assembly of Copper Sulfide Nanoplates. *Nanoscale* **2011**, *3*, 5096−5102.
(133) Bowden, N.; Choi, I. S.; Grzybowski, B. A.; Whitesides, G. M. Mesoscale Self-Assembly of Hexagonal Plates Using Lateral Capillary Force: Synthesis Using the "Capillary Bond. *J. Am. Chem. Soc.* **1999**, *121*, 5373−5391.
(134) Huang, F.; Zhou, J.; Xu, J.; Wang, Y. Reversible Self-Assembly of MxS (M = Cu, Ag) Nanocrystals through Ligand Exchange. *CrystEngComm* **2014**, *16*, 9478−9481.
(135) Zhang, H. T.; Wu, G.; Chen, X. H. Large-Scale Synthesis and Self-Assembly of Monodisperse Hexagon Cu 2S Nanoplates. *Langmuir* **2005**, *21*, 4281−4282.
(136) Paik, T.; Ko, D. K.; Gordon, T. R.; Doan-Nguyen, V.; Murray, C. B. Studies of Liquid Crystalline Self-Assembly of GdF3 Nanoplates by in-Plane, out-of-Plane SAXS. *ACS Nano* **2011**, *5*, 8322−8330.
(137) Ye, X.; Chen, J.; Engel, M.; Millan, J. A.; Li, W.; Qi, L.; Xing, G.; Collins, J. E.; Kagan, C. R.; Li, J.; et al. Competition of Shape and Interaction Patchiness for Self-Assembling Nanoplates. *Nat. Chem.* **2013**, *5*, 466−473.
(138) Ou, Z.; Wang, Z.; Luo, B.; Luijten, E.; Chen, Q. Kinetic Pathways of Crystallization at the Nanoscale. *Nat. Mater.* **2020**, *19*, 450−455.
(139) Erwig, M. The Graph Voronoi Diagram with Applications. *Int. J. Netw. Sci.* **2000**, *36*, 156−163.
(140) Lee, Y. H.; Lay, C. L.; Shi, W.; Lee, H. K.; Yang, Y.; Li, S.; Ling, X. Y. Creating Two Self-Assembly Micro-Environments to Achieve Supercrystals with Dual Structures Using Polyhedral Nanoparticles. *Nat. Commun.* **2018**, *9*. DOI: 10.1038/s41467-018-05102-x.
(141) Gong, J.; Newman, R. S.; Engel, M.; Zhao, M.; Bian, F.; Glotzer, S. C.; Tang, Z. Shape-Dependent Ordering of Gold Nanocrystals into Large-Scale Superlattices. *Nat. Commun.* **2017**, *8*. DOI: 10.1038/ncomms14038.
(142) O'Brien, M. N.; Lin, H. X.; Girard, M.; Olvera De La Cruz, M.; Mirkin, C. A. Programming Colloidal Crystal Habit with Anisotropic Nanoparticle Building Blocks and DNA Bonds. *J. Am. Chem. Soc.* **2016**, *138*, 14562−14565.
(143) Chang, W. Application of Tessellation in Architectural Geometry Design. *E3S Web Conf.* **2018**, *38*, 03015.
(144) O'Brien, M. N.; Girard, M.; Lin, H.-X.; Millan, J. A.; Olvera de la Cruz, M.; Lee, B.; Mirkin, C. A. Exploring the Zone of Anisotropy

and Broken Symmetries in DNA-Mediated Nanoparticle Crystallization. *Proc. Natl. Acad. Sci. U. S. A.* **2016**, *113*, 10485−10490.
(145) Zhang, J.; Luo, Z.; Quan, Z.; Wang, Y.; Kumbhar, A.; Smilgies, D. M.; Fang, J. Low Packing Density Self-Assembled Superstructure of Octahedral Pt 3Ni Nanocrystals. *Nano Lett.* **2011**, *11*, 2912−2918.
(146) Liao, C. W.; Lin, Y. S.; Chanda, K.; Song, Y. F.; Huang, M. H. Formation of Diverse Supercrystals from Self-Assembly of a Variety of Polyhedral Gold Nanocrystals. *J. Am. Chem. Soc.* **2013**, *135*, 2684−2693.
(147) Chiu, C. Y.; Chen, C. K.; Chang, C. W.; Jeng, U. S.; Tan, C. S.; Yang, C. W.; Chen, L. J.; Yen, T. J.; Huang, M. H. Surfactant-Directed Fabrication of Supercrystals from the Assembly of Polyhedral Au-Pd Core-Shell Nanocrystals and Their Electrical and Optical Properties. *J. Am. Chem. Soc.* **2015**, *137*, 2265−2275.
(148) Liu, J.; Enomoto, K.; Takeda, K.; Inoue, D.; Pu, Y.-J. Simple Cubic Self-Assembly of PbS Quantum Dots by Finely Controlled Ligand Removal through Gel Permeation Chromatography. *Chem. Sci.* **2021**, *12*, 10354.
(149) Wang, Y.; Peng, X.; Abelson, A.; Xiao, P.; Qian, C.; Yu, L.; Ophus, C.; Ercius, P.; Wang, L.-W.; Law, M.; et al. Dynamic Deformability of Individual PbSe Nanocrystals during Superlattice Phase Transitions. *Sci. Adv.* **2019**, *5*, No. eaaw5623.
(150) Whitham, K.; Smilgies, D.-M.; Hanrath, T. Entropic, Enthalpic, and Kinetic Aspects of Interfacial Nanocrystal Superlattice Assembly and Attachment. *Chem. Mater.* **2018**, *30*, 54−63.
(151) Wang, Y.; Chen, J.; Zhong, Y.; Jeong, S.; Li, R.; Ye, X. Structural Diversity in Dimension-Controlled Assemblies of Tetrahedral Gold Nanocrystals. *J. Am. Chem. Soc.* **2022**, *144*, 13538−13546.
(152) Zhou, S.; Li, J.; Lu, J.; Liu, H.; Kim, J.-Y.; Kim, A.; Yao, L.; Liu, C.; Qian, C.; Hood, Z. D.; et al. Chiral Assemblies of Pinwheel Superlattices on Substrates. *Nature* **2022**, *612*, 259−265.
(153) He, M.; Gales, J. P.; Ducrot, É.; Gong, Z.; Yi, G.-R. R.; Sacanna, S.; Pine, D. J. Colloidal Diamond. *Nature* **2020**, *585*, 524−529.
(154) Srivastava, S.; Santos, A.; Critchley, K.; Kim, K.-S.; Podsiadlo, P.; Sun, K.; Lee, J.; Xu, C.; Lilly, G. D.; Glotzer, S. C.; et al. Light-Controlled Self-Assembly of Semiconductor Nanoparticles into Twisted Ribbons. *Science* **2010**, *327*, 1355−1359.
(155) Wang, W.; Erofeev, I.; Nandi, P.; Yan, H.; Mirsaidov, U. Evolution of Anisotropic Arrow Nanostructures during Controlled Overgrowth. *Adv. Funct. Mater.* **2021**, *31*, 1−9.
(156) Wang, Q.; Wang, Z.; Li, Z.; Xiao, J.; Shan, H.; Fang, Z.; Qi, L. Controlled Growth and Shape-Directed Self-Assembly of Gold Nanoarrows. *Sci. Adv.* **2017**, *3*, 1−9.
(157) Chen, C.; Zheng, L.; Guo, F.; Fang, Z.; Qi, L. Programmable Self-Assembly of Gold Nanoarrows via Regioselective Adsorption. *Research* **2021**, *2021*, 1−10.
(158) Pavlopoulos, N. G.; Dubose, J. T.; Liu, Y.; Huang, X.; Pinna, N.; Willinger, M. G.; Lian, T.; Char, K.; Pyun, J. Type I: Vs. Quasi-Type II Modulation in CdSe@CdS Tetrapods: Ramifications for Noble Metal Tipping. *CrystEngComm* **2017**, *19*, 6443−6453.
(159) Zanella, M.; Bertoni, G.; Franchini, I. R.; Brescia, R.; Baranov, D.; Manna, L. Assembly of Shape-Controlled Nanocrystals by Depletion Attraction. *Chem. Commun.* **2011**, *47*, 203−205.
(160) Arciniegas, M. P.; Kim, M. R.; De Graaf, J.; Brescia, R.; Marras, S.; Miszta, K.; Dijkstra, M.; Van Roij, R.; Manna, L. Self-Assembly of Octapod-Shaped Colloidal Nanocrystals into a Hexagonal Ballerina Network Embedded in a Thin Polymer Film. *Nano Lett.* **2014**, *14*, 1056−1063.
(161) Miszta, K.; De Graaf, J.; Bertoni, G.; Dorfs, D.; Brescia, R.; Marras, S.; Ceseracciu, L.; Cingolani, R.; Van Roij, R.; Dijkstra, M.; et al. Hierarchical Self-Assembly of Suspended Branched Colloidal Nanocrystals into Superlattice Structures. *Nat. Mater.* **2011**, *10*, 872−876.
(162) Castelli, A.; De Graaf, J.; Marras, S.; Brescia, R.; Goldoni, L.; Manna, L.; Arciniegas, M. P. Understanding and Tailoring Ligand Interactions in the Self-Assembly of Branched Colloidal Nanocrystals into Planar Superlattices. *Nat. Commun.* **2018**, *9*. DOI: 10.1038/s41467-018-03550-z.
(163) Castelli, A.; De Graaf, J.; Prato, M.; Manna, L.; Arciniegas, M. P. Tic-Tac-Toe Binary Lattices from the Interfacial Self-Assembly of Branched and Spherical Nanocrystals. *ACS Nano* **2016**, *10*, 4345−4353.
(164) Lee, Y. H.; Shi, W.; Lee, H. K.; Jiang, R.; Phang, I. Y.; Cui, Y.; Isa, L.; Yang, Y.; Wang, J.; Li, S.; et al. Nanoscale Surface Chemistry Directs the Tunable Assembly of Silver Octahedra into Three Two-Dimensional Plasmonic Superlattices. *Nat. Commun.* **2015**, *6*, 4−10.
(165) Henzie, J.; Andrews, S. C.; Ling, X. Y.; Li, Z.; Yang, P. Oriented Assembly of Polyhedral Plasmonic Nanoparticle Clusters. *Proc. Natl. Acad. Sci. U. S. A.* **2013**, *110*, 6640−6645.
(166) Brodin, J. D.; Auyeung, E.; Mirkin, C. A. DNA-Mediated Engineering of Multicomponent Enzyme Crystals. *Proc. Natl. Acad. Sci. U. S. A.* **2015**, *112*, 4564−4569.
(167) Zhu, J.; Avakyan, N.; Kakkis, A.; Hoffnagle, A. M.; Han, K.; Li, Y.; Zhang, Z.; Choi, T. S.; Na, Y.; Yu, C. J.; et al. Protein Assembly by Design. *Chem. Rev.* **2021**, *121*, 13701−13796.
(168) Lai, Y. T.; Cascio, D.; Yeates, T. O. Structure of a 16-Nm Cage Designed by Using Protein Oligomers. *Science* **2012**, *336*, 1129.
(169) Lai, Y.-T.; Reading, E.; Hura, G. L.; Tsai, K.-L.; Laganowsky, A.; Asturias, F. J.; Tainer, J. A.; Robinson, C. V.; Yeates, T. O. Structure of a Designed Protein Cage That Self-Assembles into a Highly Porous Cube. *Nat. Chem.* **2014**, *6*, 1065−1071.
(170) Cannon, K. A.; Nguyen, V. N.; Morgan, C.; Yeates, T. O. Design and Characterization of an Icosahedral Protein Cage Formed by a Double-Fusion Protein Containing Three Distinct Symmetry Elements. *ACS Synth. Biol.* **2020**, *9*, 517−524.
(171) Padilla, J. E.; Colovos, C.; Yeates, T. O. Nanohedra: Using Symmetry to Design Self Assembling Protein Cages, Layers, Crystals, and Filaments. *Proc. Natl. Acad. Sci. U. S. A.* **2001**, *98*, 2217−2221.
(172) Laniado, J.; Yeates, T. O. A Complete Rule Set for Designing Symmetry Combination Materials from Protein Molecules. *Proc. Natl. Acad. Sci. U. S. A.* **2020**, *117*, 31817−31823.
(173) Hsia, Y.; Bale, J. B.; Gonen, S.; Shi, D.; Sheffler, W.; Fong, K. K.; Nattermann, U.; Xu, C.; Huang, P.-S.; Ravichandran, R.; et al. Design of a Hyperstable 60-Subunit Protein Icosahedron. *Nature* **2016**, *535*, 136−139.
(174) Golub, E.; Subramanian, R. H.; Esselborn, J.; Alberstein, R. G.; Bailey, J. B.; Chiong, J. A.; Yan, X.; Booth, T.; Baker, T. S.; Tezcan, F. A. Constructing Protein Polyhedra via Orthogonal Chemical Interactions. *Nature* **2020**, *578*, 172−176.
(175) King, N. P.; Sheffler, W.; Sawaya, M. R.; Vollmar, B. S.; Sumida, J. P.; André, I.; Gonen, T.; Yeates, T. O.; Baker, D. Computational Design of Self-Assembling Protein Nanomaterials with Atomic Level Accuracy. *Science* **2012**, *336*, 1171−1174.
(176) Bale, J. B.; Gonen, S.; Liu, Y.; Sheffler, W.; Ellis, D.; Thomas, C.; Cascio, D.; Yeates, T. O.; Gonen, T.; King, N. P.; et al. Accurate Design of Megadalton-Scale Two-Component Icosahedral Protein Complexes. *Science* **2016**, *353*, 389−394.
(177) King, A. M.; Reid-Yu, S. A.; Wang, W.; King, D. T.; De Pascale, G.; Strynadka, N. C.; Walsh, T. R.; Coombes, B. K.; Wright, G. D. Aspergillomarasmine A Overcomes Metallo-β-Lactamase Antibiotic Resistance. *Nature* **2014**, *510*, 503−506.
(178) Wargacki, A. J.; Wörner, T. P.; van de Waterbeemd, M.; Ellis, D.; Heck, A. J. R.; King, N. P. Complete and Cooperative in Vitro Assembly of Computationally Designed Self-Assembling Protein Nanomaterials. *Nat. Commun.* **2021**, *12*, 883.
(179) Malay, A. D.; Miyazaki, N.; Biela, A.; Chakraborti, S.; Majsterkiewicz, K.; Stupka, I.; Kaplan, C. S.; Kowalczyk, A.; Piette, B. M. A. G.; Hochberg, G. K. A.; et al. An Ultra-Stable Gold-Coordinated Protein Cage Displaying Reversible Assembly. *Nature* **2019**, *569*, 438−442.
(180) Sinclair, J. C.; Davies, K. M.; Vénien-Bryan, C.; Noble, M. E. M. Generation of Protein Lattices by Fusing Proteins with Matching Rotational Symmetry. *Nat. Nanotechnol.* **2011**, *6*, 558−562.
(181) Gonen, S.; DiMaio, F.; Gonen, T.; Baker, D. Design of Ordered Two-Dimensional Arrays Mediated by Noncovalent Protein-Protein Interfaces. *Science* **2015**, *348*, 1365−1368.

(182) Ben-Sasson, A. J.; Watson, J. L.; Sheffler, W.; Johnson, M. C.; Bittleston, A.; Somasundaram, L.; Decarreau, J.; Jiao, F.; Chen, J.; Mela, I.; et al. Design of Biologically Active Binary Protein 2D Materials. *Nature* **2021**, *589*, 468−473.
(183) Li, Z.; Wang, S.; Nattermann, U.; Bera, A. K.; Borst, A. J.; Yaman, M. Y.; Bick, M. J.; Yang, E. C.; Sheffler, W.; Lee, B.; et al. Accurate Computational Design of Three-Dimensional Protein Crystals. *Nat. Mater.* **2023**, *22*, 1556−1563.
(184) Ballister, E. R.; Lai, A. H.; Zuckermann, R. N.; Cheng, Y.; Mougous, J. D. In Vitro Self-Assembly of Tailorable Nanotubes from a Simple Protein Building Block. *Proc. Natl. Acad. Sci. U. S. A.* **2008**, *105*, 3733−3738.
(185) Sendai, T.; Biswas, S.; Aida, T. Photoreconfigurable Supramolecular Nanotube. *J. Am. Chem. Soc.* **2013**, *135*, 11509−11512.
(186) Kashiwagi, D.; Sim, S.; Niwa, T.; Taguchi, H.; Aida, T. Protein Nanotube Selectively Cleavable with DNA: Supramolecular Polymerization of "DNA-Appended Molecular Chaperones. *J. Am. Chem. Soc.* **2018**, *140*, 26−29.
(187) McMillan, J. R.; Mirkin, C. A. DNA-Functionalized, Bivalent Proteins. *J. Am. Chem. Soc.* **2018**, *140*, 6776−6779.
(188) Sim, S.; Niwa, T.; Taguchi, H.; Aida, T. Supramolecular Nanotube of Chaperonin GroEL: Length Control for Cellular Uptake Using Single-Ring GroEL Mutant as End-Capper. *J. Am. Chem. Soc.* **2016**, *138*, 11152−11155.
(189) Zhou, K.; Zang, J.; Chen, H.; Wang, W.; Wang, H.; Zhao, G. On-Axis Alignment of Protein Nanocage Assemblies from 2D to 3D through the Aromatic Stacking Interactions of Amino Acid Residues. *ACS Nano* **2018**, *12*, 11323−11332.
(190) Suzuki, Y.; Cardone, G.; Restrepo, D.; Zavattieri, P. D.; Baker, T. S.; Tezcan, F. A. Self-Assembly of Coherently Dynamic, Auxetic, Two-Dimensional Protein Crystals. *Nature* **2016**, *533*, 369−373.
(191) Yang, G.; Zhang, X.; Kochovski, Z.; Zhang, Y.; Dai, B.; Sakai, F.; Jiang, L.; Lu, Y.; Ballauff, M.; Li, X.; et al. Precise and Reversible Protein-Microtubule-like Structure with Helicity Driven by Dual Supramolecular Interactions. *J. Am. Chem. Soc.* **2016**, *138*, 1932−1937.
(192) Partridge, B. E.; Winegar, P. H.; Han, Z.; Mirkin, C. A. Redefining Protein Interfaces within Protein Single Crystals with DNA. *J. Am. Chem. Soc.* **2021**, *143*, 8925−8934.
(193) Alberstein, R.; Suzuki, Y.; Paesani, F.; Tezcan, F. A. Engineering the Entropy-Driven Free-Energy Landscape of a Dynamic Nanoporous Protein Assembly. *Nat. Chem.* **2018**, *10*, 732−739.
(194) Zhang, S.; Alberstein, R. G.; De Yoreo, J. J.; Tezcan, F. A. Assembly of a Patchy Protein into Variable 2D Lattices via Tunable Multiscale Interactions. *Nat. Commun.* **2020**, *11*, 3770.
(195) Hayes, O. G.; McMillan, J. R.; Lee, B.; Mirkin, C. A. DNA-Encoded Protein Janus Nanoparticles. *J. Am. Chem. Soc.* **2018**, *140*, 9269−9274.
(196) Kashiwagi, D.; Shen, H. K.; Sim, S.; Sano, K.; Ishida, Y.; Kimura, A.; Niwa, T.; Taguchi, H.; Aida, T. Molecularly Engineered "Janus GroEL": Application to Supramolecular Copolymerization with a Higher Level of Sequence Control. *J. Am. Chem. Soc.* **2020**, *142*, 13310−13315.
(197) Hayes, O. G.; Partridge, B. E.; Mirkin, C. A. Encoding Hierarchical Assembly Pathways of Proteins with DNA. *Proc. Natl. Acad. Sci. U. S. A.* **2021**, *118*, No. e2106808118.
(198) Mueller, N. S.; Okamura, Y.; Vieira, B. G. M.; Juergensen, S.; Lange, H.; Barros, E. B.; Schulz, F.; Reich, S. Deep Strong Light-Matter Coupling in Plasmonic Nanoparticle Crystals. *Nature* **2020**, *583*, 780−784.
(199) Huh, J. H.; Lee, J.; Lee, S. Soft Plasmonic Assemblies Exhibiting Unnaturally High Refractive Index. *Nano Lett.* **2020**, *20*, 4768−4774.
(200) Sun, S.; Yang, S.; Xin, H. L.; Nykypanchuk, D.; Liu, M.; Zhang, H.; Gang, O. Valence-Programmable Nanoparticle Architectures. *Nat. Commun.* **2020**, *11*, 2279.
(201) Malay, A. D.; Miyazaki, N.; Biela, A.; Chakraborti, S.; Majsterkiewicz, K.; Stupka, I.; Kaplan, C. S.; Kowalczyk, A.; Piette, B. M. A. G.; Hochberg, G. K. A.; et al. An Ultra-Stable Gold-Coordinated Protein Cage Displaying Reversible Assembly. *Nature* **2019**, *569*, 438−442.
(202) King, N. P.; Bale, J. B.; Sheffler, W.; McNamara, D. E.; Gonen, S.; Gonen, T.; Yeates, T. O.; Baker, D. Accurate Design of Co-Assembling Multi-Component Protein Nanomaterials. *Nature* **2014**, *510*, 103−108.
(203) Zhou, Z.; Harris, K. D. M. Optimizing the Number of Components in a Molecular Quasicrystal: A Three-Component Material Based on the Penrose Tiling. *J. Phys. Chem. C* **2008**, *112*, 16186−16188.
(204) Zhou, Z.; Harris, K. D. M. Design of a Molecular Quasicrystal. *ChemPhysChem* **2006**, *7*, 1649−1653.

https://doi.org/10.1021/acs.chemrev.4c00299
Chem. Rev. 2024, 124, 11063−11107